nagra.

Arbeitsbericht NAB 14-01

Geomechanical properties, rock models and in-situ stress conditions for Opalinus Clay in Northern Switzerland

December 2014

S. Giger & P. Marschall

**Nationale Genossenschaft
für die Lagerung
radioaktiver Abfälle**

Hardstrasse 73
CH-5430 Wettingen
Telefon 056-437 11 11

www.nagra.ch

nagra.

Arbeitsbericht NAB 14-01

Geomechanical properties, rock models and in-situ stress conditions for Opalinus Clay in Northern Switzerland

December 2014

S. Giger & P. Marschall

KEYWORDS

SGT-E2, Opalinus Clay, geomechanical properties, rock model, in-situ stress, constitutive law, strength

Nationale Genossenschaft für die Lagerung radioaktiver Abfälle

Hardstrasse 73
CH-5430 Wettingen
Telefon 056-437 11 11

www.nagra.ch

Nagra Working Reports concern work in progress that may have had limited review. They are intended to provide rapid dissemination of information.

Zusammenfassung

Für die Beurteilung der bautechnischen Machbarkeit geologischer Tiefenlager sind das Verständnis des Deformationsverhaltens des Wirtgesteins sowie die Abschätzung der in den Standortgebieten vorherrschenden geologischen Verhältnisse (Spannungsfeld, Porendruck) und des tektonischen Baus (Störungssysteme, Trennflächen) von zentraler Bedeutung. Der Opalinuston wurde im Rahmen der Etappe 1 des Sachplans geologische Tiefenlager (SGT) als Wirtgestein für hochaktive Abfälle (BE/HAA) bestimmt. Opalinuston ist auch ein mögliches Wirtgestein für schwach- und mittelaktive Abfälle (SMA).

Der vorliegende Bericht fasst den Kenntnisstand geomechanischer Eigenschaften des Opalinustons zusammen ("geomechanische Referenzparameter"). Zusätzlich zu den geomechanischen Eigenschaften wie Steifigkeit und Festigkeit werden auch Daten zu Strukturelementen ("Gebirgsmodelle") sowie des In-situ-Spannungszustands auf Lagerebene für die verschiedenen Standortgebiete diskutiert. Das Hauptprodukt des Berichts ist der sogenannte "geomechanische Geodatensatz für bautechnische Anwendungen" (GDS-AB-WG). Er besteht in der Tabellierung von Referenzparametern sowie der Formulierung von Gebirgsmodellen für numerische Modellrechnungen im Rahmen der Beurteilung der bautechnischen Machbarkeit geologischer Tiefenlager im Opalinuston.

Opalinuston kann mineralogisch als ein karbonatischer, sandiger Tonstein klassifiziert werden, wobei die Korngrössenverteilung von der Siltfraktion dominiert wird. Geotechnisch gesehen handelt es sich um einen überkonsolidierten Tonstein mit geringer bis mittlerer Plastizität. Die Überkonsolidierung kommt in Deformationsexperimenten durch eine ausgeprägte Spitzenfestigkeit und sprödes Nachbruchverhalten im für geologische Tiefenlager relevanten Spannungsbereich zum Ausdruck. Die Zunahme der Steifigkeit, der Festigkeit und der Quelleigenschaften mit grösserer Versenkungstiefe bzw. grösserer effektiver Belastung werden für Opalinuston ebenfalls beobachtet. Das elasto-plastische Spannungs-Dehnungsverhalten kann konzeptuell durch die Theorie der kritischen Zustände ("critical state theory)" beschrieben werden, in der die Tiefenabhängigkeit der geomechanischen Eigenschaften des Opalinustons implizit berücksichtigt wird. Für bautechnische Zwecke werden in der Regel vereinfachte Materialgesetze verwendet, die auf dem Mohr-Coulomb Kriterium zur Formulierung der Festigkeit beruhen. Deshalb werden für den GDS-AB-WG zwei Parametersätze abgeleitet:

- Der geomechanische Datensatz *Opalinuston untief*, basierend auf den Grundlagedaten von Kernproben des Felslabors Mont Terri, wird als prioritär angesehen für die Untersuchung des Deformationsverhalten von Opalinuston bis maximal etwa 400 m Tiefe.
- Der geomechanische Datensatz *Opalinuston tief*, basierend auf den Grundlagedaten von Kernproben der Bohrungen Benken und Schlattingen-1, wird als prioritär angesehen für die Untersuchung des Deformationsverhaltens von Opalinuston im Tiefenbereich von etwa 400 – 900 m.

Diskrete Bruchflächen oder Störungszonen werden im Opalinuston zwar beobachtet, sind jedoch in Kernbohrungen der Nordschweiz generell selten. Um eine mögliche Entfestigung des Gebirges durch Strukturelemente in vergleichenden Modellrechnungen zu berücksichtigen, werden skalenunabhängige Gebirgsmodelle formuliert.

Zur Ergänzung der Datenlage der In-situ Gebirgsspannungen, insbesondere bezüglich der Ungewissheiten in der Magnitude der maximalen lateralen Hauptspannung, werden verschiedene Ansätze aus der Fels- und Bodenmechanik eingeführt. Diese erlauben die Formulierung verschiedener Szenarien des vorherrschenden Spannungsfelds auf Lagerebene, die abdeckend sind für das Spektrum der geologischen Situationen in den Standortgebieten.

Table of Contents

Zusammenfassung I

Table of Contents III

List of Tables V

List of Figures VI

1 Background and objectives 1

2 Structural and stress data of Opalinus Clay in Northern Switzerland 3
2.1 Source locations for characterization and testing 3
2.2 Structural data 4
2.2.1 Fracture orientation and frequencies 4
2.2.2 Fault anatomy and fault scaling 8
2.3 Stress data 11
2.3.1 Orientation of principal stresses 11
2.3.2 Stress magnitudes 11
2.3.2.1 Minimum horizontal stress magnitude (Sh) 12
2.3.2.2 Maximum horizontal stress magnitude (SH) 14
2.4 Pore fluid pressure 14

3 Mineralogy and basic physical properties 15
3.1 Mineralogy 15
3.2 Density and water content 17
3.3 Porosity and void ratio 18
3.4 Geotechnical characterization 20
3.4.1 Grain size distribution 20
3.4.2 Atterberg limits 21

4 Deformation and strength behavior 23
4.1 Convention of sample orientation in deformation tests 23
4.2 Consolidation and swelling behavior 23
4.2.1 Compressibility during one-dimensional consolidation 23
4.2.2 Overconsolidation ratio from preconsolidation stress 25
4.2.3 Time-dependent settlement (consolidation and creep) 26
4.2.4 Swelling parameters 27
4.3 Static elastic moduli and Poisson's ratio 28
4.4 Tensile strength 35
4.5 Uniaxial compressive strength 36
4.6 Hydromechanical coupling parameters 38
4.7 Triaxial strength 39
4.7.1 Volumetric behavior during shear 40

4.7.2 Effective stress analysis (p'-q space) 42
4.7.3 Total stress analysis (undrained shear strength) 51
4.8 Residual strength 52
4.9 Stiffness of joint/bedding planes and dilation angle 53

5 Data evaluation 55
5.1 Porosity and water content 55
5.2 Stiffness and strength 55

6 Constitutive framework and application to modelling 57
6.1 Critical state approach 57
6.2 Constitutive law for assessment of engineering feasibility 59

7 Recommended parameter values for numerical modelling 61
7.1 Geomechanical parameters 61
7.2 Swelling parameters 67
7.3 Rock models ('Gebirgsmodelle') 68
7.4 In-situ stress 75
7.5 Site-specific reference data sets 79

References 81

Appendices:

A Independent evidence A-1

B Effect of pore pressure in regression lines of Benken data B-1

C Estimation of minimum horizontal stress magnitudes C-1

D Electronic datafiles D-1

List of Tables

Tab. 2-1: Overburden depth of the Opalinus Clay in the siting regions of Northern Switzerland. 3
Tab. 3-1: Reference mineralogy for Opalinus Clay. 17
Tab. 3-2: Opalinus Clay reference porosity and density with upper and lower bounds..... 18
Tab. 3-3: Opalinus Clay porosity values from borehole samples and the URL MT. 19
Tab. 4-1: Compilation of overconsolidation ratios (OCR) from selected locations..... 25
Tab. 4-2: Types of E-moduli derived in drained and undrained tests. 30
Tab. 4-3: Summary of tensile strength results..... 35
Tab. 4-4: Results from uniaxial compressive strength (UCS) tests..... 36
Tab. 4-5: Best fit parameters in p'-q space and calculated Mohr-Coulomb parameters..... 43
Tab. 4-6: Overview of selected studies and assigned quality levels for regression analysis of sample from Mont Terri rock laboratory. 44
Tab. 7-1: Recommended parameter sets for Opalinus Clay for effective stress analysis using a bi-linear Mohr-Coulomb constitutive law with tension cut-off. 61
Tab. 7-2: Recommended swelling parameters for Opalinus Clay..... 68
Tab. 7-3: Recommended Mohr-Coulomb effective strength parameters for the different rock models. 70
Tab. 7-4: Recommended parameter values to derive undrained shear strength values (Su) for different rock models at a given water content. 73
Tab. 7-5: Reference principal total normal stress values as a function of depth. 76
Tab. 7-6: Recommended geomechanical reference datasets for site specific analyses. 79
Tab. B1-1: Comparison of fit analysis with variable pore fluid pressure values for the geomechanical tests by Rummel & Weber (1999). B-1
Tab. D1-1: Overview of electronic datafiles. D-1

List of Figures

Fig. 2-1: Regional tectonic map of Northern Switzerland with source localities of Opalinus Clay used for characterization and geomechanical testing. 4
Fig. 2-2: Orientation of fractures and slip indicators from surface mapping. 5
Fig. 2-3: Structural analysis of Opalinus Clay from cores in deep boreholes of Northern Switzerland. 8
Fig. 2-4: Orientation of induced fractures in hydraulic fracturing tests. 8
Fig. 2-5: Examples of fault architecture in Opalinus Clay. 10
Fig. 2-6: Comparison of in-situ stress with paleo stress data for Northern Switzerland. 11
Fig. 2-7: Stress magnitude data from hydraulic fracturing at Benken and Schlattingen. 12
Fig. 2-8: Comparison of Opalinus Clay horizontal to vertical stress ratios between conceptual considerations and measurements by hydraulic fracturing. 13
Fig. 3-1: Opalinus Clay mineralogy in the ternary diagram by Füchtbauer. 15
Fig. 3-2: Clay mineral content of Opalinus Clay from boreholes at HLW siting areas. 16
Fig. 3-3: Opalinus Clay porosity as function of current burial depth below ground. 19
Fig. 3-4: Grain size distribution of Opalinus Clay. 20
Fig. 3-5: Plasticity chart for Opalinus Clay samples. 21
Fig. 4-1: Convention of sample orientation. 23
Fig. 4-2: Schematic of oedometric curve with interpreted parameters. 24
Fig. 4-3: Coefficient of consolidation versus vertical effective stress for samples from Schlattingen-1. 26
Fig. 4-4: Swelling pressures as a function of water content. 28
Fig. 4-5: Non-cyclic (left) versus cyclic test (right). 29
Fig. 4-6: Influence of suction on sample stiffness in Oedometer tests. 30
Fig. 4-7: Compilation of static E-Moduli for samples from Mont Terri. 32
Fig. 4-8: Compilation of static E-Moduli for samples from Schlattingen and Benken. 33
Fig. 4-9: Summary of E-Moduli from geomechanical testing. 34
Fig. 4-10: Results from tensile strength tests at variable humidity conditions. 35
Fig. 4-11: Results from UCS tests as a function of sample orientation. 36
Fig. 4-12: UCS test results as function of natural water content. 37
Fig. 4-13: Stress-strain results from UCS tests with samples from URL MT at variable humidity conditions. 38
Fig. 4-14: Evolution of (deviator) stress with axial strain in Opalinus Clay from Schlattingen. 40
Fig. 4-15: Volumetric strain as a function of deviator stress for Opalinus Clay Benken. 41
Fig. 4-16: Volumetric strain as a function of deviator stress for Opalinus Clay Schlattingen. 41

Fig. 4-17: Peak and post-peak matrix strength of samples from URL Mont Terri. 45
Fig. 4-18: Mont Terri peak matrix trength with respect to water content. 46
Fig. 4-19: Peak and post-peak bedding strength of samples from URL Mont Terri. 47
Fig. 4-20: Peak and post-peak matrix strength of samples from BEN and SLA-1. 48
Fig. 4-21: Benken/Schlattingen-1 peak matrix strength with respect to water content. 49
Fig. 4-22: Peak and post-peak bedding strength of samples from BEN and SLA-1. 50
Fig. 4-23: Comparison of measured and calculated UCS values. 51
Fig. 4-24: Undrained shear strength as a function of water content. 52
Fig. 6-1: State boundary surface in three dimensions. 58
Fig. 6-2: p'-q section of the 3D state boundary surface in Fig. 5-1 58
Fig. 7-1: Bilinear regression for matrix strength from Benken and Schlattingen-1. 63
Fig. 7-2: Bilinear regression for bedding strength from Benken and Schlattingen-1. 64
Fig. 7-3: Strength results projected onto q-*v* section. 65
Fig. 7-4: Forced regression for matrix post-peak strength of Mont Terri test results. 66
Fig. 7-5: Forced regression for bedding peak strength of Mont Terri test results. 66
Fig. 7-6: Forced regression for bedding post-peak strength of Mont Terri test results. 67
Fig. 7-7: Schematic destructuring of intact, anisotropic Opalinus Clay rock mass. 69
Fig. 7-8: Schematic of assigned laboratory strength parameters to progressively destructured Opalinus Clay 69
Fig. 7-9: Strength values of different rock models for *Opalinus Clay shallow* 71
Fig. 7-10: Strength values of different rock models for *Opalinus Clay deep* 72
Fig. 7-11: Rock models interpreted in Su-w space 74
Fig. 7-12: Recommended depth trend of reference and alternative stress scenarios. 78
Fig. A-1: Empirical correlation of effective friction angle with Plasticity Index (I_p or PI) after Terzaghi et al. (1996). A-1
Fig. A-2: Empirical correlation of effective residual friction angle with liquid limit (w_L) and clay size fraction (CF) after Stark & Eid (1994). A-2
Fig. A-3: Comparison of normalized undrained shear strength between Opalinus Clay and North Sea shales A-3

1 Background and objectives

The evaluation of construction feasibility of underground structures is a critical aspect of Stage 2 in the site selection process of the Sectoral Plan for Deep Geological Repositories ("SGT", SFOE 2008). In stage 1 of the SGT, Opalinus Clay was selected as the host rock for high-level waste (HLW), and as a potential host rock for low- and intermediate-level waste (L/ILW).

Conventional engineering feasibility assessment is conducted by using analytical and numerical methods which require the following geomechanical and state properties as input data:

- Laboratory intact rock properties and constitutive behavior
- Scaling of intact rock properties to rock mass properties by consideration of structural and other inhomogeneities not captured by the rock properties
- Magnitudes and orientation of the principal in-situ stress components

The objective of this report is to compile such input data. It provides first an overview of locations at which Opalinus Clay was sampled for geomechanical characterization and testing in the laboratory (Chapter 2). Structural and stress data for Opalinus Clay in northern Switzerland are also compiled in Chapter 2.

Chapter 3 is dedicated to the compilation of basic physical, mineralogical and index properties.

Geomechanical test results of Opalinus Clay are compiled in Chapter 4. A brief general assessment of the data is provided in Chapter 5. Chapter 6 attempts to outline a constitutive context for the observed test results and concludes with a simplified elasto-plastic material law of Opalinus Clay for numerical modelling of underground structures.

Chapter 7 concludes with recommended reference parameter sets consisting of i) rock properties, ii) rock (mass) models ("Gebirgsmodelle") and iii) stress scenarios.

All electronic data files used for documentation and regression analyses in Chapter 3 to 7 can be found on the CD attached to this report. Appendix D provides an overview of the electronic data files and details where the data was used in the various figures and tables.

2 Structural and stress data of Opalinus Clay in Northern Switzerland

2.1 Source locations for characterization and testing

Opalinus Clay was sampled across Northern Switzerland at depths of several meters to more than 1000 m. At the proposed siting regions, Opalinus Clay is found at depths of approximately 300 to 900 m below ground (Tab. 2-1). Besides differences in current burial depth, Opalinus Clay in the different siting regions was also exposed to variable tectonic deformation during Neogene shortening. It is estimated (Nagra 2008 and ongoing work at Nagra with structural restoration of seismic sections) that Opalinus Clay at the siting regions of Nördlich Lägern and Jura Ost was transported several hundred meters to the north, and in the case of Jura-Südfuss as much as several kilometers.

Extensive geomechanical testing programs were conducted by Nagra on core samples from the Mont Terri underground lab (URL MT) in Northwestern Switzerland, and with core samples from the boreholes of Benken and Schlattingen-1 in Northeastern Switzerland (Fig. 2-1). Geomechanical testing was also conducted on samples retrieved from more shallow depths (< 100 m) in academic studies (Bellwald 1990; Nüesch 1991; Aristorenas 1992) and industry reports (Büchi & Müller AG 1988) (cf. indices 1 to 4 in Fig. 2-1). In addition, basic physical and mineralogical properties were derived from Opalinus Clay samples from several deep boreholes (Fig. 2-1).

Tab. 2-1: Overburden depth of the Opalinus Clay in the siting regions of Northern Switzerland.

After Nagra (2010).

Siting region	min	max	median
Südranden (SR)	310	410	380
Jura Ost (JO)	300	510	410
Jura-Südfuss (JS)	490	700	560
Zürich Nordost (ZNO)	570	850	700
Nördlich Lägern (NL)	700	910	810

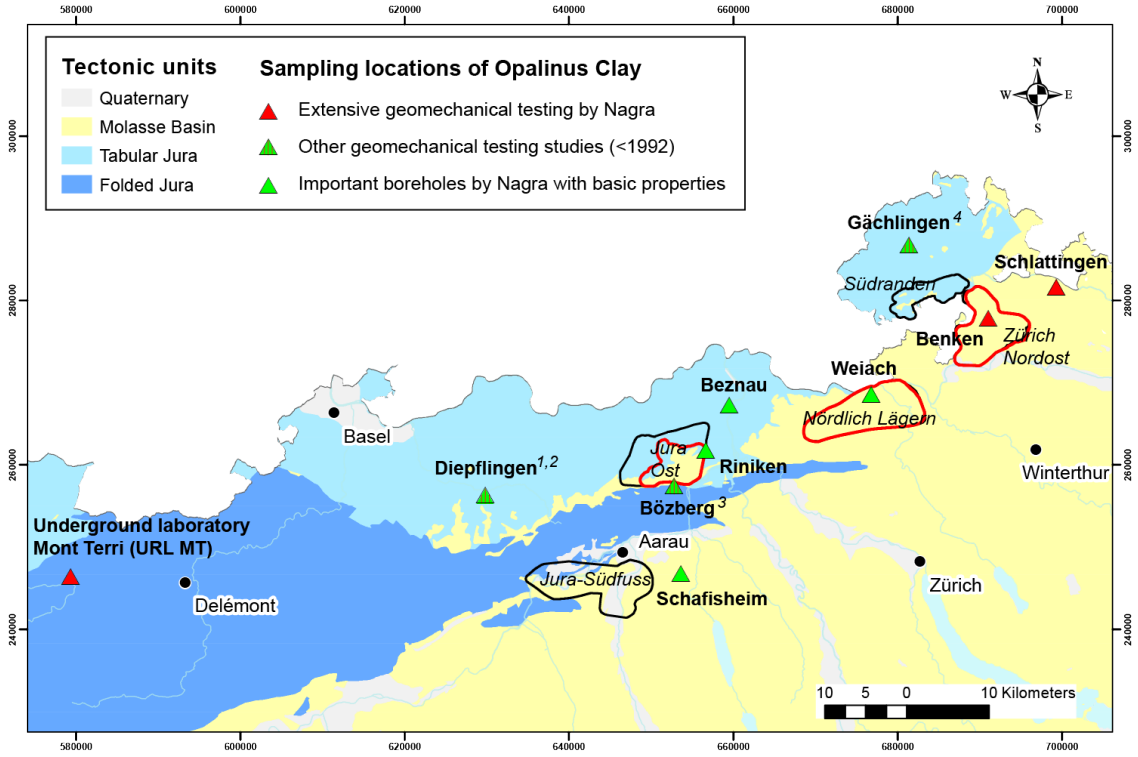

Fig. 2-1: Regional tectonic map of Northern Switzerland with source localities of Opalinus Clay used for characterization and geomechanical testing.

Numbers relate to geomechanical characterisation and testing conducted on Opalinus Clay without Nagra involvement: [1] Bellwald (1990), [2] Aristorenas (1992), [3] Nüesch (1991), [4] Büchi & Müller AG (1988).

2.2 Structural data

2.2.1 Fracture orientation and frequencies

Opalinus Clay outcrops are generally of poor quality and structural description generally limited to quarries (cf. Fig. 2-5a,b). Madritsch & Hammer (2012) conducted field investigations in different siting regions on Tertiary and Upper/Middle Jurassic rocks (Fig. 2-2). The dominant azimuth of the fractures is in N-S to NNE-SSW direction. A WNW-ESE direction is also prominent in the siting areas of JS and NL. Inclinations of fractures in all siting areas are generally steep (80 – 90° to horizontal). Many of these steep fractures may be attributed to unloading effects (decompaction joints). However, between 60 to 80% of the recorded fractures also contain a kinematic indicator (slip striation) on the fracture surface and can therefore be distinguished from pure mode 1 fractures (joints). Gently dipping fractures (< 30 – 40°) are generally rare (NL, JS, JO) or not detected at all (SR/ZNO) at outcrops. Fracture spacing in all siting regions is approximately 0.5 – 1 m for subvertical fractures and several meters for moderately to gently dipping fractures. Frequencies are elevated for mechanically more competent and thinly bedded layers (Madritsch & Hammer 2012).

The key structural databases in the subsurface are boreholes. The near-to-vertical trajectory of deep boreholes in Northern Switzerland implies that subvertical fractures tend to be undersampled.

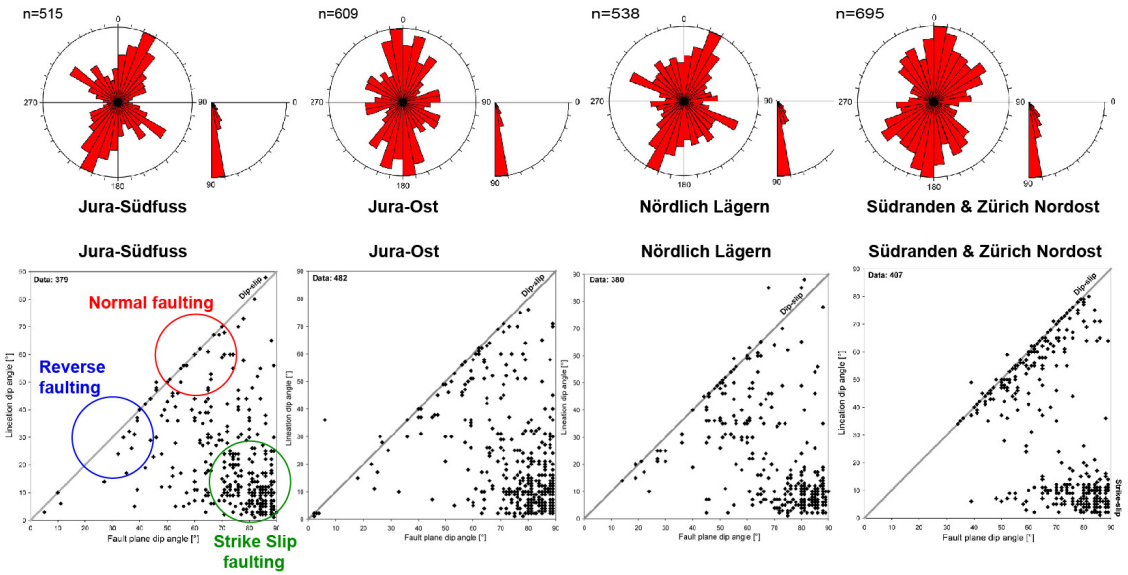

Fig. 2-2: Orientation of fractures and slip indicators from surface mapping.

Above: Rose diagrams for all fractures (n = number of measurements). *Below:* Only fractures with slip component (excluding joints). From Madritsch & Hammer (2012).

Conversely, the fracture frequency derived from borehole data will provide an upper boundary, as some fractures may be induced mechanically during drilling or by chemical interaction between the drilling fluid and the rock.

In the Schafisheim borehole, fractures in the Malm and the upper Dogger strike SW-NE (Chapter 6.3.3.4 in Matter et al. 1988), in good agreement with the dominant direction from surface mapping in the siting region of Jura-Südfuss further to the west. At the level of the Opalinus Clay, fractures strike more WNW-ESE, which is perpendicular to the mean in-situ orientation of SH (Fig. 2-6) and roughly parallel with the azimuth of the second most dominant fracture family reported from surface mapping (Fig. 2-2). Fractures in Opalinus Clay are very rare over the uppermost 90% of the core interval with frequencies of 0.1 – 0.2 per core meter (Fig. 2-3). The lowermost 10 m of the Opalinus Clay show a much higher frequency (up to 10/m) of fractures with very small to gentle dip (< 30 – 40°) with respect to the bedding (Matter et al. 1988). It has been suggested that significant deformation was localized in this zone of the Opalinus Clay at the contact with the 'more rigid' upper Lias (Matter et al. 1988). A rigidity contrast may be defined by the clay mineral content, which appears to decrease sharply from some 55 – 60% in the Opalinus Clay to under 20% in the upper Lias (Albert & Schwab 2013).

Fractures in Opalinus Clay of the Riniken borehole within the siting region of Jura Ost have a dominant azimuth in WSW-ENE direction (Beilage 31 in Matter et al. 1987). As in Schafisheim, this orientation is orthogonal to the current in-situ direction of SH and subparallel to the dominant thrust systems in the region, the Mandach thrust in the north, the Siglistorf Anticline immediately to the east and the Jura main thrust in the south (e.g. Nagra 2008). Dip angle of the fractures vary typically between 10 and 70° (Matter et al. 1987, and Fig. 2-3). Fractures are rare in the upper and central part of the formation (0.1-1/m), with intervals of 20 - 40 m without indication of any structural discontinuity. As in Schafisheim, the lowermost 20 to 30 m of the Opalinus Clay in Riniken are much more disturbed and was interpreted to consist of either two main and isolated fault zones of 2 m thickness each, or a larger fault zone of approximately 7 m thickness, covering the two fault strands with a relatively intact central

part. If out-of-sequence reverse thrusting at the base of the Opalinus Clay was responsible for the greater thickness of 13 m in Riniken in comparison with Weiach (as speculated in Nagra 1987) the associated throw would be of the order of 20 to 80 m assuming fault inclinations of 45 and 10 degrees, respectively.

Only very few and isolated fractures are reported from Opalinus Clay cores of the Weiach and Benken boreholes in the siting areas of NL and ZNO. These dip moderately to steep. The only fault explicitly described in the two boreholes has a central core of some 4 cm thickness and a peripheral damage zone approximately one order of magnitude wider (Fig. 5-11 and Beilage 5.2C in Nagra 2001) (cf. Benken at a depth of 602 m in Fig. 2-3).

Induced fractures in hydraulic fracturing tests in both the boreholes Benken and Schlattingen strike parallel to the present main horizontal stress direction (SH) at the level of the OPA. In the case of the borehole Benken, the azimuth of the induced fractures is also subparallel to the dominant fracture orientation at the surface (Fig. 2-2). In addition, the induced fractures in Benken are very steep (85 – 90°) in the uppermost 400 m, but are inclined 70 – 80° at greater depths.

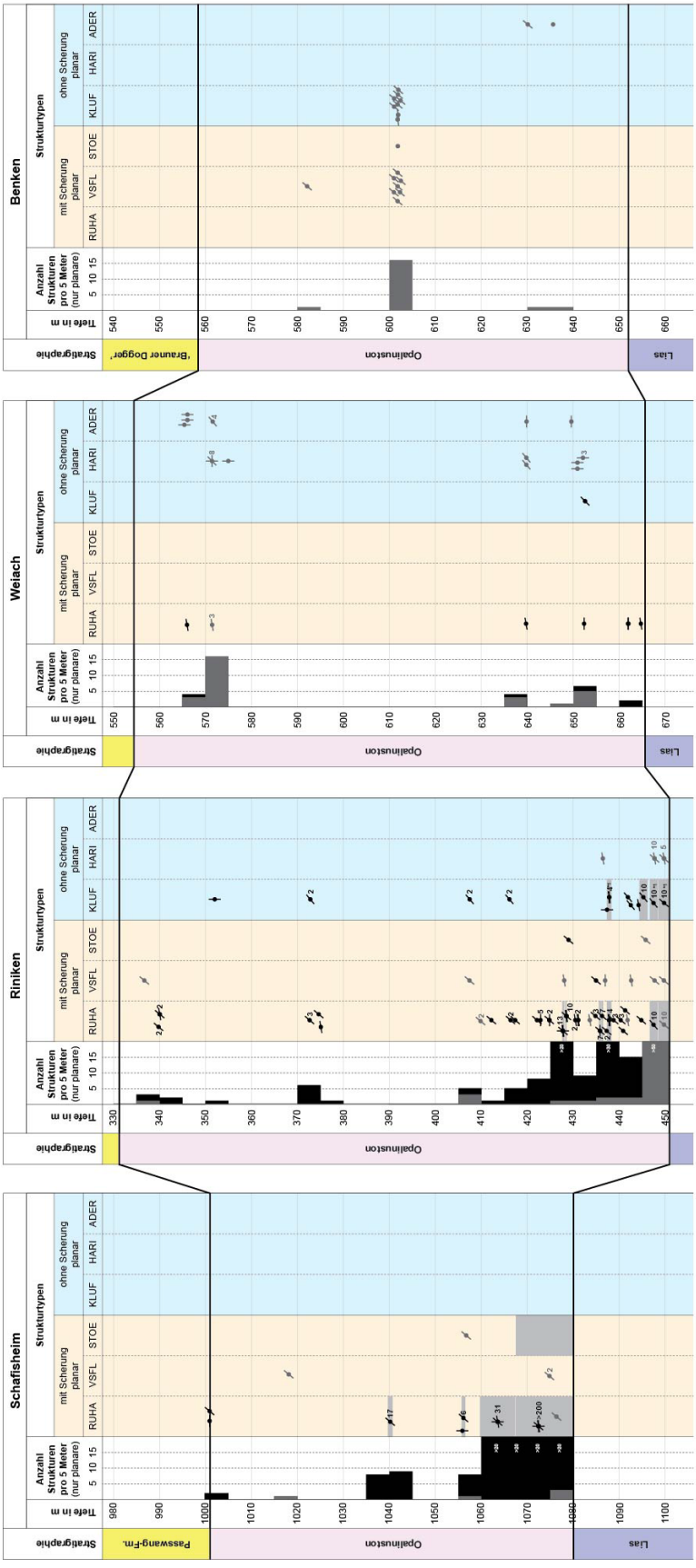
Schafisheim
Riniken
Weiach
Benken
Strukturtypen
mit Scherung planar
ohne Scherung planar
RUHA
VSFL
STOE
KLUF
HARI
ADER
Anzahl Strukturen pro 5 Meter (nur planare)
Tiefe in m
Stratigraphie
Passwang-Fm.
Opalinuston
Lias
'Brauner Dogger'

Fig. 2-3: Structural analysis of Opalinus Clay from cores in deep boreholes of Northern Switzerland.

A distinciton is made for planar structures with shear indicators (RUHA = slickensides, VSFL = fault plane, relative movement constrained, STOE = fault zone) and without shear indicators (KLUF = joint, HARI = hair-line cracks, ADER = vein). Detailed definition of interpreted structures and analysis procedure is provided in Ebert (2014).

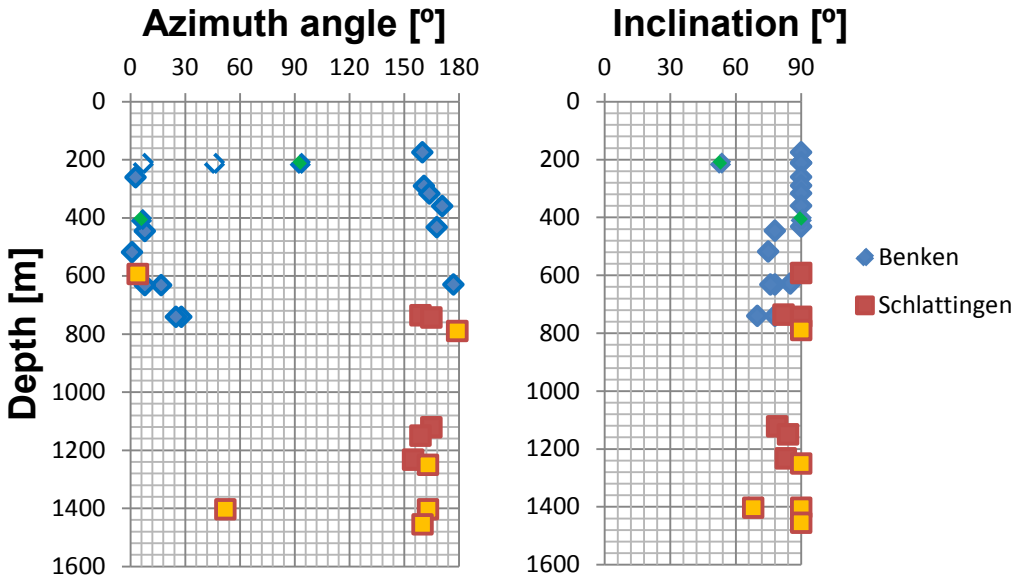

Fig. 2-4: Orientation of induced fractures in hydraulic fracturing tests.

Blue and red symobls = fractures induced during testing. Green and orange filling = fractures interpreted to be present prior to testing. Open symbols = unclear whether present prior to testing. Note: Opalinus Clay interval between 540 and 650 m in Benken, and 830 to 950 m in Schlattingen. Compiled from Klee & Rummel (2000) and Klee (2012).

2.2.2 Fault anatomy and fault scaling

Faults within the Opalinus Clay can be observed in various quarries, boreholes and in the URL at Mont Terri (Fig. 2-5). Their general architecture can be approximated by a relatively narrow, strongly disturbed 'core' zone containing multiple fractures with narrow spacing and in subparallel orientation, confined by much wider zones of increasingly more isolated fractures ('damage zone') and of more variable orientation away from the core. Where the disturbed zone is oriented at low angle to the bedding, a damage zone may be less pronounced as deformation can be accommodated by bedding-parallel slip (Fig. 2-5c). In the disturbed zone, the bedding fabric is either rearranged towards parallel orientation with the dominant fractures, or entirely obliterated along discrete planes. Mineralized zones in the fault zones are very rare.

The described fault architecture for Opalinus Clay is qualitatively comparable to fault zones in siliziclastic sequences for which scaling relationships were proposed (e.g. Torabi & Berg 2011). Following this approach, fault size attributes may be estimated from other attributes by empirical data correlation, although with very large scatter of approximately one order of magnitude. For example, vertical seismic resolution at the level of the Opalinus Clay in the recent 2D Seismic acquisition is estimated at approximately 15 – 20 m (Madritsch et al. 2013). Hence fault zones with a throw of < 20 m are not expected to be resolved, especially not in the absence of favorable impedance contrasts. For a realistic scenario with an inclined fault zone dominated by dip-slip the displacement of potentially unresolved faults in the seismic survey is then of the order of 25 to 40 m for normal and thrust faults, respectively, and potentially much larger for faults at very low angle with respect to bedding (bedding-parallel slip) or for steeply inclined faults with a dominant strike-slip component. According to empirical relationships (Torabi & Berg 2011), this would equate to fault zones of several hundred meters in length with a peripheral fracture or 'damage' zone of a few meters to decameters, and a 'fault core' of several decimeters to approximately 1 m. The 'main fault' at the URL Mont Terri may be an example of such a fault, with a 'core' thickness of 1 – 3 m and a damage zone of several meters. The increased fracture frequency and disturbed zone at the base of the Opalinus Clay in the Schafisheim and Riniken boreholes may also correspond to fault zones of this order of magnitude.

A somewhat smaller fault was described in the quarry of Siblingen (Nagra 2002) (Fig. 2-5a). It consists of a core of one to several decimeters and a 'damage' zone of a few meters. Following local structural mapping based on borehole analysis, the fault has a throw borehole below 10 meters and is striking SE over a length of at least a few hundred meters (Büchi & Müller AG 1983). The fault is part of a fairly consistent fault pattern in the quarry of Siblingen and the nearby quarry and waste site of Pflumm approximately 1 km to the north (Büchi & Müller AG 1988). Based on the location and striking direction, these faults are likely branches of the Neuhausen fault zone extending from the southeast.

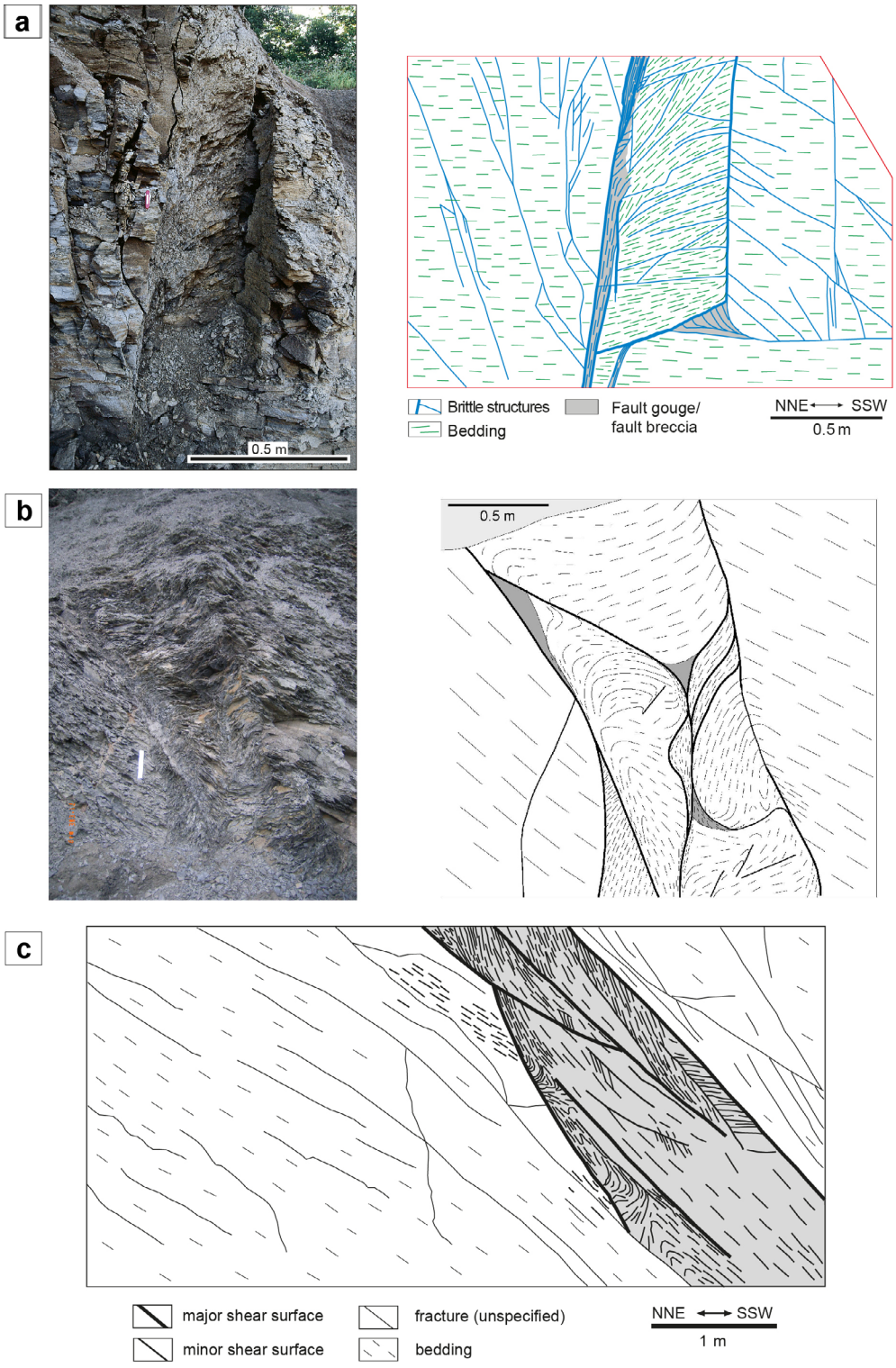

Fig. 2-5: Examples of fault architecture in Opalinus Clay.

(a) Siblingen quarry, north of the siting area of SR (from Nagra 2002). (b) Holderbank quarry, south of JO (courtesy of M. Mazurek, unpublished). (c) Interpretation of the 'main fault' at the URL Mont Terri (from Nagra 2002).

2.3 Stress data

2.3.1 Orientation of principal stresses

Present day orientation of maximum horizontal stress (SH) in Northern Switzerland was derived from borehole breakouts and earthquake focal mechanisms. New data and re-examination of previous analysis of borehole breakouts confirm a relatively uniform NNW-SSE direction (166 ± 12°) for SH in the Mesozoic and Cenozoic cover (Heidbach & Reinecker 2013). Formation-specific borehole breakout analyses have shown that the dominant average orientation of SH deduced from all formations at a particular location are also representative for the Opalinus Clay.

2.3.2 Stress magnitudes

Relative stress magnitudes can be estimated from earthquake focal mechanisms. In the upper 7 – 8 km of Northern Switzerland, these mechanisms are dominated by strike-slip movement, with only minor normal faulting and virtually no thrust faulting (Heidbach & Reinecker 2013). This indicates a dominant stress regime between transpression (Sh < Sv ≈ SH, with Sh = minimum horizontal stress and Sv = overburden stress) and transtension (Sh ≈ Sv < SH).

Extensive field work with analysis of kinematic indicators on fracture planes indicates that the direction of SH has not changed significantly in Northern Switzerland since the Late Miocene (Madritsch & Hammer 2012; Fig. 2-6).

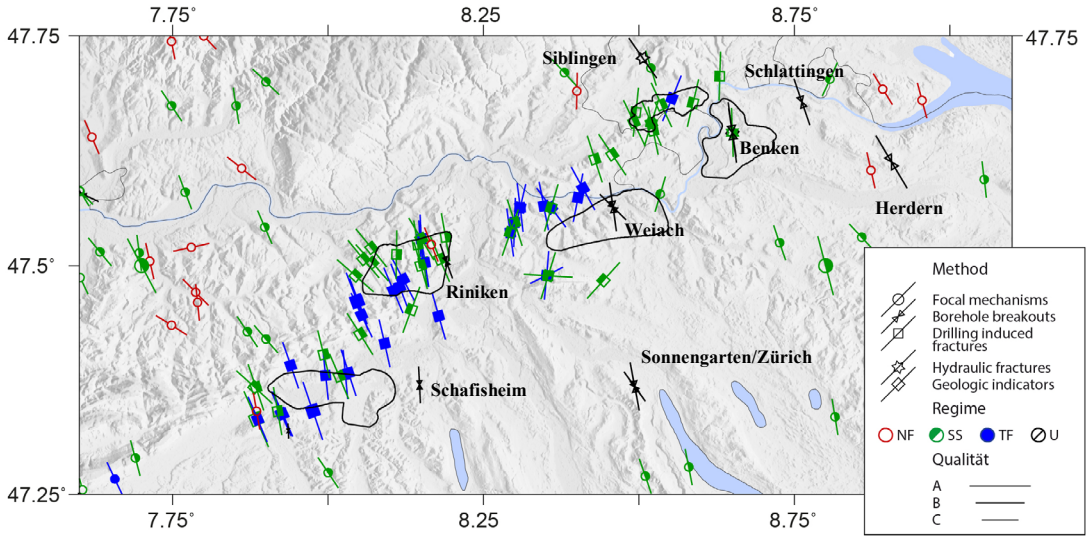

Fig. 2-6: Comparison of in-situ stress with paleo stress data for Northern Switzerland.

Paleo stress data are derived from geological field indicators (slip analysis) and are plotted as squares (from Madritsch & Hammer 2012). All other data represent current in-situ stresses (Heidbach & Reinecker 2013). The bar indicates the direction of SH, and its length the quality of the data (A = best, applies only to current in-situ data). Colours indicate tectonic regime: NF = normal fault, SS = strike slip, TF = thrust, U = unknown.

Further evidence for a relatively stable orientation of SH over geological time scale stems from the fact that SH directions derived from stylolites (e.g. Schafisheim, Beilage 6.28 in Matter et al. 1988; Benken, Chapter 5.3.10.6 in Nagra 2001), and Benken (Nagra 2001) are comparable with current SH orientation derived from borehole breakouts (Heidbach & Reinecker 2013). Stylolites are interpreted to form by dissolution of carbonate at elevated temperature and hence generally deeper burial depths than encountered today in boreholes of Northern Switzerland.

The paleo slip analysis by Madritsch & Hammer (2012) does however indicate an abundance of thrust fault indicators (Sh < Sv < SH) in the paleo stress data, suggesting that the magnitudes of the horizontal stress magnitudes have decreased from compressive to transpressive/transtensive, at least for the siting areas of JS, JO and NL. This is also consistent with the geodynamic concept of active thrusting in the Jura fold-and-thrust belt from Miocene to Pliocene time (e.g. Nagra 2008).

2.3.2.1 Minimum horizontal stress magnitude (Sh)

Sh magnitude values within the Opalinus Clay were constrained from hydraulic fracturing tests in the borehole Benken (Nagra 2001; Fig. 2-7) and yielded values very close to Sv ($K_{Sh/Sv}$ = 0.95) at a depth of approximately 630 m. The same qualitative observation is valid for all other tested formations with elevated clay mineral content (> 35%). In formations with lower clay mineral content, Sh was generally much lower than Sv ($0.6 \leq K_{Sh/Sv} \leq 0.8$) except for two measurements in the upper Malm limestones. Increasing Sh-values with increasing clay mineral content and similar absolute magnitude values of Sh and Sv have also been reported for the Oxfordian to Dogger sequence in the underground lab at Bure, France (Willeveau 2007).

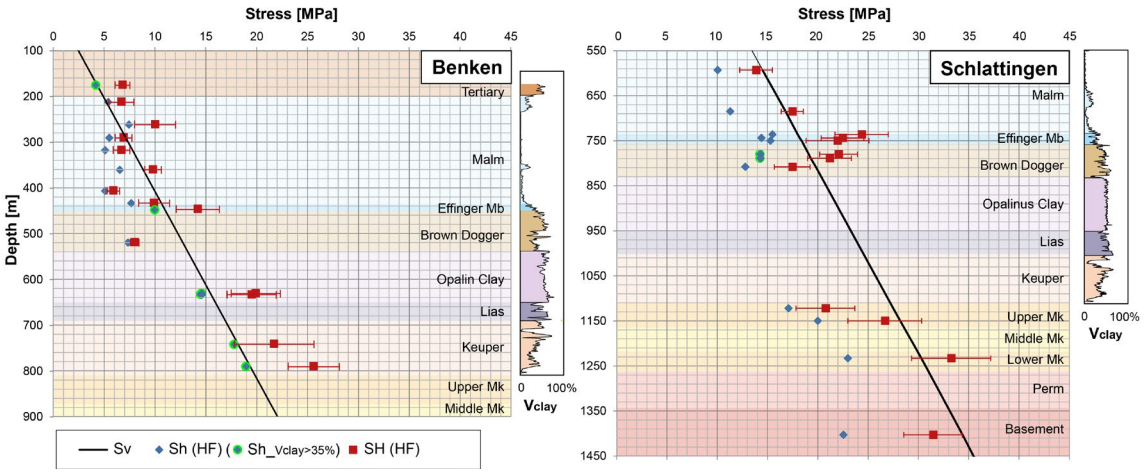

Fig. 2-7: Stress magnitude data from hydraulic fracturing at Benken and Schlattingen.

Black line indicates the overburden stress assuming constant density of 2500 kg/m^3. Highlighted in green are Sh magnitude measurements in formations with more than 35% clay mineral content (V_{clay}, constrained by Albert & Schwab 2013).

More recent magnitude data stem from hydraulic fracture tests at the geothermal borehole of Schlattingen-1 (Klee 2012). All derived Sh values are much smaller than Sv ($0.6 < K_{Sh/Sv} < 0.8$). But in contrast to Benken, formations with elevated clay mineral content (e.g. Tertiary, Opalinus Clay to Keuper) could not be tested in Schlattingen-1, except for two measurements in the upper Dogger. The $K_{Sh/Sv}$ -values from these two measurements were not elevated with respect to other tested intervals ($K_{Sh/Sv} \approx 0.75$).

Minimum horizontal stress values in overconsolidated claystones may also be estimated using semi-empirical relationships from soil mechanics (e.g. Brooker & Ireland 1965). The background for this approach is elucidated in more detail in Appendix C. The method estimates horizontal stress magnitudes during the unloading path (e.g. exhumation) and accounts for the empirical finding that stress ratios are elevated with respect to values at identical depth during initial loading (e.g. burial). Mayne & Kulhawy (1982) suggested that the controlling factors in constraining Sh for the unloading path in overconsolidated claystones are the angle of internal friction and the overconsolidation ratio, two parameters which can be constrained by appropriate geomechanical testing. The calculated horizontal stress magnitude using this "overconsolidation approach" can be assumed to mimic an idealized scenario where horizontal stress is controlled by the present-day overburden stress and the burial stress history only (i.e. *no lateral tectonic loading*). It is therefore considered a lower bound for the Sh magnitude.

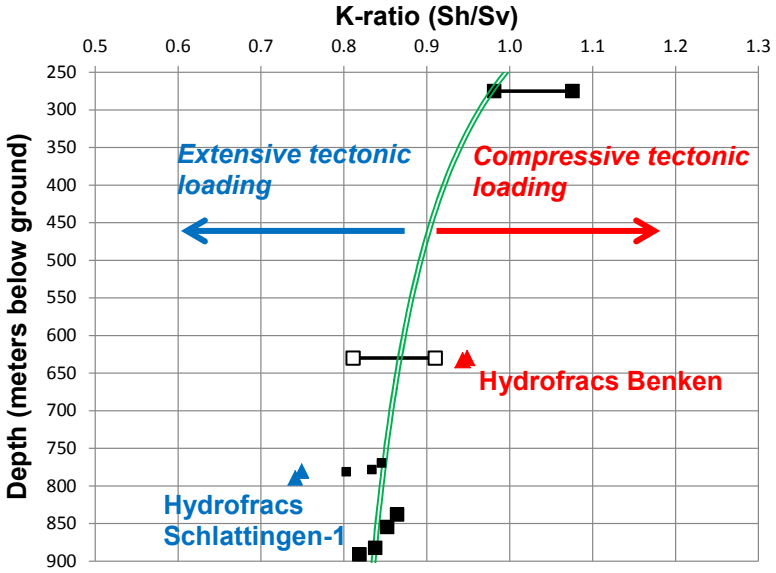

Fig. 2-8: Comparison of Opalinus Clay horizontal to vertical stress ratios between conceptual considerations and measurements by hydraulic fracturing.

Triangles indicate in-situ K-ratios from hydraulic fracturing (red = Benken; blue = Schlattingen-1). Black squares are K-ratios calculated on the basis of Equation C1-1 (App. C) using $\varphi = 25°$ and overconsolidation ratios (Equation 4-1) constrained by oedometer testing[1]. The green line is the regression according to Equation C3-1d (Appendix C) and may be considered as a depth trend of K-ratios *without* lateral tectonic stresses.

[1] Open white squares refer to data from the Benken borehole. Overconsolidation ratio for the Benken samples was not constrained by oedometer testing but a combination of other indicators (Nagra 2002).

Comparison between magnitude data derived by the semi-empirical relationships and hydrofrac data is given in Fig. 2-8. The hydrofrac measurements in Benken are elevated with respect to the overconsolidation approach, which assumes no tectonic loading, suggesting a weak lateral tectonic stress component in Benken. In Schlattingen-1, the hydrofrac data plot slightly below the expected values from the overconsolidation approach. This result is in qualitative agreement that some lateral stress was released in the graben border zone of the Bodensee-Hegau Graben.

Geomechanical, numerical modeling using an elasto-plastic framework indicates that Sh/Sv-ratios are not very sensitive to changes in the applied stress boundary conditions due to the relatively low stiffness of Opalinus Clay with respect to other Mesozoic Formations (Heidbach et al. 2014).

2.3.2.2 Maximum horizontal stress magnitude (SH)

The abundance of regular borehole breakouts in Opalinus Clay, and derived SH-orientations which are consistent with the general trend at a particular location (Heidbach & Reinecker 2013), are in support for a certain differential stress between the Sh and SH magnitudes. SH magnitudes were constrained on the basis of Sh values in the boreholes Benken and Schlattingen-1 (Fig. 2-7). Since the estimation of SH is based on a number of assumptions and further parameter assignments, the errors in evaluating SH magnitudes are considerably larger than for the Sh magnitudes.

Albert (2000) gave further consideration to possible ranges of SH magnitudes in the Opalinus Clay at Benken by taking into account laboratory strength tests. He concluded that a stress ratio SH/Sh between approximately 1.1 and 1.6 is required for breakouts to occur. The reported value of SH/Sh for Benken is approximately 1.35 (Nagra 2001). This value is similar and somewhat greater than the ratio reported for the Callovo-Oxfordian claystone at the underground lab at Bure in France ($1.0 < SH/Sh < 1.2$, Willeveau et al. 2007). Furthermore, the geomechanical-numerical modeling study by Heidbach et al. (2014) again shows that SH ratios are not very sensitive to changes in the applied stress field and therefore lends support that lateral stress ratios similar to those reported in Benken may also be transferable to other siting regions.

Since stress magnitudes are limited by the capacity of a particular material to resist the exerted stresses, an upper bound of SH magnitude values can also be estimated from strength considerations of the Opalinus Clay. Assuming residual bedding plane strength values for the angle of internal friction ($\varphi = 20°$) and cohesion ($C = 0.5$ MPa) the calculated maximum SH/Sh values in the depth range of the proposed repository levels are between 1.7 and 1.8 (cf. Equation 6-6 in Chapter 6.2).

2.4 Pore fluid pressure

Hydraulic head distributions in Opalinus Clay are discussed for the boreholes of Benken, Riniken and Schafisheim in Beauheim (2013). To a first approximation, pore fluid pressure in Opalinus Clay can be considered as hydrostatic.

3 Mineralogy and basic physical properties

3.1 Mineralogy

Clay mineral content of Opalinus Clay is typically of the order of 60 wt.-%. The other three main constituents are quartz (20 wt.-%), calcite (13 wt.-%) and siderite (4 wt.-%), with the latter two variably present as cement (Nagra 2002; Tab. 3-1). With relevance to material behavior, it is noted that expansive (swelling) clays typically account for less than 10 wt.-% of the bulk clay mineral content, but can be as high as 25 wt.-% (cf. illite/smectite alternating layers in Tab. 3-1).

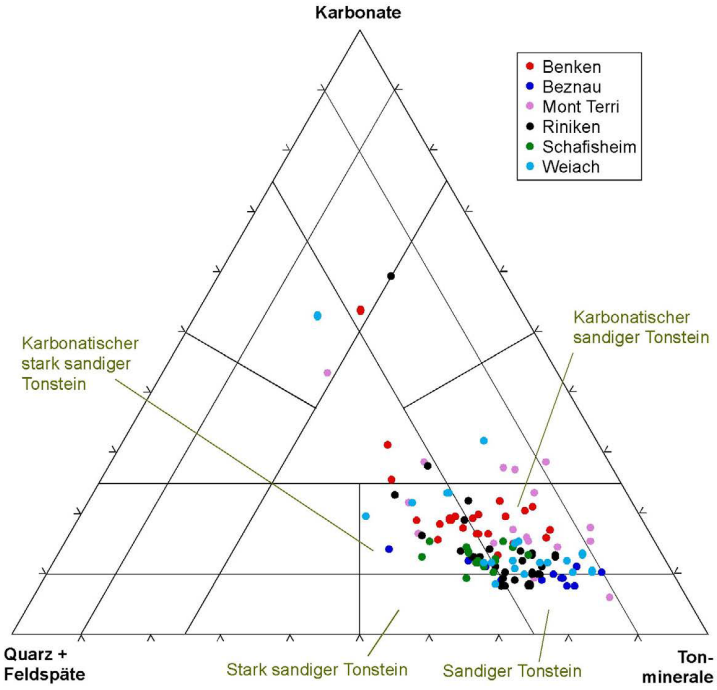

Fig. 3-1: Opalinus Clay mineralogy in the ternary diagram by Füchtbauer.

Plotted are only data from bulk mineral analysis of core samples from the boreholes indicated in the legend. Figure from Mazurek (2011). Cf. Fig. 2-1 for localities.

In a compilation of analyses from core samples and logs of 6 deep boreholes at the URL MT, Traber & Blaser (2013) summarize that the average clay mineral contents at the various sites investigated are fairly homogeneous with values between 54 wt.-% (Benken) and 68 wt.-% (Beznau). At the URL MT the average value is 61 wt.-%. There is a scatter of more than 20 wt.-% at particular sites (Figs. 3-1 and 3-2), however only 5% of all analyzed values resulted in clay mineral contents < 40 wt.-%, and only 5% above 75 wt.-%. Accordingly, the derived reference values with lower and upper bounds (5 and 95 percentile, respectively) are given in Tab. 3-1.

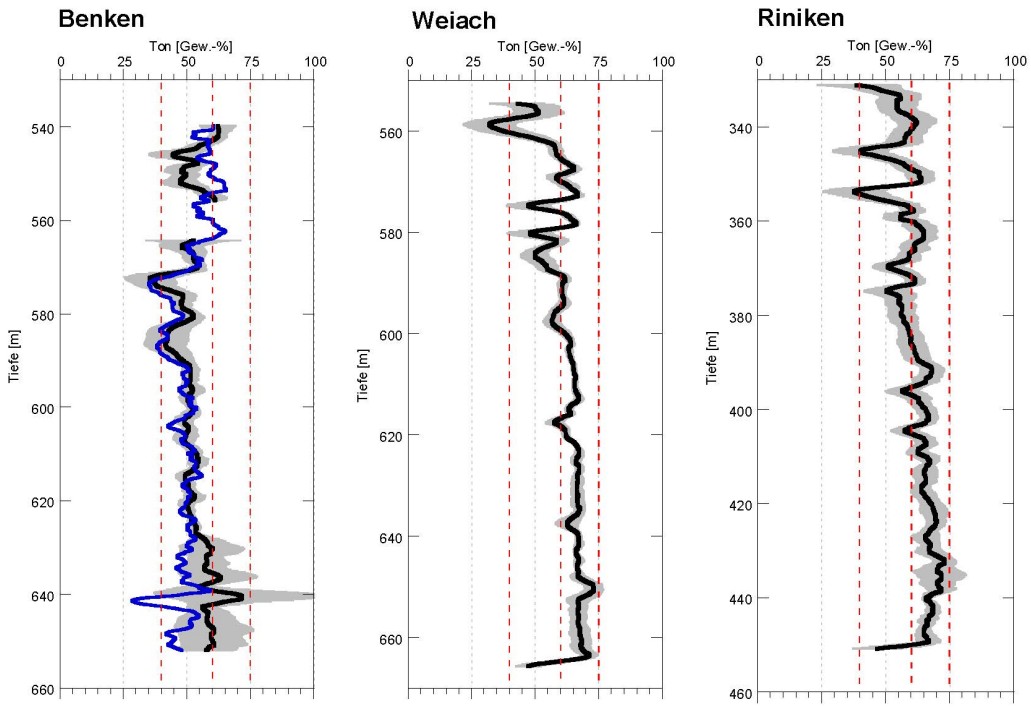

Fig. 3-2: Clay mineral content of Opalinus Clay from boreholes at HLW siting areas.

Calculated from geophysical logs (sonic, electric resistivity and gamma ray) calibrated on core data (from Albert & Schwab 2013). Black lines = median value, dashed red lines = reference values with upper and lower bounds, grey area = standard deviation based on three logs. Blue line = elemental capture spectroscopy (ECS log), which is only available for the Benken borehole. Figures adapted from Traber & Blaser (2013).

Tab. 3-1: Reference mineralogy for Opalinus Clay.

According to Traber & Blaser (2013).

	Reference value	Lower bound	Upper bound
Bulk mineralogy [wt.-%]			
Clay minerals	60	40	75
Quartz	20	10	30
Calcite	13	5	35
Orthoclase	2	0	5
Plagioclase	0.9	0	2
Dolomite + ankerite	0.4	0	2
Siderite	4	0	15
Anhydrite	0	0	0
Gipsum	0	0	0
Pyrite	1	0.3	3
Sum	101.3		
Clay mineralogy [wt.%]			
Illite	24	15	35
Ill/Sm alternating layers	9	4	25
Smectite	0	0	0
Kaolinite	18	10	30
Chlorite	9	2	15
Chl-Sm alternating layers	0	0	0
Sum	60	-	-

3.2 Density and water content

Bulk density: $\rho = \frac{m}{V}$, with m and V = mass and volume of bulk sample.

In a compilation of 574 samples from the URL MT, Bock (2009) reports a mean value of ρ = 2.43 ± 0.02 g/cm^3. At Benken, 281 analyses yielded a mean value ρ = 2.52 ± 0.03 (Nagra 2002). Analyses from the borehole of Schlattingen-1 are within the standard deviation of the values from Benken (Favero et al. 2013; Traber & Blaser 2013).

Water content: $w = \frac{m_w}{m_s} \times 100$, with m_w = mass of free water, m_s = mass of solids.

The water content is generally constrained by the oven drying method at a temperature of 105°C, with duration of at least 24 hours. For the URL MT, Bock (2009) reports an average value of 6.4 ± 1% (n = 367). Rummel & Weber (1999) state average w = 4.5 ± 0.8% (n = 36) for cores from Benken. Similar values are reported for samples from the Schlattingen-1 borehole by Gesteinslabor Jahns (2013) with w = 4.4 ± 0.3% (n = 33), and somewhat lower values by Favero et al. (2013) with w = 3.9 ± 0.7% (n = 5), although with a smaller sample size.

Dry density: $\rho_d = \frac{m_s}{V}$

Dry density is generally calculated from bulk density and water content ($\rho_d = \rho/(1+w)$), although other methods were used in the past (cf. Mazurek 2011, for details). A compilation of 6 boreholes and the URL MT yields a median value of 2.41 g/cm^3 (Tab. 3-2). For the URL MT, Bock (2009) suggests an average of ρ_d = 2.33 ± 0.05 g/cm^3 (n = 56). An average value of ρ_d = 2.43 ± 0.06 g/cm^3 (n = 8) was constrained for samples of the Benken borehole (Nagra 2002), and ρ_d = 2.46 ± 0.04 g/cm^3 (n = 38) for Schlattingen-1 (Gesteinslabor Jahns 2013).

Grain density: $\rho_s = \frac{m_s}{V_s}$, with V_s= volume of solids.

Specific gravity: $G_s = \frac{\rho_s}{\rho_w}$, with ρ_w= density of water

Grain density relates to density of all solids and is measured in pulverized and dried material in a pycnometer. A value of ρ_s = 2.71 g/cm3 is the suggested reference value according to Traber & Blaser (2013) (Tab. 3-2). Bock (2009) states ρ_s = 2.70 ± 0.02 g/cm^3 (n = 67), whereas a value of ρ_s = 2.72 ± 0.01 g/cm^3 was constrained for samples from Benken (n = 8; Nagra 2002).

Tab. 3-2: Opalinus Clay reference porosity and density with upper and lower bounds.
Figure adapted from Traber & Blaser (2013).

Physical porosity Vol.-%		Grain density g/cm^3	Calculated dry density ρ_d g/cm^3		Statistics (incl. FMT)
Lower bound	6.0	2.71	**2.55**	**Upper bound**	2.53 (P95)
Reference value	11.0	2.71	**2.41**	**Reference value**	2.41 (Median)
Upper bound	17.0	2.71	**2.25**	**Lower bound**	2.30 (P5)

3.3 Porosity and void ratio

Physical porosity: $\phi = \left(1 - \left[\frac{\rho_d}{\rho_s}\right]\right) \times 100$

Void ratio: $e = \frac{\phi/100}{1-\phi/100}$

Specific volume: $v = 1 + e$

Average porosity values from samples of boreholes and the URL MT are between 8 and 16% (Tab. 3-3). Despite significant scatter at individual locations, porosity correlates broadly with present burial depth (Fig. 3-3). However, the correlation may also reflect the result of different burial paths in geological history. According to basin modelling (Nagra 2002), maximum burial depth of Opalinus Clay in the boreholes of Benken, Riniken and Weiach was comparable and reached a maximum of approximately 1500 – 1700 m in late Tertiary. In the Schafisheim borehole, maximum burial depth probably exceeded 2000 m. At the URL MT, maximum burial depth is inferred to have been reached at an earlier stage (late Cretaceous) with lower absolute burial (1350 m) compared to cores from boreholes in Northern Switzerland (Nagra 2002).

It is also emphasized that the specified values for porosity are determined in the laboratory after extraction of cores from greater depth and after unloading from in-situ conditions.

Tab. 3-3: Opalinus Clay porosity values from borehole samples and the URL MT.

Abbreviations relate to borehole location from which samples were analyzed:
BEN = Benken, WEI = Weiach, BEZ = Beznau, RIN = Riniken, SHA = Schafisheim,
FMT = URL MT. Figure adapted from Traber & Blaser (2013).

	N total	Mean	Standard Deviation	Minimum	1. Quartile	Median	3. Quartile	Maximum	P5	P95
Alle Daten	65	10.9	2.9	3.5	8.8	10.9	12.5	17.0	6.3	16.1
BEN	10	10.8	1.7	7.4	10.0	11.1	12.4	13.1	7.4	13.1
WEI	15	9.0	2.7	3.5	8.0	9.4	11.2	12.6	3.5	12.6
BEZ	12	12.6	1.5	10.4	11.6	12.5	14.0	14.7	10.4	14.7
RIN	12	10.4	1.2	7.6	10.1	10.4	11.2	11.7	7.6	11.7
SHA	8	7.9	1.5	5.8	6.8	8.0	8.9	10.1	5.8	10.1
FMT	8	15.9	1.0	14.0	15.4	16.0	16.5	17.0	14.0	17.0

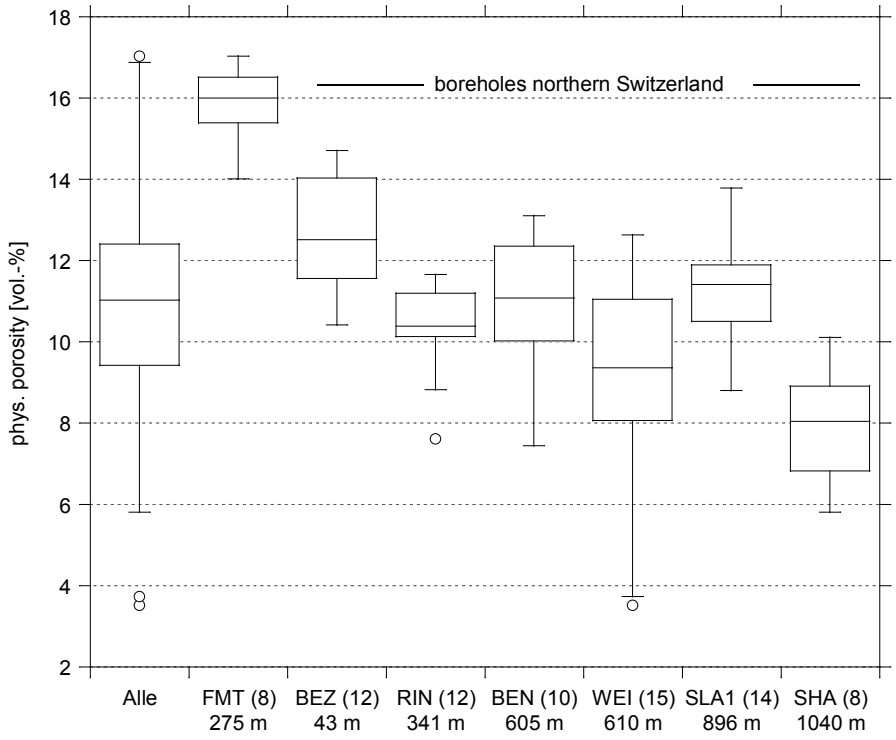

Fig. 3-3: Opalinus Clay porosity as function of current burial depth below ground.

Boxes indicate first, second (median) and third quartile, and whiskers comprise 5th and 95th percentile. Number in brackets indicate quantities of analyzed samples (from Traber & Blaser 2013). Second row indicates average depth of Opalinus Clay at particular locality (c.f. Fig. 2-1).

3.4 Geotechnical characterization

3.4.1 Grain size distribution

Grain size analysis was conducted by sedimentation analysis for samples from the URL MT (Ferrari et al. 2009; Minon et al. 2010; Schanz et al., unpublished) and Schlattingen-1 (Ferrari et al. 2012) (Fig. 3-4). Silt fraction accounts typically for 50 – 60% of the grain fraction, followed by clay (20 – 40%) and sand (5 – 20%). The highest clay fraction (40%) from URL MT samples stem from a fault gouge analysis by Ferrari et al. (2009) and are indicated by open circles in Fig. 3-4. Aristorenas (1992) reports clay fractions from two boreholes in the vicinity of Diepflingen (cf. Fig. 2-1), which are comparable to the clay fractions from the URL MT. Grain size distributions were also reported for one sample of the shallow Bözberg borehole (Nüesch 1991). The clay fraction in this sample was exceptionally high (> 50%) and the distribution generally similar to the fault gouge sample from the URL MT by Ferrari et al. (2009). In this context it is noted that the Bözberg borehole sampled Opalinus Clay from a highly tectonized zone (Figure 2 in Nüesch 1991).

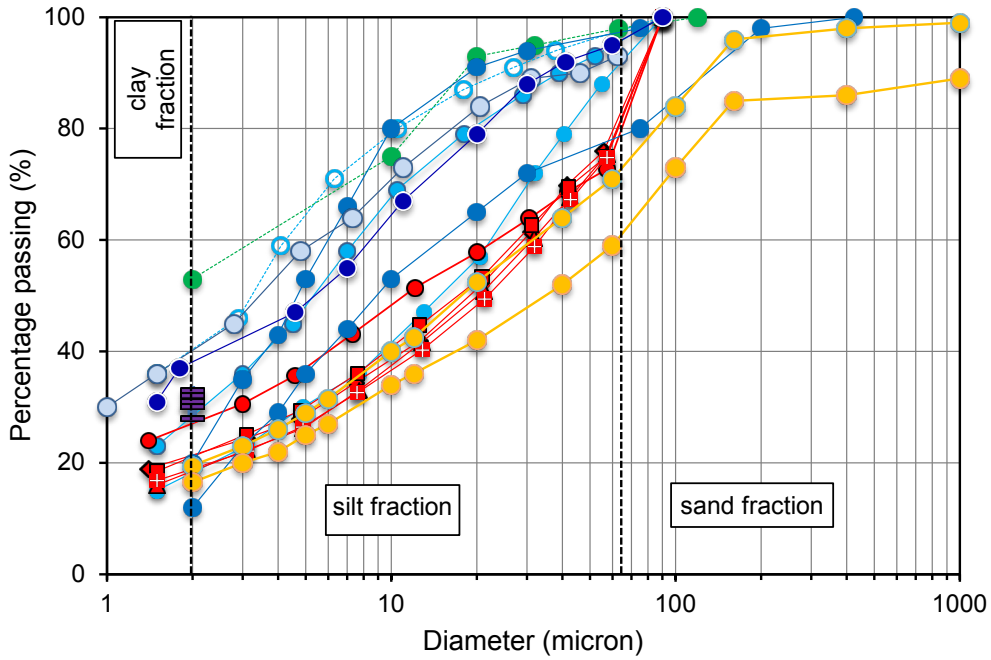

Fig. 3-4: Grain size distribution of Opalinus Clay.

Blue symbols represent results from the URL MT (Ferrari et al. 2009; Ferrari et al. 2012b; Minon et al. 2010; Schanz et al., unpublished), green symbols from Bözberg (Nüesch 1991), orange symbols from Gächlingen (Büchi & Müller AG 1988), red symbols from Schlattingen-1 (Ferrari et al. 2012a). Also indicated in purple are clay fractions for samples of borehole near Diepflingen (Aristorenas 1992). Open symbols are from fault gouge samples.

3.4.2 Atterberg limits

Plasticity Index: $PI = w_L - w_P$, with w_L= water content at liquid limit

and w_P= water content at plastic limit

The plasticity chart in Fig. 3-5 summarises w_L vs. PI results of Opalinus Clay samples from URL MT (Ferrari et al. 2012; Olalla et al. 1999; Schanz et al., unpublished data), Schlattingen (Ferrari et al. 2012) and from Diepflingen (Aristorenas 1992). The data plot broadly along the A-line, which separates clayey from silty soils based on the unified soil classifications system. The reported values for w_L and PI range between approximately 30 to 50% and approximately 10 to 25%, respectively. According to SN 670 004-2a, the samples classify predominantly as lean clay with sand, with minor silty clay with sand or silt with sand.

Activity: $A = \frac{PI}{CF}$, with CF= clay size fraction (< 2 µm)

Activity can be calculated for the data points shown in Fig. 3-4 in the range of $30 < w_L < 40\%$, yielding values between 0.30 and 0.76. Data from Büchi & Müller AG (1988) with w_L of approximately 40 yield activity values of 0.8 to 1.1. The data with higher PI values in the range of $40 < w_L < 50\%$, are from Olalla et al. (1999) and grain size distributions are not reported. Clays with $A < 0.75$ are generally classified as "inactive", values $0.75 < A < 1.25$ as "normal" and $A > 1.25$ as "active" (e.g. Holtz et al. 2011).

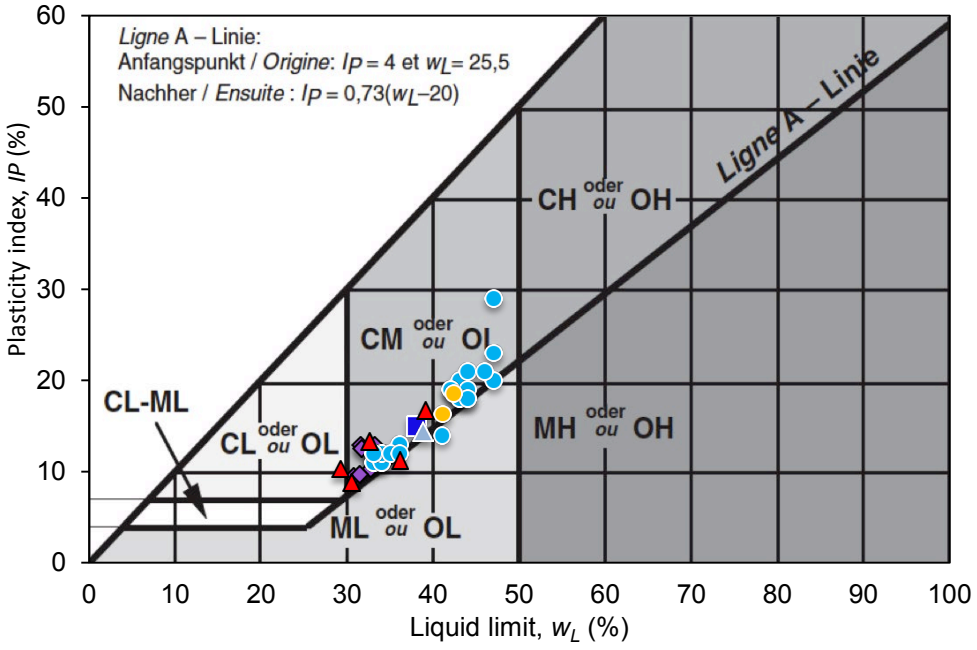

Fig. 3-5: Plasticity chart for Opalinus Clay samples.

Blue symbols represent results from the URL MT (Ferrari et al. 2012b; Olalla et al. 1999; Schanz & Al-Badran. 2011), purple symbols from Diepflingen (Aristorenas 1992), red symbols from Schlattingen-1 (Ferrari et al. 2012a) and orange symbols from Gächlingen (Büchi & Müller AG 1988).

4 Deformation and strength behavior

4.1 Convention of sample orientation in deformation tests

Test sample configuration in this report refers to the angle of the dominant sample fabric ('bedding') with respect to the cylinder sample axis (Fig. 4-1). In all mechanical tests but tensile strength tests, the loading direction is parallel to the sample axis. In tensile strength tests, samples are prepared as P-samples and loading direction is perpendicular to sample axis, but can be either parallel (P-orientation) or perpendicular (S-orientation) to bedding. The one-dimensional compression or consolidation tests (Chapter 4.2), all presented results were obtained in S-configuration.

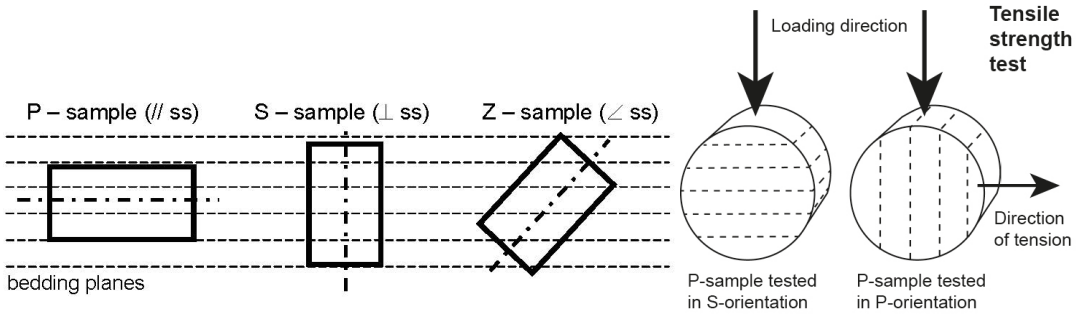

Fig. 4-1: Convention of sample orientation.

Left: Dot-pointed line indicates sample long axis, which is at an angle of 0° for P-samples, 30° for X-samples (not shown), 45° for Z-samples and 90° for S-samples. Figure from Bock (2009). Right: sample convention in tensile strength tests. Note that both samples are prepared as P-*samples*, but that tests can be conducted in both P- and S-*orientation*. Mechanical results in this report always refer to test orientation (distinction only relevant for tensile strength tests).

4.2 Consolidation and swelling behavior

4.2.1 Compressibility during one-dimensional consolidation

The volumetric behaviour upon applied stress can be studied ideally in one-dimensional compression or consolidation tests. In a typical test of an overconsolidated claystone, loading increments are first approximately log-linear with void ratio e (or vertical strain ε_v) and define the initial loading line (ILL, Fig. 4-2). With increasing effective vertical stress (σ_v'), the slope of the curve fit between stress increments increases. This change in slope is interpreted to reflect an irreversible compaction by particle re-arrangement (e.g. Holtz 2011) as the applied effective stress becomes greater than the stresses previously experienced by the sample. When the slope of the steeper curve is again approximately linear in semilogarithmic space consolidation occurs along the normal consolidation line (NCL). When the load increments are reversed the sample expands again (void ratio increases) along the unload-reload line (URL). This leads to the following definitions (cf. Fig. 4-2):

Compression index: $C_c = -\Delta e/\Delta \log \sigma_v'$ [-], slope of the NCL recorded during loading

Swelling index: $C_s = -\Delta e/\Delta \log \sigma_v'$ [-], slope of the URL recorded during unloading

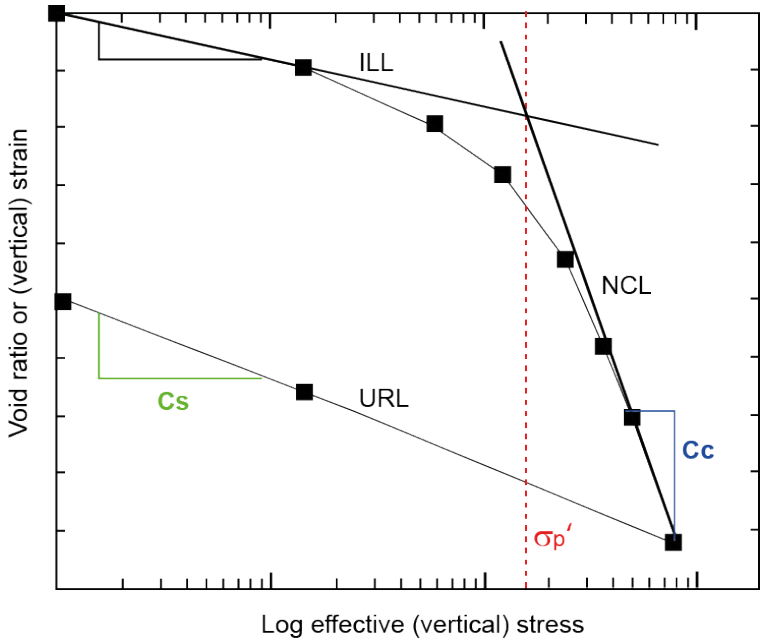

Fig. 4-2: Schematic of oedometric curve with interpreted parameters.

Different loading stages: ILL = initial loading line, NCL = normal consolidation line, URL = unloading-reloading line. The preconsolidation stress (σ_p') can be estimated by intersection of the ILL with the NCL (chap. 4.2.2). Cc = compression index, Cs = s welling index.

Compression and swelling index are sometimes derived from the natural logarithm of the effective stress and expressed as λ (= Cc/ln(10)) and κ (= Cs/ln(10)).

There is considerable scatter in the Cc and Cs values reported from the URL MT. Chiffoleau & Robinet (1999) specify $0.07 < Cc < 0.09$ and $0.007 < Cs < 0.013$ after consolidating to a maximum stress of 60 MPa, and they also demonstrate that the values in three tests correlate positively with an increase in relative humidity.Ferrari et al. (2012) and Minon et al. (2010) find much smaller values for Cc (0.03 to 0.04) but similar values for Cs (around 0.01) after consolidation to 25 and 50 MPa, respectively. Péron et al. (2009) specify Cc of 0.09 and Cs of 0.005. In an attempt to correct the effective stress values by considering saturation state before and after consolidation, they conclude that the effective values are much higher with Cc = 0.134 and Cs = 0.019.

For the Schlattingen cores Ferrari et al. (2012) found $0.02 < Cc < 0.04$ in four tested samples. Contrary to expectations, the Cs values increased when consolidated to progressively higher stresses in unload-reload loops. The authors attributed this observation to the formation of micro-fractures during the loading phase.

One-dimensional consolidation tests were not conducted on core samples from Benken. However, Horseman & Harrington (2002) conducted a very long-term (6 months) permeameter test, from which they could deduce a Cs value of 0.017 (κ = 0.0075).

4.2.2 Overconsolidation ratio from preconsolidation stress

The preconsolidation stress (σ_p') represents the maximum effective vertical stress the sample has experienced in its geological history. As indicated in Fig. 4-2 the preconsolidation stress can be estimated from one-dimensional compression by intersecting the ILL and the NCL line. In the absence of significant lateral tectonic stresses, elevated pore pressures or chemical alterations, the maximum vertical effective stress is then also a measure of the maximum burial depth in the geological history. The overconsolidation ratio can therefore be defined as (e.g. Azizi 2000):

$$OCR = 1 + \frac{z_1}{z} \approx \frac{\sigma_p'}{\sigma_v'} \quad (4\text{-}1)$$

where z_1 is the maximum burial depth and z is the present burial depth. Apart from one-dimensional compression tests the maximum burial depth can also be estimated from temperature data or quantification of eroded strata. The results of the different techniques are summarized in Tab. 4-1.

It is noted that maximum burial depth of Opalinus Clay at the URL MT is poorly constrained (Nagra 2002), and that lateral tectonic stresses were definitely significant in the recent geological history of the area. With the current average depth of approximately 275 m, the overconsolidation ratio (OCR) of Opalinus Clay at the URL MT is greater (OCR ≈ 3 – 5) than in samples from Northern Switzerland (OCR ≈ 1.5 – 3) with the exception of samples from the Riniken borehole (OCR ≈ 4).

Tab. 4-1: Compilation of overconsolidation ratios (OCR) from selected locations.

[a] Maximum burial depths from basin modelling (Nagra 2002). Present effective burial depth calculated assuming an effective stress gradient of 0.015 MPa/m. [b] Maximum effective burial stress determined from Oedometer tests. For URL MT: Chiffoleau & Robinet (1999), Horseman et al. (2006), and Minon et al. (2010); for Schlattingen-1: Ferrari et al. (2012). [c] Assuming z_1 of Schlattingen-1 equal to Benken given the proximity of the two locations.

Location	Max. burial depth[a] (z_1)	Present burial depth (z)	OCR (depth)	Max. effective burial stress in past[b] (σ_p')	Present effective burial stress[a] (σ_v')	OCR (stress)
	[m]	[m]	[-]	[MPa]	[MPa]	[-]
URL MT	1350	275	4.9	17 ± 5	4.0	3.0-4.9
Riniken	1550	390	4.0		5.7	
Weiach	1700	610	2.8		9.0	
Benken	1650	605	2.7		8.9	
Schafisheim	2150	1040	2.1		15.3	
Schlattingen-1	1650[c]	890	1.9	24 ± 2	13.1	1.5-1.8

4.2.3 Time-dependent settlement (consolidation and creep)

The vertical strain associated with each vertical stress increment during one-dimensional compression as plotted in Figure 4-2 relate to the recorded *primary settlement*. During consolidation, excess pore water pressure generated by the volume reduction during loading is dissipated by water outflow. The rate at which water pressures can dissipate in clays and shales is controlled by the low values of intrinsic permeability. The *coefficient of vertical consolidation (c_v)* captures the time-dependent primary settlement. Results from high-pressure oedometric tests with cores from Schlattingen-1 are given in Figure 4-3.

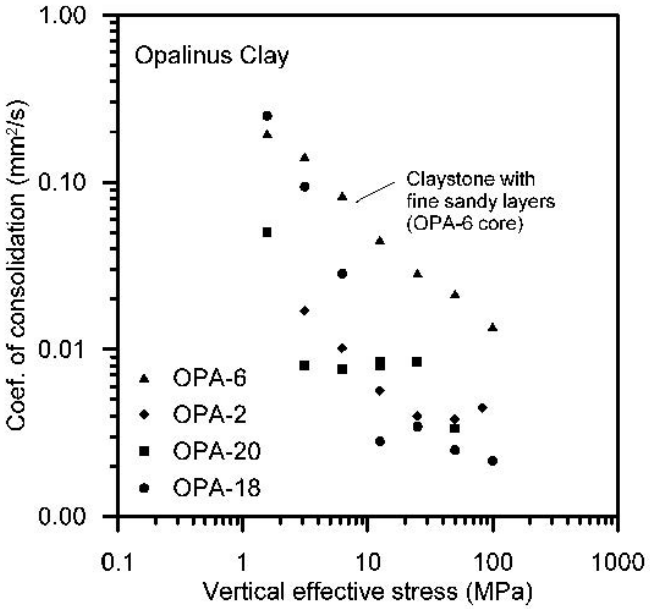

Fig. 4-3: Coefficient of consolidation versus vertical effective stress for samples from Schlattingen-1.

Loading of samples is vertical to bedding (S-configuration). From Ferrari et al. (2012).

Secondary settlement is the continuation of volume change that started during (primary) consolidation, but it takes places at a constant effective stress. Hence after essentially all the excess pore pressure has dissipated.

Secondary compression index: $C_\alpha = \Delta e / \Delta \log t$ [-]

The secondary compression is also known as the *creep* component of settlement (e.g. Azizi 2000), and its rate is much smaller compared to primary consolidation. In the one-dimensional compression tests conducted to constrain the compression index Cc, the total settlement is usually corrected for the secondary compression. For example, in four tested samples from Schlattingen by Ferrari et al. (2012) maximum values of $C_\alpha \approx 0.001$ can be deduced (personal communication by V. Favero, EPFL). However, these values must be considered with caution, as the tests from which the values were derived were not designed to investigate the long-term settlement. Yet the data is in good agreement with literature data. Terzaghi et al. (1996) specify typical ratios of C_α/Cc of 0.03 ± 0.01 for shales and mudstones.

Using C_α = 0.001 and 0.02 < Cc < 0.04 for the Schlattingen-1 samples (according to Ferrari et al. 2012) yields C_α/Cc ratios of 0.025 to 0.05.

4.2.4 Swelling parameters

Swelling strain (heave): $S_\varepsilon = \left(\frac{d}{L}\right) \times 100$ [%],

where d = maximum displacement in free swelling tests and L = initial sample thickness before swelling. Swelling strain or heave is measured in free swelling tests until an asymptotic value is reached, typically over 5 to 10 days.

Swelling pressure (p_s) is measured in constrained swelling tests.

Vögtli & Bossart (1998) report 0.4 < p_s < 0.6 MPa and S_ε of 3 to 9% in S-orientation (perpendicular to bedding), and approximately 0.1 MPa pressure and up to 3% heave in P-orientation for URL MT samples. More recent tests by Ferrari et al. (2009) with URL MT samples in S-orientation roughly confirmed these findings with $S_\varepsilon \approx 10\%$ and p_s of 0.5 to 0.6 MPa.

Mathier et al. (1999) evaluated the swelling parameters of Benken samples published in Nagra (2002). They found swelling pressures in the range 0.8 < p_s < 1.4 MPa with 1.4 < S_ε < 7.5% in S-orientation, and p_s of approximately 0.1 - 0.2 MPa and 0.7 < S_ε < 4.7% in P-orientation. Ferrari et al. (2012) again found slightly higher heave values (S_ε = 11%) but confirmed 0.9 < p_s < 1.4 MPa in three tests with cores from Schlattingen-1.

Figure 4-4[2] summarizes the swelling pressures of the different data sources from URL MT and Benken (BEN) and Schlattingen-1 (SLA-1). It illustrates the clear anisotropy of swelling pressure between samples of P- and S-orientation. In addition, a weak negative correlation can be deduced between swelling pressure and water content for samples in S-orientation.

[2] Test compilation (incl. depth of samples) can be found in the electronic data file *3_Swelling.xlsx*

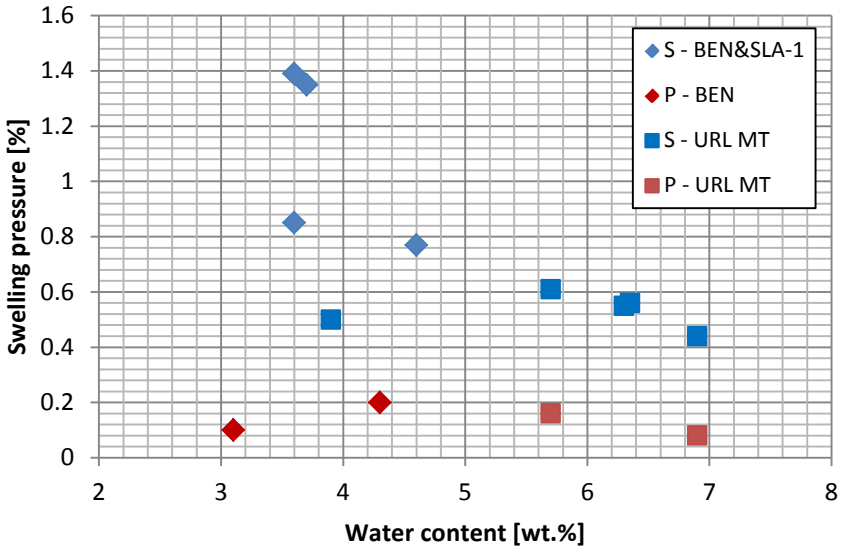

Fig. 4-4: Swelling pressures as a function of water content.

Data source: Benken tests = Mathier et al. (1999), Schlattingen-1 = Ferrari et al. (2012), URL MT = Vögtli and Bossart (1998) and Ferrari et al. (2009).

4.3 Static elastic moduli and Poisson's ratio

Static Young's modulus (E) and static Poisson's ratio (υ) are measured from uniaxial loading. E is derived by the slope of the axial stress versus axial strain curve, υ by the slope of lateral strain versus axial strain. Other elastic moduli (bulk modulus, shear modulus) may be computed using these two values under the assumption that the theory of elasticity for homogeneous, isotropic material is valid.

The most straightforward evaluation of E and υ is by unconfined compressive strength (UCS) tests. Problematic with deriving these values from UCS tests is that the test boundary conditions for very-low permeability samples such as the Opalinus Clay are poorly defined. Due to the generally fast, imposed strain rate (typically 10^{-5} s^{-1}) and the low intrinsic permeability, the test may essentially be considered as undrained. However, undrained conditions imply perfect fluid saturation and constant volume during deformation, two attributes that are not met in UCS tests. The derived values should therefore be considered with care.

In triaxial testing, E can be determined only if the confining pressure is held constant in the relevant test interval (generally met), and υ if the test is conducted under drained conditions (generally not met). All the triaxial test results presented below can be considered undrained, that is with pore fluid disconnected from the reservoir supply. This means that all E-Moduli relate to *undrained* (E_u) values, and measurements of Poisson's ratio are considered unreliable since the values should approach 0.5 under perfectly undrained conditions.

Important is further the distinction between E values determined on the primary loading path at 50% of peak strength ($E_{t\text{-}50}$), and the more common procedure of measuring E on an unloading-reloading path (E_{UR}) at approximately 30 – 70% of peak strength (Fig. 4-5). The latter tends to stiffer values (steeper slope of the stress-strain curve).

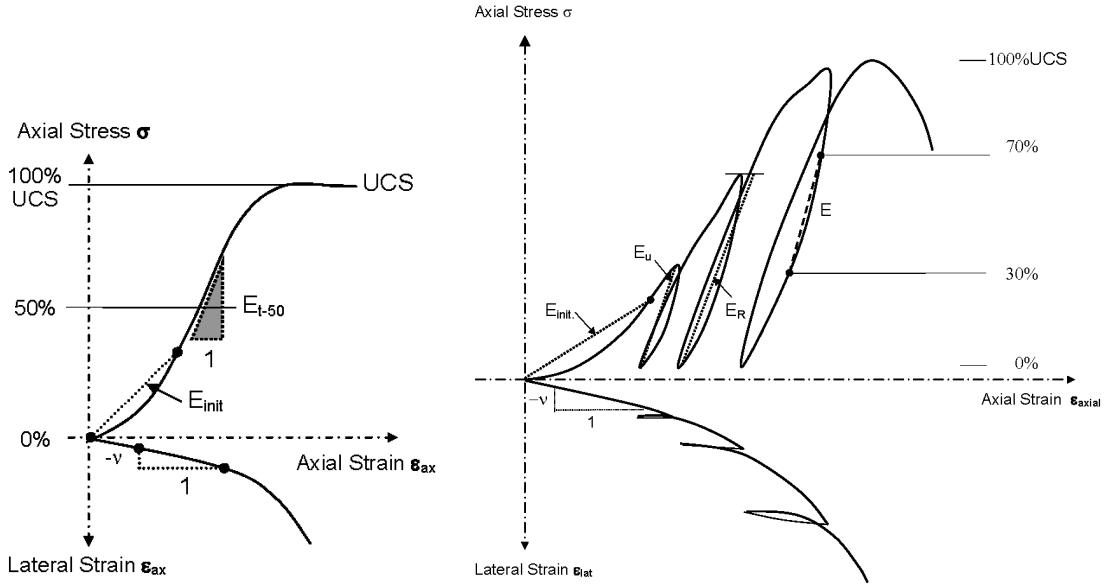

Fig. 4-5: Non-cyclic (left) versus cyclic test (right).

E_{init} = first-loading Modulus, E_{t-50} = tangent modulus at 50% UCS, E_U = unloading modulus, E_R = reloading modulus, E = Youngs's modulus. Note $E_U \approx E_R \approx E_{UR}$ (unload-reload cycle. From Bock (2009).

In one-dimensional oedometer tests, the oedometric modulus (E_{oed}) can be calculated by the following relationship (e.g. Lambé & Whitman 1979):

$$E_{Oed} = -\Delta\sigma_v'/\Delta\varepsilon_v \tag{4-2}$$

where $\Delta\sigma_v'$ and $\Delta\varepsilon_v$ are increments in vertical effiective stress and vertical strain, respectively.

Since oedometer testing is generally conducted under drained conditions, the drained E-Moduli (E_d) can be related to E_{oed} through the Poisson's ratio υ (e.g. Favero et al. 2013):

$$E_d = E_{oed}\frac{(1+\upsilon)(1-2\upsilon)}{(1-\upsilon)} \tag{4-3}$$

A summary of the types of different E-moduli measured in the various tests is given in Tab. 4-2.

Tab. 4-2: Types of E-moduli derived in drained and undrained tests.

* Since Oedometer tests are conducted under laterally fixed boundaries, E_d is not directly measured but calculated from the oedometric modulus E_{oed} in the loading-unloading loop according to Equations 4-2 and 4-3. Note that the static Poisson's ratio υ needs to be constrained in separate geomechanical tests.

Type of Test	Direct loading to peak (t-50)	Unload-reload interval (UR)
Drained test *(Permeameter, Oedometer)*	$E_{d\_t\text{-}50}$	E_{d_UR}*
Undrained test *(Triaxial)*	$E_{u\_t\text{-}50}$	E_{u_UR}
'Pseudo-undrained' test *(Unconfined compressive strength)*	$E_{UCS\_t\text{-}50}$	E_{UCS_UR}

It is emphasized that unsaturated conditions (i.e. development of suction) can affect measured E-moduli (Fig. 4-6). This qualitative observation is of particular importance when comparing E-moduli measured in testing devices without fluid saturation control (UCS) with those measured in configurations where sample saturation can be achieved prior to testing (triaxial tests with fluid backpressure).

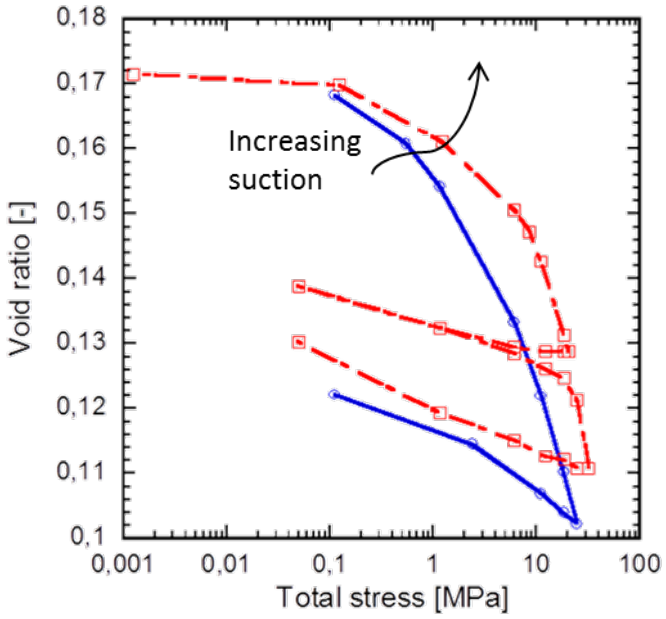

Fig. 4-6: Influence of suction on sample stiffness in Oedometer tests.

Tests on samples of URL MT. Blue line = consolidation at zero suction, red line = consolidation at -20 MPa suction. Figure from Favero et al. (2013).

A compilation of E-Moduli from samples of the URL MT is given in Fig. 4-7. The undrained E-values are average values from triaxial testing for a particular stress interval using a larger number of samples, as compiled by Bock (2009)[3]. Undrained E-Moduli constrained in unloading-reloading loops (green circles in Fig. 4-7) indicate a positive correlation with stress, and a clear anisotropy between values in P- and S-orientation (Eu_p/ Eu_s ≈ 2:1) at a particular effective confining stress (σ_3'). Values from UCS tests are higher than expected if the trend of the undrained tests was projected to $\sigma_3' = 0$. This observation is in qualitative agreement with results from Fig. 4-6, since fluid saturation cannot be established and maintained during UCS testing. It is also in good agreement with observations by Wild et al. (2014) who demonstrate a strong dependence of stiffness values on suction.

$E_{u\_t\text{-}50}$ values (striped filling pattern) are lower and do not show a stress dependency. E_d values (open circles) were constrained from oedometer tests (all samples in S-orientation) of three different studies and using Equations (4-2) and (4-3). Effective confining stresses for these tests were calculated from measured effective vertical stresses σ_v' using Equation C1-1 (see Appendix C), assuming $\varphi = 25°$ and OCR calculated from the maximum value of σ_v' during the test prior to unloading. It is noted that for all results of E_d-values in Fig. 4-7 (below) the maximum effective stress reached during the oedometer tests prior to unloading was greater than the interpreted maximum effective burial stress. E_d-values also exhibit a positive stress dependency with absolute values reaching approximately 50% of the undrained values.

The qualitative observations from E-values of URL MT samples are also reflected in the samples from Benken and Schlattingen-1 (Fig. 4-8): a positive stress-dependency in undrained E-moduli (blue filled circles) with anisotropy of the order of Eu_p/Eu_s ≈ 2:1, elevated values from UCS tests with respect to projected values at $\sigma_3' = 0$ considering the Eu_UR results, no stress dependency in Et-50 values, positive stress dependency of drained tests (blue open circles) with absolute values approximately 50% of the undrained values. The results of the drained oedometer tests in Schlattingen-1 were taken from the summary by Favero et al. (2013).

The undrained E-moduli from triaxial testing are summarized for Mont Terri and Schlattingen-1 with respect to loading orientation in Figure 4-9.

In the absence of drained triaxial test results, Poisson ratios may be estimated from UCS tests. Lack of effective stress control in UCS tests will also affect the recorded Poisson's Ratio, but it appears that this parameter is not very sensitive to the effect of suction (e.g. Wild et al. 2014). Bock (2009) recommends values of 0.35 and 0.25 for P- and S-orientation as representative at the URL MT. For Benken core samples, UCS tests yield median values of $\upsilon = 0.21$ (n = 5) in P-orientation and $\upsilon = 0.31$ (n = 3) in S-orientation (Mathier et al. 1999)[4]. More recent data from Schlattingen-1 show good agreement with Benken samples in P-orientation with average $\upsilon = 0.22$ (n = 3), but strong discrepancy in S-orientation with $\upsilon = 0.10$ (n = 3) (Gesteinslabor Jahns 2013).

In Nagra (2002), the reference value for the Poisson ratio was given as $\upsilon = 0.27$ for both P- and S-orientation. This value is also identical to the dynamic Poisson ratio calculated from ultrasonic measurements (Nagra 2002).

---

[3] Only values from the review period 2000 to 2009 are considered, as values prior to that were considered 'unreliable' by Bock (2009) – cf. his Table 4-3.

[4] See Data file *5_Poisson ratio.xlsx* (Appendix D) for details.

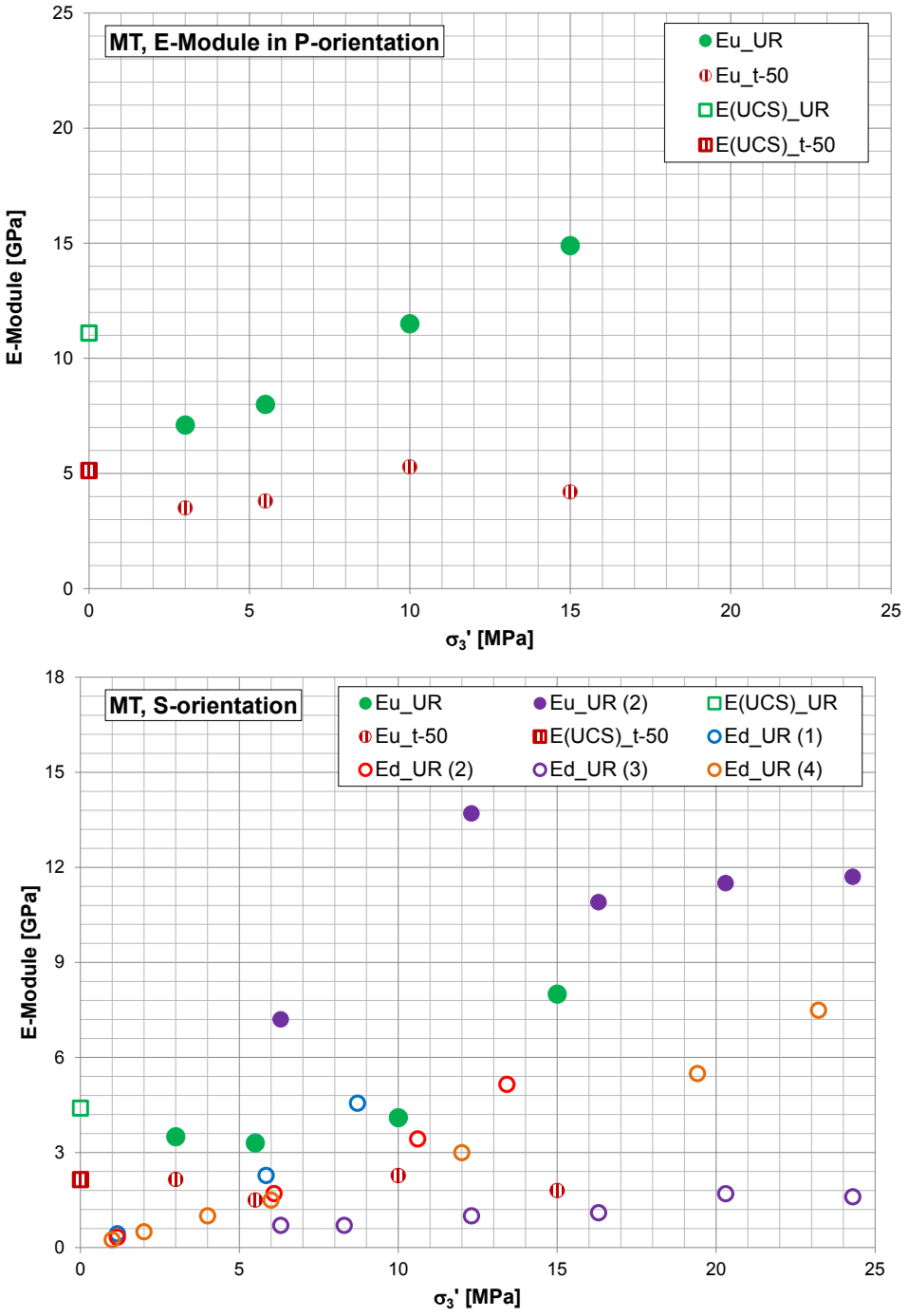

Fig. 4-7: Compilation of static E-Moduli for samples from Mont Terri.

Above: values in P-orientation (loading parallel to bedding). *Below*: values in S-orientation (loading perpendicular to bedding). The indices 1-4 in Ed_UR-values relate to the following references: (1 & 2) = Péron et al. (2009); (3) = Horseman et al. (2006) and (4) = Chiffoleau & Robinet (1999).

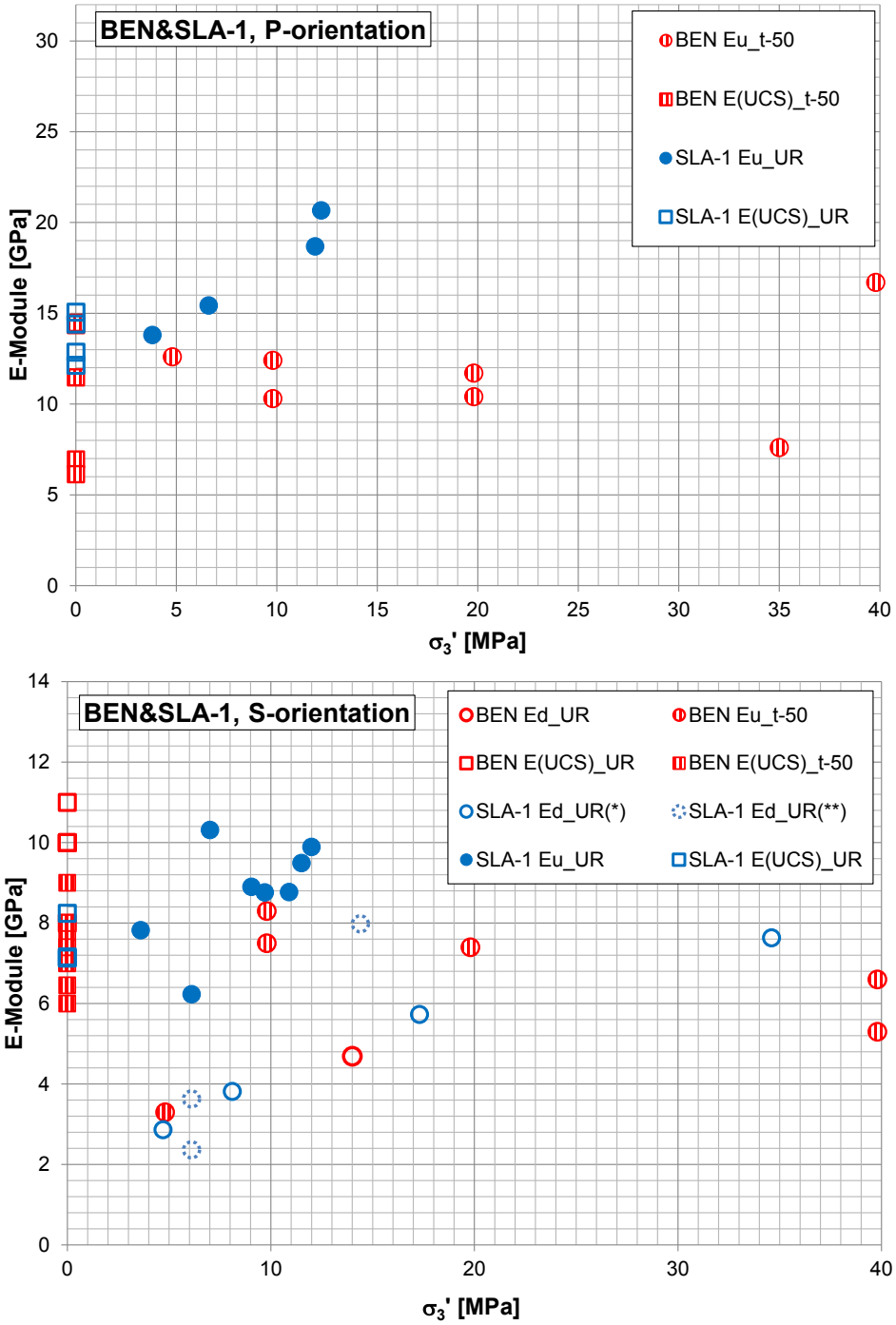

Fig. 4-8: Compilation of static E-Moduli for samples from Schlattingen and Benken.

Above: values in P-orientation (loading parallel to bedding). *Below*: values in S-orientation (loading perpendicular to bedding). Filled circles = undrained conditions (triaxial tests, Gesteinslabor Jahns 2013), striped filling pattern = $E_{t\text{-}50}$ (Rummel & Weber 1999), open squares = uniaxial tests (Mathier et al. 1999; Klee & Rummel 2000; Gesteinslabor Jahns 2013), open circles = drained conditions constrained from (i) oedometer tests with E-values constrained during loading (*) and unloading (**) from Favero et al. (2013) and ii) from a long-term permeameter test by Horseman & Harrington (2002) (red circle).

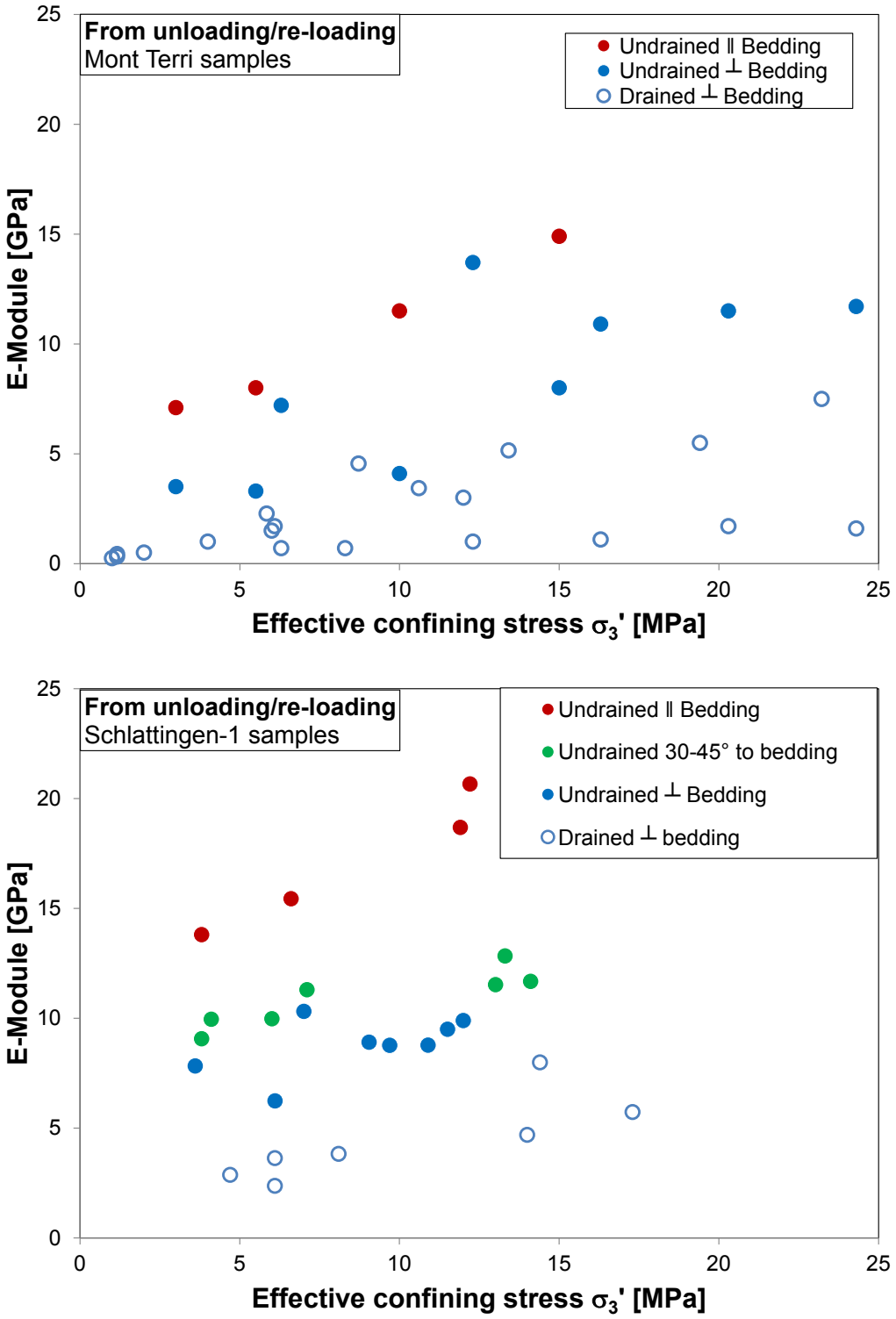

Fig. 4-9: Summary of E-Moduli from geomechanical testing.

Above: values for the URL MT, *Below*: values for SLA-1. Green points are from Jahns (2013) for Schlattingen-1.

4.4 Tensile strength

In good agreement with Wild et al. (2014), Backers (2010) demonstrated in one suite of experiments that relative humidity (as a measure of suction) can significantly influence tensile strength results (Fig. 4-10). Regulated lower humidity values resulted in elevated matrix suction and in turn to higher strength values. However, Backers (2010) also notes that small heterogeneities and possible damage during sample preparation strongly influence crack initiation and propagation. This could explain why in two other suites of experiments the correlation between tensile strength and humidity was poor.

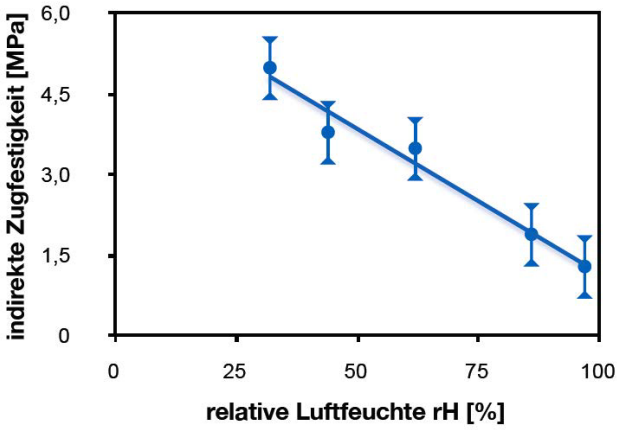

Fig. 4-10: Results from tensile strength tests at variable humidity conditions.

Figure from Backers (2010) demonstrating the influence of humidity on test results of S-samples.

Tensile strength was also examined by Mathier et al. (1999) for samples from Benken and by Jahns (2013) for samples from Schlattingen-1. A compilation of available data from samples of the URL MT and the BEN and SLA-1 boreholes is provided in Tab. 4-3.

Tab. 4-3: Summary of tensile strength results.

	URL MT	BEN	SLA-1
P-orientation			
Median (MPa)	1.1	1.3	2.15
Range (MPa)	1.0-1.1	0.8-1.7	1.7-2.6
Number of tests	3	6	2
S-orientation			
Median (MPa)	1.70	2.6	3.5
Range (MPa)	1.3-2.4	1.8-4.1	2.5-4.0
Number of tests	6	8	3
Sources	*Schnier & Stührenberg (2007), Backers (2010), Jahns (2010)*	*Mathier et al. (1999)*	*Jahns (2013)*

4.5 Uniaxial compressive strength

Results for samples of the URL MT, Benken and Schlattingen-1 are provided in Tab. 4-4 and illustrated with respect to sample orientation in Fig. 4-11. For this report, two studies were selected as reference data for the URL MT (Rummel & Weber 2004; Jahns 2010).

Tab. 4-4: Results from uniaxial compressive strength (UCS) tests.

	URL MT	BEN	SLA-1
P-orientation			
Median (MPa)	17	29	40
Range (MPa)	12-31	22-36	38-42
Number	9	5	4
S-orientation			
Median (MPa)	18	30	31
Range (MPa)	12-24	17-36	31-34
Number	6	8	3
X-/Z-orientation			
Median (MPa)	8	7	18
Range (MPa)	4-13	2-8	6-22
Number	8	4	4
Sources	*Rummel & Weber (2004), Jahns (2010)*	*Mathier et al. (1999), Klee & Rummel (2000)*	*Jahns (2013)*

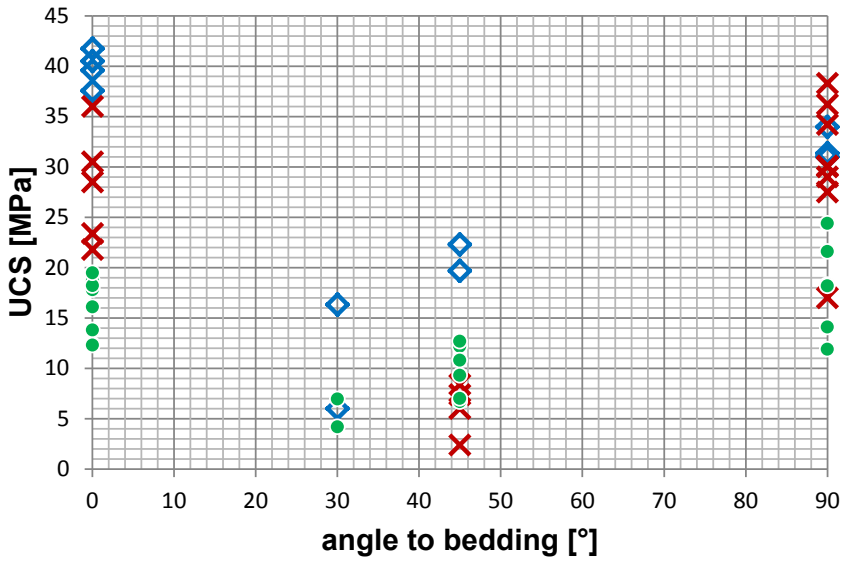

Fig. 4-11: Results from UCS tests as a function of sample orientation.

Data source as in Tab. 4-4. Blue diamonds = SLA-1 samples; red crosses = BEN samples, green circles = URL MT samples. 'Angle to bedding' refers to angle between loading direction and dominant fabric ('bedding').

In P- and S-orientation, UCS results from URL MT are consistently lowest in comparison with samples from Benken and Schlattingen-1 (Fig. 4-11). The exception is in Z-orientation, where Benken values are very low. However, it has been noted by different groups that preparation of samples in X-/Z-samples is most difficult, and due to the sample anisotropy the effect of potential weakening from induced microcracks during sample handling and preparation is expected to be most pronounced in tests of this configuration. Further evidence that UCS values from Benken in X-/Z-directions are underestimated in tests due to sample damage comes from comparison with triaxial test results (Fig. 4-24). UCS results from Benken and Schlattingen-1 in S-orientation are basically identical.

The data compiled in Tab. 4-4 and Fig. 4-11 is also plotted as a function of natural water content in Fig. 4-12. As noted in Nagra (2002), UCS strength correlates broadly with natural water content.

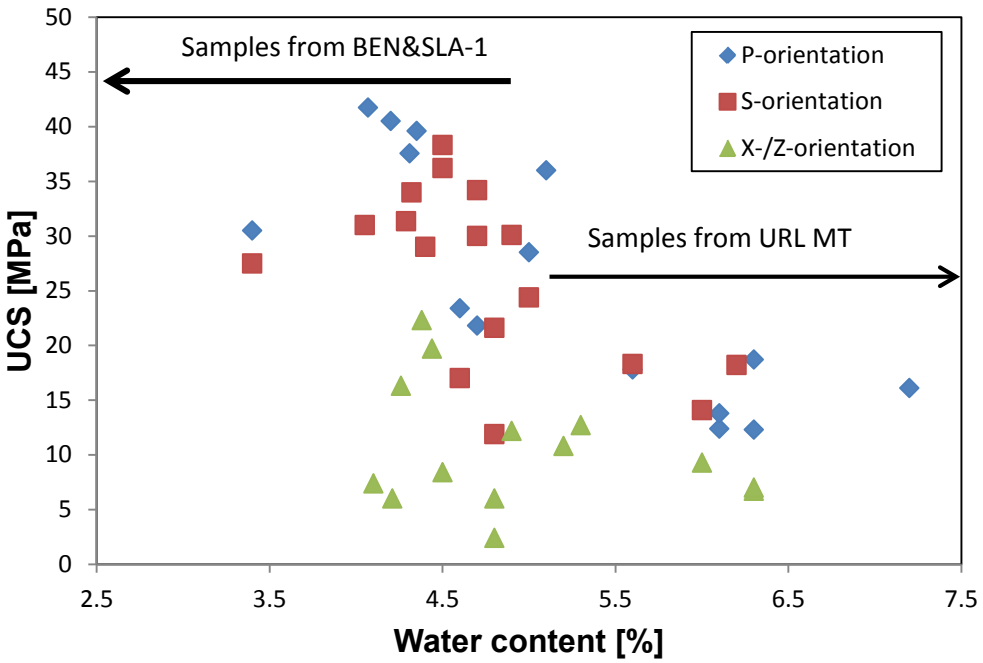

Fig. 4-12: UCS test results as function of natural water content.
Test results taken from studies in Tab. 4-4.

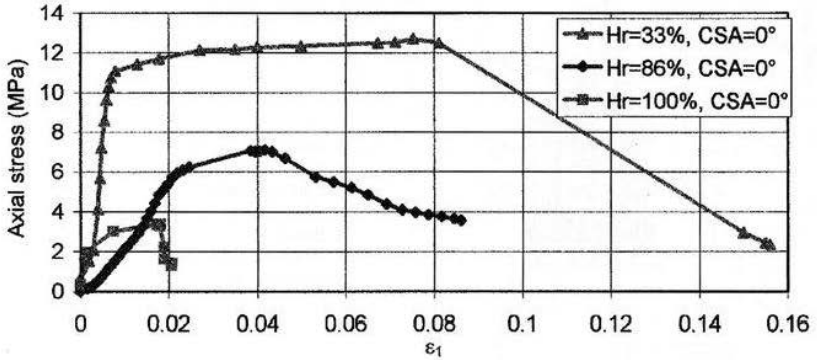

Fig. 4-13: Stress-strain results from UCS tests with samples from URL MT at variable humidity conditions.

Hr = relative humidity (controlled by saturated salt solutions). CSA = core sampling angle (0° = P-orientation). From Chiffoleau & Robinet (1999).

Nüesch (1991) performed UCS tests on Opalinus Clay samples from an exploration borehole (N3/06 5256.20) for the Bözberg road tunnel, in the area of the siting region of JO. In three tests he found UCS values of 16.4 ± 7 MPa in P-orientation. The samples were retrieved from a depth of less than 70 m and – importantly – they were air-dried from a natural water content of approximately 4% to a water content of 1.8 wt.-%. Wild et al. (2014) and Chiffoleau & Robinet (1999) have demonstrated that decreasing water contents (expressed as relative humidity) can strongly overestimate UCS strength (Fig. 4-13). Accordingly, the reported values by Nüesch (1991) may be regarded as upper bound.

4.6 Hydromechanical coupling parameters

Biot coefficient: $\alpha = \frac{\Delta V_f}{\Delta \varepsilon_{vol}} \approx 1 - \frac{K_d}{K_s}$

where ΔV_f = changes in pore fluid volume, $\Delta \varepsilon_{vol}$ = changes in volumetric strain of the sample, Kd = drained bulk modulus of the sample and Ks = bulk modulus of the solid phase only. Note that the bulk modulus K is defined as the volumetric strain in response to an applied external stress ($K = \Delta\sigma / \Delta\varepsilon_{vol}$).

Skempton coefficient B: $B = \frac{\Delta P_f}{\Delta \sigma}$, with ΔPf = changes of fluid pressure.

The presence of a pore fluid can strongly impact the mechanical response of a porous rock or soil sample. An increase in pore pressure can induce dilation in the sample, and inversely compression of the sample can cause a rise of pore fluid pressure. The two parameters controlling these coupled mechanisms are the Biot coefficient α and the Skempton coefficient B (e.g. Charlez 1997). Biot α measures the ratio of fluid volume changes in a material upon a volume change in the material when the pore pressure is allowed to return to its initial state (i.e. response under drained conditions). It also governs the effective stress law according to the following relationship:

$$\sigma' = \sigma - \alpha \times P_f \qquad (4\text{-}4)$$

Where σ' and σ are the effective and total stresses acting on the material, respectively. Skempton B measures the changes to the pore fluid pressure upon a change in the applied stress under undrained conditions. The range of possible values for both parameters α and B is between 0 and 1. Biot α and Skempton B can be related to each other through the drained (K_d) and undrained (K_u) bulk moduli:

$$B = \frac{K_u - K_d}{\alpha \times K_u} \tag{4-5}$$

Following the theory of linear elasticity for isotropic materials, bulk moduli may be obtained from elastic moduli and the Poisson's ratio by the following relationship:

$$K = \frac{E}{3(1-2\upsilon)} \tag{4-6}$$

Equation (4-5) and the above relationship $\alpha \approx 1\text{-}Kd/Ks$ stem from theoretical considerations of ideal porous materials characterized by fully interconnected pores and microscopically homogeneous and isotropic matrix material. For anisotropic material, especially with very low intrinsic permeability such as Opalinus Clay, the validity of this relationship must be checked experimentally (e.g. Charlez 1997).

There are no specific studies in which poroelastic parameters in Opalinus Clay were evaluated in detail. Bellwald (1990) and Aristorenas (1992) specify values of $0.88 < \alpha < 0.99$ and $0.80 < B < 0.99$, respectively. Chiffoleau & Robinet (1999) obtained $0.4 < \alpha < 0.8$ in oedometric tests using Opalinus Clay samples from the URL Mont Terri, but tests were conducted at variable saturation levels and documentation of the technique used to constrain α is poor. Monfared et al. (2011) obtained Skempton $B \approx 0.93$ also in Opalinus Clay samples from the URL Mont Terri in a hollow cylinder device.

An attempt of measureing B-values was also made in recent tests using cores from Schlattingen1 to assess the saturation and equilibration state of test samples prior to triaxial deformation (Jahns 2013). Some tests showed close to asymptotic values with $0.6 < B < 1$, but also values of $B > 1$ and $B < 0$ were constrained. Subsequent diagnostic analyses have shown that these measurements were unreliable (Favero et al. 2013; Tab. 3-1).

Quantitative information of poroelastic constants is available for the Tournemire argillite with comparable geomechanical and physical properties as the Opalinus Clay. Based on a synthesis of three different studies and own data, Noiret et al. (2011) concluded that α in Tournemire argillites is slightly stress dependent, decreasing from approximately 0.75 ± 0.2 at 5 MPa effective axial stress to approximately 0.5 ± 0.1 at 25 MPa effective axial stress.

4.7 Triaxial strength

A large number of studies were dedicated to triaxial testing of Opalinus Clay over the past 20 years. Unfortunately, the test protocols in these studies were very variable and this makes a rigorous synthesis difficult, especially for samples tested from the URL Mont Terri.

Earlier testing programs focused strongly on water content (e.g. Nüesch 1991; Rummel et al. 1999; Rummel & Weber 1999) noting that strength significantly increased with decreasing

water content. In the recent testing program on cores from the Schlattingen-1 borehole, samples were consolidated at elevated fluid pressures prior to testing (Jahns 2013). The effect of strain rate on test results was also investigated in the range between 10^{-8} s^{-1} and 10^{-4} s^{-1} (Rummel et al. 1998; Jahns 2013).

4.7.1 Volumetric behavior during shear

The vast majority of all triaxial experiments conducted on Opalinus Clay have shown a pronounced peak stress, preceded by strain-hardening and followed by significant strain weakening (Fig. 4-14). The recording of the associated volumetric behavior is somewhat restricted by conventional triaxial recording systems, especially in the post-peak phase. Rummel & Weber (1999) recorded volumetric changes of the tested samples from the Benken core by the displaced confining oil (holding confinement pressure constant). It appears that a transition from dilatant to contractant behavior during yielding occurs at approximately 20 MPa confining stress (Fig. 4-15).

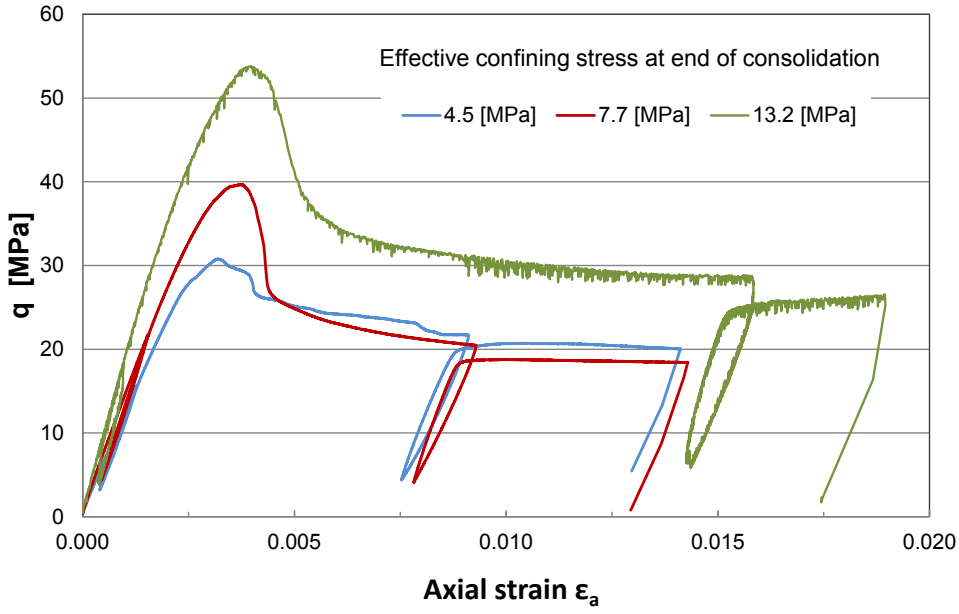

Fig. 4-14: Evolution of (deviator) stress with axial strain in Opalinus Clay from Schlattingen.

Example from Favero et al. (2013) showing results of consolidated-undrained triaxial tests with samples in P-configuration from Schlattingen.

Amann (2012) using a circumferential strain gage observed a transition of volumetric strain from negative to positive in Opalinus Clay core samples from URL MT at total confining stresses of approximately 0.5 – 2.0 MPa.

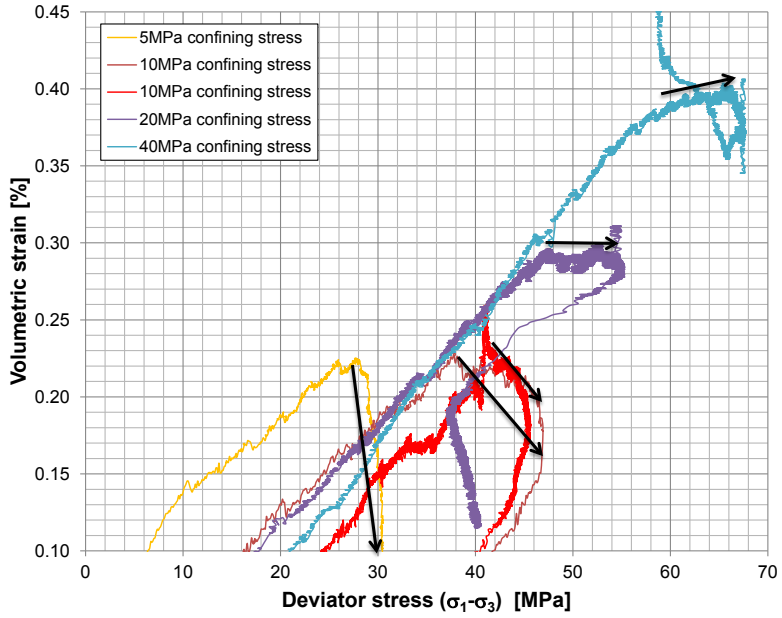

Fig. 4-15: Volumetric strain as a function of deviator stress for Opalinus Clay Benken.

Results for samples in S-orientation from Rummel & Weber (1999). Shown are curves from tests conducted at different total confining stresses. The black arrows indicate the volumetric behavior from yielding to peak. Negative slopes relate to negative volumetric strain (expansion), positive slopes to positive volumetric strain (contraction). An apparent transition from negative to positive volumetric strain during yielding is observed at a total confining stress of approximately 20 MPa.

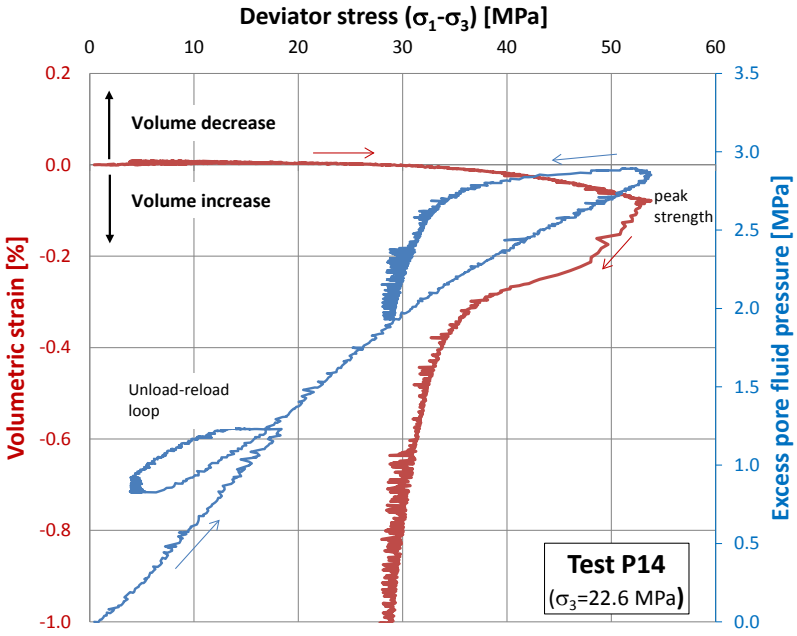

Fig. 4-16: Volumetric strain as a function of deviator stress for Opalinus Clay Schlattingen.

Dilation indicated at approximately 30 MPa deviator stress and associated with a decreasing rate of excess pore pressure build-up. At peak stress decrease of pore pressure. Test corresponds to green curve in Fig. 4-14.

In the recent triaxial testing program with samples from the Schlattingen-1 borehole (Jahns 2013) only a single diametric strain gauge was employed to monitor radial strain. One example of recorded strain and associated changes to pore pressure is is given in Fig. 4-17 for a sample in P-configuration. In this example, yielding at approximately 30 MPa is associated with dilation (volume increase indicated by negative volumetric strain) and a decrease in the rate of excess pore pressure build-up. Pore pressure declines after reaching peak strength. Samples in S-orientation indicated a rather contractant volumetric behavior. Favero et al. (2013) discuss the volumetric behavior of all the tests conducted by Jahns (2013) and emphasize the importance of proper sample saturation and equilibration during consolidation and prior to testing for a robust analysis.

4.7.2 Effective stress analysis (p'-q space)

In the following Figs. 4-17 to 4-22 strength results of triaxial tests are plotted in p'-q space, where $p' = 1/3(\sigma_1' + \sigma_2' + \sigma_3')$[5] is the *effective mean stress* and $q = \sigma_1'-\sigma_3'$ the *deviator stress*. A Biot coefficient α=1 was assumed to calculate effective stresses in Equation 4-4 for all test results.

As will be discussed below, test data from URL Mont Terri are analysed as a separate data set and test data from Benken and Schlattingen are analysed in combination. Fit results are summarized in Table 4-5. Note that linear regression in p'-q space takes the form:

$$q = a + M \times p' \tag{4-7}$$

where *a* and *M* are related to the Mohr-Coulomb parameters of *effective cohesion* (C') and *effective friction angle* (φэ) as follows (e.g. Azizi 2000):

$$a = C' \frac{6\cos(\varphi')}{3-\sin(\varphi')} \tag{4-8}$$

$$M = \frac{6\sin(\varphi')}{3-\sin(\varphi')} \tag{4-9}$$

[5] In the performed 'triaxial' (more precisely bi-axial, since $\sigma_2' = \sigma_3'$) tests, $\sigma_1' = \sigma_a'$ (axial stress) and $\sigma_2' = \sigma_3' = \sigma_c'$ (effective confining stress), it follows that $p' = 1/3(\sigma_a' + 2\,\sigma_c')$ and $q = \sigma_a'-\sigma_c'$.

Tab. 4-5: Best fit parameters in p'-q space and calculated Mohr-Coulomb parameters.

Compilation from Figs. 4-18 to 4-23 using Equations 4-7 to 4-9 to obtain the Mohr-Coulomb strength parameters.

Derived parameters	Matrix (P/S-orientations) Peak	Residual	Bedding (X/Z-orientations) Peak	Residual
URL MT				
a	6.4	0.7	2.8	1.5
M	1.15	1.13	0.76	0.70
C'	**3.1**	**0.3**	**1.3**	**0.7**
φ'	**29**	**28**	**20**	**18**
BEN&SLA-1				
a	13.0	10.9	10.4	4.59
M	1.30	0.86	0.81	0.84
C'	**6.3**	**5.1**	**4.9**	**2.2**
φ'	**32**	**22**	**21**	**22**

Also shown in the linear regression analysis of Figs. 4-18, 4-20, 4-21 and 4-23 are the 95% confidence bands, representing the limits within which the chosen fit line is adequate with a confidence of 95%. It is emphasized that these are purely statistical analyses conducted with routine analyses in Origin® software. In some examples the lower bound of the confidence intervals intersects the q-axis at negative values, without plausible physical meaning (i.e. suggesting negative cohesion values).

The results for samples from URL Mont Terri are shown in Figs. 4-18 and 4-20, grouped by matrix and bedding direction, respectively, where 'matrix' comprises test results in P- and S-orientation, and 'bedding' comprises of test results in X- and Z-orientations (cf. Fig. 4-1). Each figure consists of two graphs, with results from peak strength above and results from post-peak[6] strength below. Seven studies were selected as representative for samples from Mont Terri (Tab. 4-6). The quality of each data set was evaluated based on the test protocols and completeness of key parameters being monitored during testing. Individual data points were not assigned different qualities, although this could be inferred for some data points[7]. To honor the different qualities of the various data sets for the appropriate strength fit analysis, each Q-level is attributed a weighting factor (Tab. 4-6), which was accounted for in the regression. The weighting is reflected by different symbol sizes in Figs. 4-18 to 4-20, where larger symbols denote a higher weighting (higher confidence) of the results.

[6] Defined as q-value after reaching close to asymptotic level following peak failure and before the unload-reload loop, typically after a strain of approximately 1.5 – 2%.

[7] For example for tests where peak strength and post-peak strength are approximately identical, indicating that the sample was significantly pre-damaged.

Tab. 4-6: Overview of selected studies and assigned quality levels for regression analysis of sample from Mont Terri rock laboratory.

Weighting refers to the regression analysis and is reflected by the size of the symbols in Figs. 4-18 and 4-20.

Reference	Q-Level	Rationale	Weighting
Jahns (2010)	B	Controlled pore pressure, small samples (30mm length), low strain rate (10^{-7}-$10^{-6}s^{-1}$)	75%
Jahns (2007)	C	Controlled pore pressure, standard sample size (60mm length) and strain rate ($10^{-6}s^{-1}$)	50%
Olalla et al. (1999)*	C	Controlled pore pressure, large sample size (150mm length) but low strain rate ($10^{-7}s^{-1}$)	50%
Rummel et al. (1999)	C	Controlled pore pressure, standard sample size (60mm length) and strain rate ($10^{-6}s^{-1}$)	50%
Rummel & Weber (2004)	C	Controlled pore pressure, standard sample size (60mm length) and strain rate ($10^{-6}s^{-1}$)	50%
Popp & Salzer (2006)	D	No pore pressure control, long sample size (160mm length) and fast strain rate ($10^{-5}s^{-1}$)	25%
Schnier & Stührenberg (2007)	D	No pore pressure control, long sample size (250mm length) and fast strain rate ($10^{-5}s^{-1}$)	25%

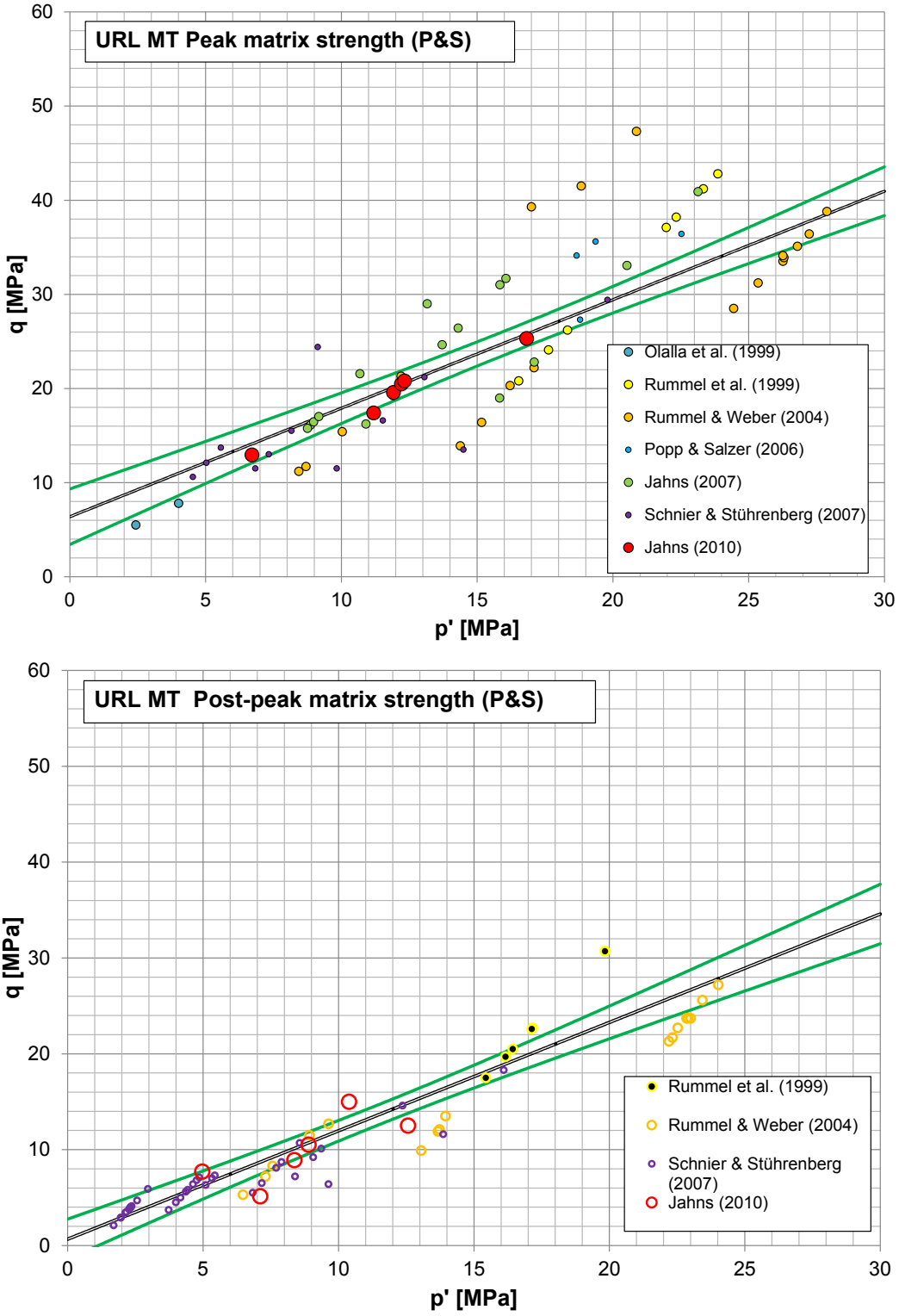

Fig. 4-17: Peak and post-peak matrix strength of samples from URL Mont Terri.

Relative sample sizes indicate qualitative weighting in fitting.
Black line = linear regression fit. Green lines = upper and lower 95% confidence band.

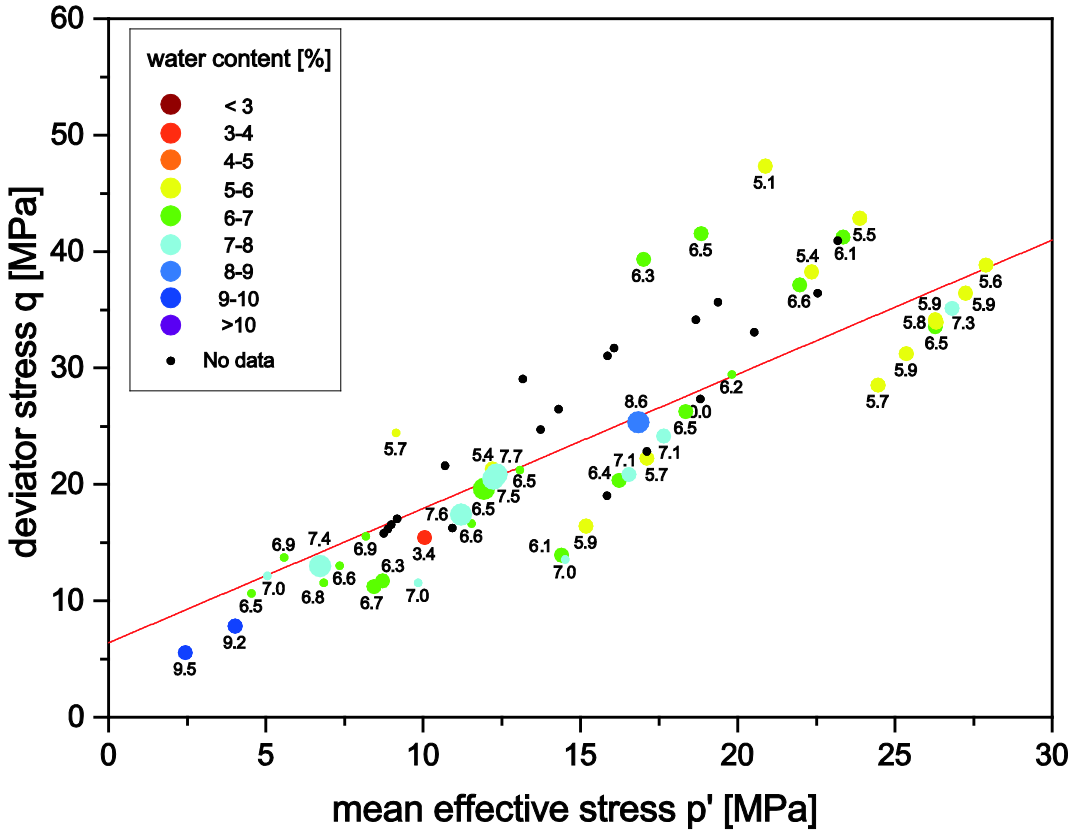

Fig. 4-18: Mont Terri peak matrix trength with respect to water content.

Data as in Fig. 4-17 (top). Numbers denote water contents in percent. As in Fig. 4-17, the size of the symbols indicates the considered realiability of the data. Red line depicts regression line as in Fig. 4-17 (top) and Tab. 4-5.

There is much larger scatter in peak strength than in post-peak strength values in Figs. 4-18 and 4-20. The scatter in peak strength can partly be attributed to different water contents, where higher water contents tend to yield lower strength values (deviator stress q) at a given mean effective stress (Fig. 4-19). On the other hand deviator stress at peak may vary by up to 50% for very similar water contents at a particular mean effective stress. This may be related to mineralogy, sample damage prior to testing or experimental artefacts, as will be discussed further in Section 5.

Peak strengths of samples in X- and Z-configuration show a particularly large scatter as indicated by the confidence bands (Fig. 4-20). Comparison with post-peak strengths indicate that a number of 'intact samples' were pre-damaged, explaining some of the very low values seen for peak strength. As emphasized in Chapter 4.5, tests in X- and Z-orientation are most sensitive to sample preparation artifacts (cf. also Footnote 4 above and last paragraph of this section).

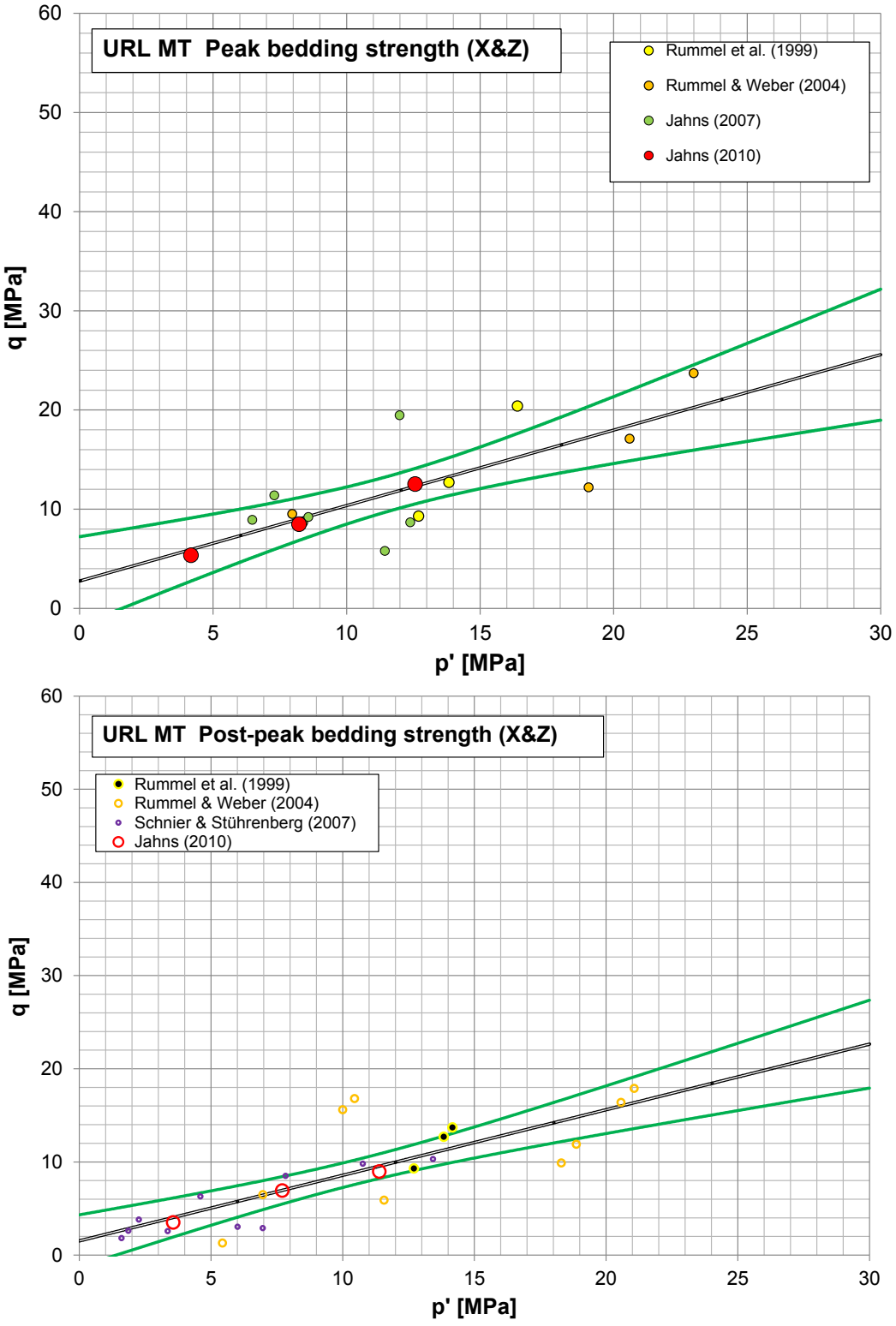

Fig. 4-19: Peak and post-peak bedding strength of samples from URL Mont Terri.

Relative sample sizes indicate qualitative weighting in fitting.
Black line = linear regression fit. Green lines = upper and lower 95% confidence band.

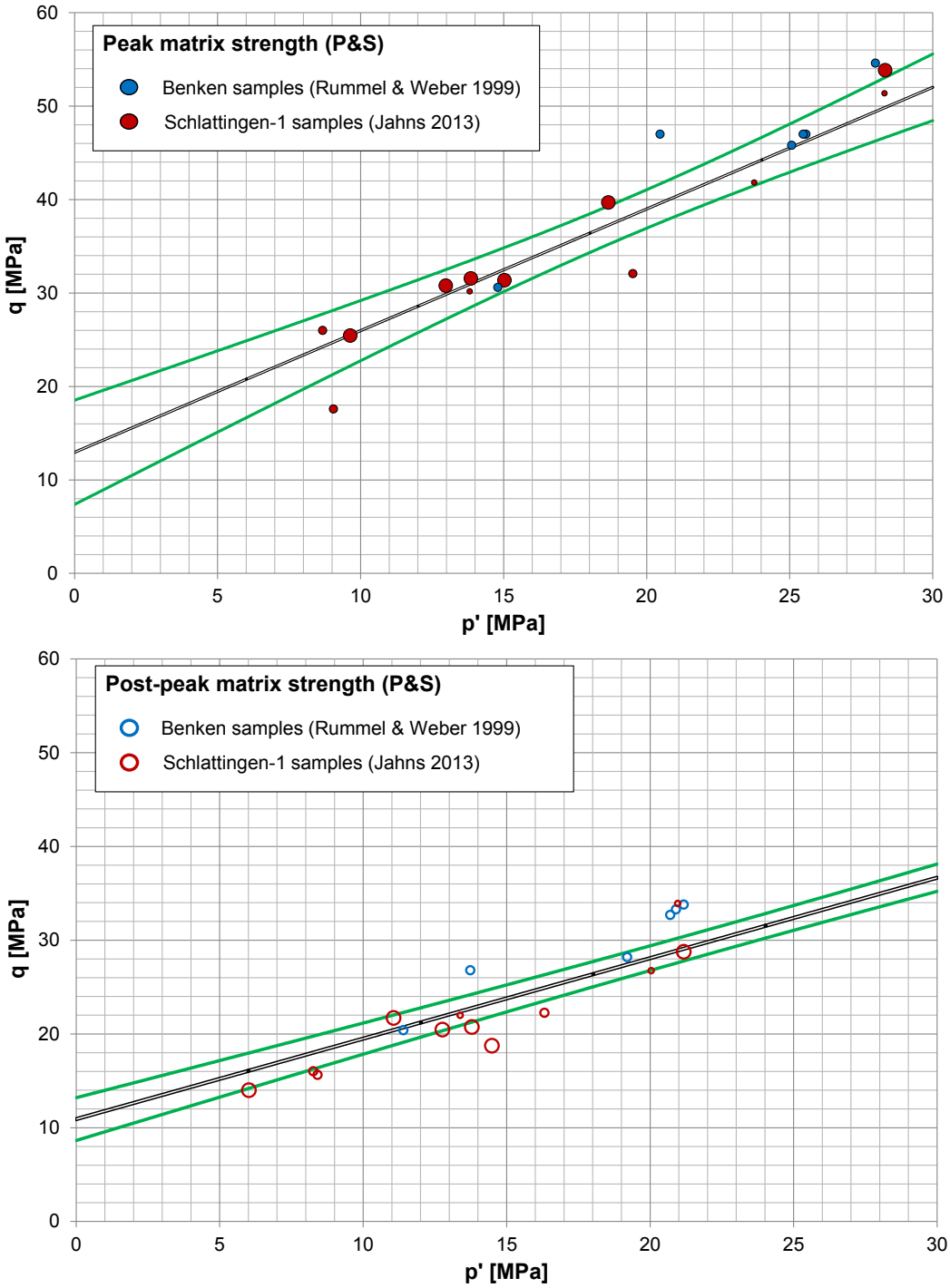

Fig. 4-20: Peak and post-peak matrix strength of samples from BEN and SLA-1.

Relative sample sizes indicate qualitative weighting in fitting.
Black line = linear regression fit. Green lines = upper and lower 95% confidence band.

The test results from Benken and Schlattingen-1 are illustrated in Figs. 4-21 to 4-23. A quality ranking was also performed on these test data. The Benken data (Rummel & Weber 1999) were assigned a C-quality as they were performed analogous to Rummel & Weber (2004) in the URL Mont Terri compilation above. The test results from Schlattingen-1 (Jahns 2013) are the only data set from which a detailed diagnostic analysis was performed (Favero et al. 2013). The quality assignment for this data set was therefore made on an individual basis for each test. The ranking for the Schlattingen-1 tests is based mainly on the saturation state and consolidation equilibration achieved prior to testing as discussed in Favero et al. (2013).

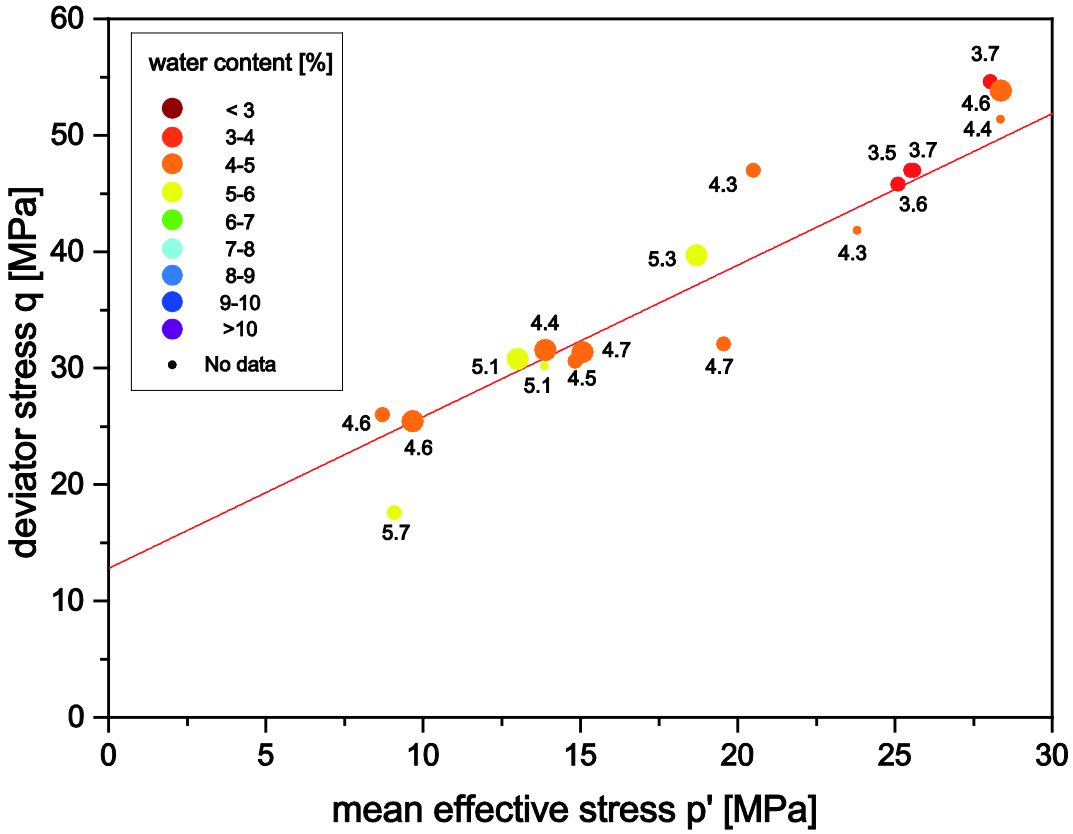

Fig. 4-21: Benken/Schlattingen-1 peak matrix strength with respect to water content.

Data as in Fig. 4-21 (top). Numbers denote water contents in percent. As in Fig. 4-21, the size of the symbols indicate the considered realiability of the data.
Red line depicts regression line as in Fig. 4-21 (top) and Tab. 4-5.

Results from Benken and Schlattingen-1 are plotted in the same graphs due to the similarity both in water contents (Fig. 4-22) and the degree of overconsolidation (cf. Table 4-1), and the apparent similarities in the actual test results. With this in mind it is noted that the *present* burial depths differ by nearly 300 m.

In summary, the URL Mont Terri data exhibit similar but lower strength than the combined data set of Benken and Schlattingen-1. Expressed in Mohr-Coulomb strength parameters, the main difference between the two data sets is seen in the apparent effective cohesion, which is greater for the samples in Benken and Schlattingen-1 then for those at the URL Mont Terri.

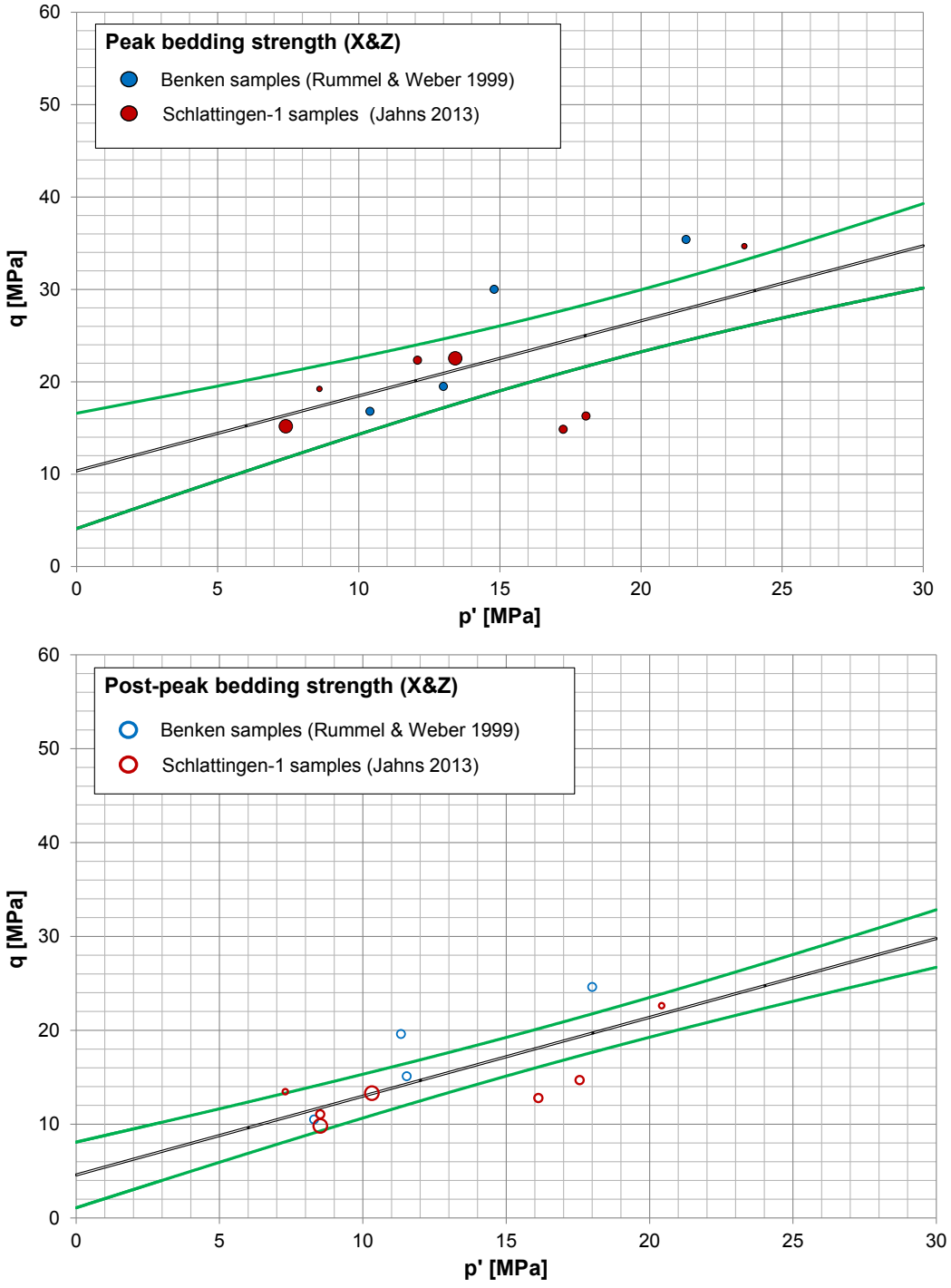

Fig. 4-22: Peak and post-peak bedding strength of samples from BEN and SLA-1.

Relative sample sizes indicate qualitative weighting in fitting.
Black line = linear regression fit. Green lines = upper and lower 95% confidence band.

Using the Mohr-Coulomb parameters from regression analysis (Tab. 4-5) UCS strength may be calculated according to the following relationship (e.g. Fjær et al. 2008):

$$UCS = 2C' \frac{\cos(\varphi)}{1-\sin(\varphi)} \tag{4-10}$$

The calculated and measured UCS values (Chapter 4.5) are compared in Fig. 4-24. The figure highlights that measured UCS strength values are generally higher because only total stresses are recorded (effective stresses are not known). The only deviation from this observation is seen systematically in all the tested UCS tests with Z-configuration from Benken, and one single test with the same configuration from Schlattingen-1. This suggests that the samples tested in Z-configuration of Benken in particular were variably pre-damaged.

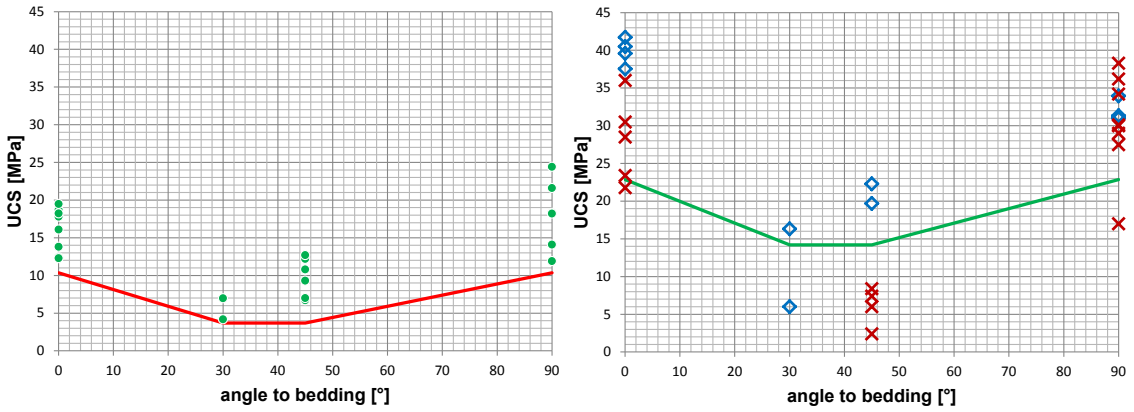

Fig. 4-23: Comparison of measured and calculated UCS values.

Left: Data from URL Mont Terri. Note that the calculated UCS values (red line) underestimate systematically measured values (green circles). *Right:* Data from Benken (red crosses) and Schlattingen-1 (blue diamonds). Calculated values (green line) underestimate values except for Benken and Schlattingen-1 tests in X- and Z-orientation.

4.7.3 Total stress analysis (undrained shear strength)

By plotting the results of triaxial experiments in effective stress (p'-q) space the underlying assumption is that pore fluid pressure is accurately monitored during deformation and that the pore pressure coupling parameters (Chapter 4.6) are known. The undrained shear strength (c_u) is an alternative way of illustrating test results as it relates only to the deviator stress which is independent of pore fluid pressure:

$$S_u = \frac{q}{2} = \frac{1}{2}(\sigma_{1f} - \sigma_{3f}) = \frac{1}{2}(\sigma_{1f}' - \sigma_{3f}') \tag{4-11}$$

Where σ_{1f} and σ_{3f} are the maximum and minimum total stress at failure and σ_{1f}' and σ_{3f}' are the maximum and minimum effective stress at failure.

The result of this analysis demonstrates a substantial increase in shear strength with decreasing water content (Fig. 4-25). In this context it is noted that the plotted water contents refer to the values determined in the laboratory (Chapter 3.2). Rummel & Weber (1999 2004) 'dried' and 'wetted' samples to increase the range of investigated water contents. These tests are indicated by open symbols in Fig. 4-25 and were not considered for effective stress analysis above.

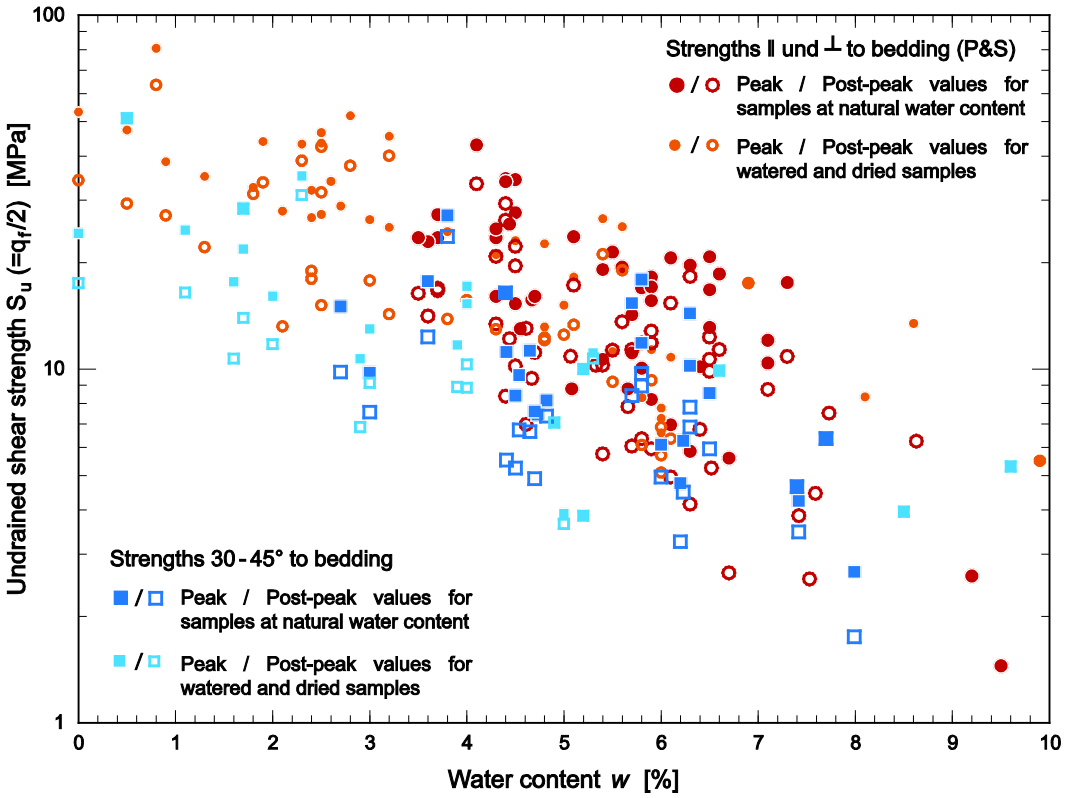

Fig. 4-24: Undrained shear strength as a function of water content.

Data are from URL Mont Terri (Rummmel et al. 1999; Rummel & Weber 2004; Jahns 2007 & 2010), Benken (Rummel & Weber 1999) and Schlattingen-1 (Jahns 2013).

4.8 Residual strength

As specified in Tab. 4-5 the lowest strength values in triaxial testing are measured as 'post-peak' in bedding directions (X- and Z-configuration), with friction angles decreasing to values of approximately 19-21° and apparent cohesion values down to approximately 0.5 to 2 MPa. In these triaxial tests the displacements achieved on the dominant slip planes were limited to approximately 2 – 3 mm. Conventional direct shear tests allow for larger absolute displacements up to 10 mm, and are somewhat better suited to address the possibility of more substantial weakening of the material at large strains. Popp & Salzer (2006) and Haug (2009) conducted experiments in such direct shear configuration with Opalinus Clay samples from the URL Mont Terri. They derived very consistent residual strength parameters with low cohesion (approximately 0.2 MPa) and an internal friction angle of approximately 20°. These results are comparable with post-peak strengths as measured in the triaxial tests, notably in terms of friction angles.

Pellet et al. (2013) report residual friction angles as low as 12° in tests with Callovo-Oxfordian claystones, with similar geomechanical properties as the Opalinus Clay (Boisson 2005). The authors attribute a dramatic decrease in the friction angles between dry and water saturated conditions to the 'lubrificant effect of water'. However, it is noted that the experiments of Pellet et al. (2013) are conducted on saw-cut samples and pore fluid pressure control during testing is not possible in direct shear configuration. Furthermore, examples of fault zones in Opalinus Clay (e.g. Fig. 2-5) indicate that localization of strain is complex and that a single sharp slip surface, as should be expected if planes with pronounced weakening would indeed have developed, is not observed. In addition, it is expected that strength can also partly be recovered on fracture surfaces in Opalinus Clay due to swelling (Chapter 4.2.3), (e.g. also Bock 2010). Appendix A relates index properties to residual strength from empirical correlations in literature lending further support that effective friction angles below 15 to 20° are unrealistic for Opalinus Clay.

4.9 Stiffness of joint/bedding planes and dilation angle

Normal stiffness: $k_n = \Delta\sigma_n/\Delta u_n$ [GPa/m],

Shear stiffness: $k_s = \Delta\tau_s/\Delta u_s$ [GPa/m],

where σ_n and τ_s are normal and shear stress components acting normal to the plane, and un and us are displacement normal and parallel to the plane.

Joint stiffness tests have only been conducted on Opalinus Clay samples from URL MT. Bock (2009) compiled values from two studies (Popp & Salzer 2006; Schnier & Stührenberg 2007) and found $k_n = 8$ and $k_s = 10$ for $\sigma_n \leq 4$ MPa. Haug (2009) found similar results with $k_n = 6 \pm 3$ for $0 < \sigma_n < 2$ MPa and $k_n = 10 \pm 3$ for $2 < \sigma_n < 4$ MPa, and $k_s = 6 \pm 5$ for $0 < \tau_s < 4.5$ MPa.

Dilation angle: $\psi = \tan^{-1}(\Delta u_n/\Delta u_{ns})$ [°]

Positive dilation angles (i.e. volume increase during direct shear testing on planes) were observed on samples from URL MT by Popp & Salzer (2007), with values decreasing form approximately 30° to 0° when increasing σ_n from 0 to 4 MPa. In a compilation of triaxial tests conducted with samples in Z-orientation and at a confining pressure of 10 MPa Bock (2002) suggested a value of 0 ± 2° (compilation Bock 2009). Haug (2009) noted that with a few exceptions, positive dilation angles were generally not observed in his direct shear tests using also samples from URL MT.

5 Data evaluation

The index and geomechanical properties of Opalinus Clay reported in Sections 3 and 4 are based on analyses of core samples in the laboratory. Recovering core samples of claystones such as Opalinus Clay from in-situ conditions and characterize them in the laboratory with minimum disturbance, including re-establishing such conditions in geomechanical testing is very challenging. The following paragraphs provide an overview of inherent uncertainties in data compilation.

5.1 Porosity and water content

Porosity values in Chapter 3.3 were calculated on samples in unconfined conditions. From oedometric testing, it can be estimated that porosity values at effective stress conditions comparable to potential repository depths (i.e. 400 to 900 m) would be approximately 5 – 10% lower. This difference can broadly be attributed to swelling and damage (e.g. microcracks) during and following sample recovery. However, samples can also reduce in volume under ambient conditions in the lab by desiccation. There are many other factors which can affect the porosity and water content of the sample with respect to in-situ conditions. These are mainly related to the drilling process and sample handling (storage, sub-coring and preparation) and are difficult to quantify.

The water content is constrained by the oven-drying method, and it is assumed that the specimen was fully saturated by water prior to drying. When measuring the particle density and the bulk density separately, the degree of saturation can then be established. It is generally found that Opalinus Clay samples are saturated at approximately 80 to 95% even after careful handling (e.g. Ferrari et al. 2012; Wild et al. 2014). Comparing water contents before and after geomechanical testing yields the same qualitative observation (e.g. Jahns 2010).

5.2 Stiffness and strength

The effect of unsaturated conditions on recorded stiffness and strength values was discussed and visualized in Chapter 4 (Figs. 4-6, 4-10, 4-13). In an unsaturated state, capillary forces and osmotic processes lead to suction, which in terms of strength can be seen as an apparent cohesive strength component (e.g. Fredlund & Rahardjo 1993). This is particularly important for UCS tests, where no pore fluid is supplied to the sample during testing. As indicated in Fig. 4-23, measured UCS on unsaturated samples may result in values which are up to a factor two greater than calculated values from triaxial testing data.

Strength (expressed by the deviator stress, i.e. $q = \sigma_1 - \sigma_3$) is influenced by the strain rate in undrained geomechanical testing. Jahns (2013) varied the strain rate in the range between 10^{-4} and 10^{-7} s^{-1} and found that strength decreased by approximately 15% for intact samples and 30% for post-peak values, respectively. Between strain rates of 10^{-6} and 10^{-7} s^{-1} the difference was negligible for peak strength and less than 10% for post-peak strength. This is broadly consistent with the findings of Rummel et al. (1998). Most of the test results in Chapter 4.7.2 were conducted at a strain rate of 10^{-6} s^{-1}. Strain rate was also an important parameter considered in the evaluation of the quality of the data (Tab. 4-6).

The strain rate also affects the pore water pressure development to failure, and hence the effective mean stress ($p' = [\sigma_1' + \sigma_2' + \sigma_3']/3$). In a diagnostic analysis of the strain rate variation in the tests by Geseinslabor Jahns (2013) Favero et al. (2013) show that generated excess pore pressure at a strain rate at 10^{-6} s^{-1} isapproximately 85% of the value at 10^{-7} s^{-1}. In comparison, at a strain rate of 10^{-4} s^{-1} the recorded excess pore pressure was only 25% of the value at a strain rate of 10^{-7} s^{-1}. It is noted that pore pressure in triaxial tests are measured at the end faces of cylindrical samples. In a number of experimental programs hardly any change in pore fluid pressure was recorded during testing (Rummel et al. 1998; Rummel & Weber 1999; Rummel & Weber 2004). This is manifested by apparent total stress paths (with slope $\Delta q = 3\,\Delta p'$) in the p' - q diagram and suggests that fluid saturation was not established during the consolidation phase. Quantification of this effect is difficult, but two qualitative effects can be envisaged (cf. Nagra 2002).

- Suction may lead to an overestimation of the deviator stress (i.e. q for a particular p' is overestimated)
- If desaturation affects mainly the external part of the sample, the pore fluid pressure in the centre of the sample could be much greater than what is recoreded at the end plates, hence p' is overestimated for a particular q.

This can explain part of the data scatter with similar water content in p'-q space (e.g. Fig. 4-18). Conversely, core drilling, sub-sampling and sample preparation can disturb the sample and lead to damage. The peak strength of a specimen measured in the laboratory may therefore also underestimate the strength of the actual rock mass (Underwood 1967; Steiner 2000).

By plotting the triaxial test results in effective stress (p'-q) it was assumed that the Biot coefficient α equals 1. From limited experimental data this value may also be lower. Using for example $\alpha = 0.6$ instead of $\alpha = 1$ for matrix peak strength values in the data of Benken and Schlattingen-1, the resulting Mohr-Coulomb strength parameters in a regression analysis would yield C' = 4.6 MPa and $\varphi' = 32$ (instead of C' = 6.3 MPa and $\varphi' = 32$, cf. Tab. 4-5)[8]. The corresponding line in p'-q space would broadly coincide with the lower 95% confidence band in Fig. 4-20 (top).

Empirical correlations of index properties and strength parameters provide independent evidence of the derived strength parameters, at least concerning the effective friction angles. For Opalinus Clay, it is expected that the effective friction angle is of the order of 25° for intact samples and 20° for residual strength (Appendix A). This is in good agreement with derived values in Tab. 4-5. The uncertainties in effective cohesion values are more difficult to constrain, also because experiments at very low p' were not conducted. The analysis with variable α above also demonstrates a greater relative sensitivity of C' than for φ'. Normalizing the undrained shear strength to the effective consolidation (or burial stress), offers a means of comparing strength data independent of the pore fluid pressure during testing. A comparison of Opalinus Clay test results with a large data set of 25 different shales from the North Sea (Gutierrez et al. 2008) shows that the positive correlation of strength with the overconsolidation ratio is similar (Appendix A, Fig.A-3). The absolute values of normalized undrained shear strength are also comparable, at least for samples which were loaded oblique to the dominant fabric (Appendix A).

[8] This is documented in the electronic datafiles 8_LinearFits_p'-q.opj and 15_BENSLA1_matrix_alpha0.6.xlsx (see Appendix D).

6 Constitutive framework and application to modelling

6.1 Critical state approach

The Opalinus Clay is an overconsolidated claystone which can be classified as a weak to medium strong rock based on the International Society for Rock Mechanics (ISRM) Classification scheme. This classificiation is underlined by distinct strain softerning at failure in the laboratory over the effective stresses relevant for depths of a potential repository. But Opalinus Clay also exhibits ample evidence of characteristics more pertinent to stiff soils. Observed examples of this are:

- Hysteresis (irreversible compaction) in loading-unloading cycle when consolidated beyond an apparent preconsolidation stress
- Moderate swelling pressure and heave
- Pronounced hydro-mechanical coupling
- Complex non-saturated behavior (e.g. shrinkage, apparent cohesion resulting from water retention mechanisms)

Accounting for these features the conceptual framework to describe the deformation behavior of Opalinus Clay was outlined in Nagra (2002) by a combination of the critical state concept and a limit state for higher overconsolidation. The critical state concept is founded on the supposition that when sheared, a porous material will eventually reach a critical state at which large shear distortions will occur without further changes in volume, deviator stress or mean stress (Schofield & Wroth 1968). The following three equations provide a basis for the volumetric behavior in the critical state concept for consolidation, for loading and unloading in an overconsolidated state, and for shear deformation (e.g. Azizi 2000):

Normal Consolidation Line (NCL): $$v = v_{\lambda 0} - \lambda \ln(\frac{p'}{p_r}) \quad (6\text{-}1)$$

Unload-Reload Line (URL): $$v = v_{\kappa 0} - \kappa \ln(\frac{p'}{p_r}) \quad (6\text{-}2)$$

Critical State Line (CSL): $$v = v_{\Gamma 0} - \lambda \ln(\frac{p'}{p_r}) \quad (6\text{-}3)$$

The slopes of the NCL and URL (or swelling) lines in semilogarithmic space were already introduced as Cc and Cs, respectively, in Chapter 4.2. Also in Chapter 4.2 it was mentioned that Cc and Cs are easily converted to λ and κ by multiplying with a factor of ln(10). The specifiv volume v was defined in Chapter 3.3. The subscripts $\lambda 0$, $\kappa 0$ and $\Gamma 0$ denote the intercepts of the different lines at a reference stress p'_r equal to 1 on a logarithmic scale. The different values for the slopes κ and λ emphasize that not all of the volumetric strain during (normal) consolidation is recoverable. Specific to the Opalinus Clay, the associated data base was introduced in Chapter 4.2, demonstrating that during normal consolidation elastoplastic deformation occurs. The vertical surface with the URL at its base and along which deformations are purely elastic is known as the *elastic wall* (Fig. 6-1). If sheared in a normally consolidated stress state, according to critical state the sample would be contractant and follow a stress path along the *Roscoe boundary surface* (Fig. 6-1). The CSL is the locus of all possible critical states in the

p'-q-*v* parameter field (Fig. 6-1) and it represents the stress state at which failure occurs. The slope of the projected CSL on the p'-q plane is defined by *M* as specified in Equation (4-7).

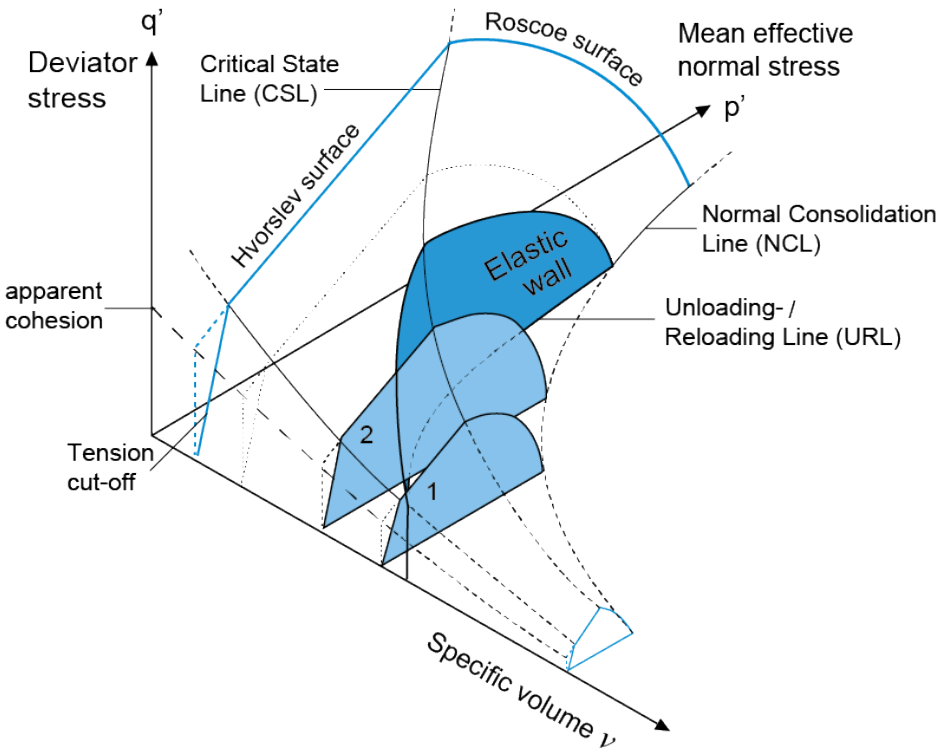

Fig. 6-1: State boundary surface in three dimensions.

The numbers 1 and 2 are sections at two different specific volumes. Note the larger surface area in 2 with respect to 1 at greater specific volume.

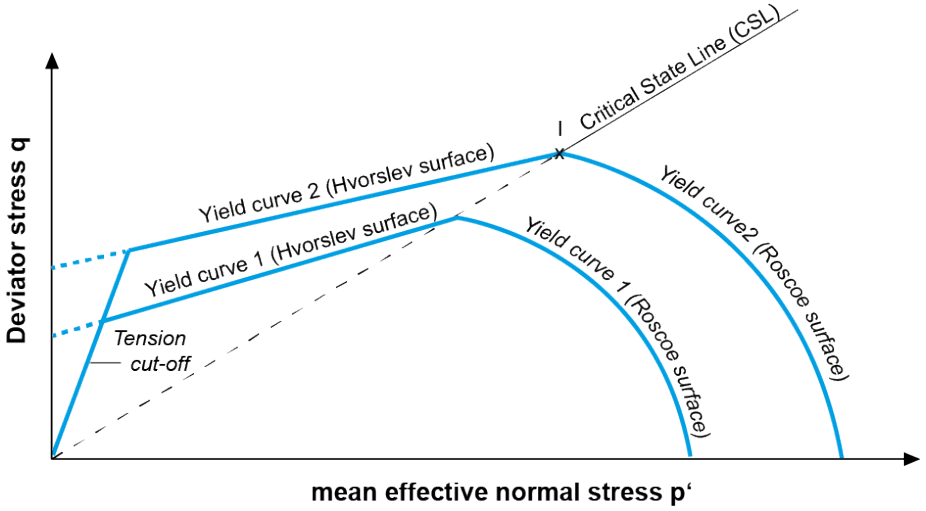

Fig. 6-2: p'-q section of the 3D state boundary surface in Fig. 5-1.

The yield curves (intersection of the p'-q plane with the 3D state boundary surface) for two sections at different specific volumes (1 and 2 in Fig. 6-1) are projected to the same plane.

For (strongly) overconsolidated clays characterized by more brittle behavior associated with dilation at yielding the *Hvorslev surface* is a more appropriate boundary surface (e.g. Azizi 2000). The Hvorslev surface intersects with the Roscoe surface at the CSL (I in Fig. 6-2), and with the *v*-q' plane at an intercept > 0 suggesting the existence of apparent cohesion. Since no geomechanical tests at very low and controlled effective stresses are available it remains unclear whether the tension cut-off applies also for Opalinus Clay (cf. dashed line for the yield surface in Figs. 6-1 and 6-2). In the absence of effective cohesion which would allow the material to withstand tensile pressure the Hvorslev surface is limited by the *tension cut-off*. As negative values of the minimum effective stress are not allowed by the tension cut-off, the relationship between deviator and effective mean stress is given by q = 3p'.

The combination of the Roscoe and the Hvorslev surface with the tension cut-off define a complete state boundary in p'-q-*v* space (Fig. 6-1). The boundary surface limits the stress states and volume of the material which can be achieved before yielding. When the boundary is reached the stress path follows the boundary surface to the CSL and failure.

Peak strengths visualized in Figs. 4-17 to 4-22 essentially represent p'-q sections of the 3D boundary surface for the Opalinus Clay. Schematically, the samples from URL MT with a water content of typically 6-7% may be regarded as section 1 in Fig. 6-1, the samples from Benken and Schlattingen with a lower water content (lower specific volume) of 4 to 4.5% as section 2. Since the critical state theory was developed on remoulded clays it assumes isotropic mechanical properties. The peak strength anisotropy, i.e. the deviations of peak strengths in X- and Z-direction with respect to P- and S-direction as seen in Figs. 4-17 to 4-22 is not reflected in the single state boundary surface as shown in Fig. 6-1. A second state boundary would need to be contructed or, alternatively, the shape of the boundary surface would need to be calibrated for anisotropic clays (Graham & Houlsby 1983). The data base on Opalinus Clay does not currently allow for such a refined conceptualization.

The projection of undrained shear strength values of Opalinus Clay to the *v*-q plane is given in Fig. 4-24. It highlights the increasing shear strength towards lower water contents (lower specific volume). From the critical state concept, the water content is related to undrained shear strength as follows (e.g. Azizi 2000):

$$w = Z - \frac{\lambda}{G_s}\ln(S_u) \tag{6-4}$$

where Z is a constant related to critical state parameters and G_s is the specific gravity (cf. Chapter 3.2). This relationship will be referred to again in Chapter 7, when reference parameter values are formulated

6.2 Constitutive law for assessment of engineering feasibility

The above introduced constitutive framework is important from a conceptual point of view, but the data base currently not mature enough for rigorous numerical parametrization. For the assessment of engineering feasibility, a simpler material law is therefore required. To capture the elasto-plastic behavior of Opalinus Clay with respect to short-term cavern stability, Nagra has previously used the *subiquitous joint model* (SUBI) implemented in FLAC software (Nagra 2002; TeKamp 2008). SUBI is a transversal isotropic, bilinear strain-hardening-softening model and capable of accounting for a number of features observed in geomechanical testing of Opalinus Clay, notably:

- Strain-hardening prior to peak and strain-softening following peak strength
- Strength anisotropy ("matrix" and "bedding" direction)
- Stress-dependent cohesion and friction values (bilinear strength envelope[9]).

Other features in the geomechanical behavior of Opalinus Clay are explicitly not accounted for in the SUBI model. These include:

- Stiffness anisotropy between "matrix" and "bedding"
- Crack evolution and associated volumetric changes (dilation)
- Time dependent processes such as consolidation, swelling or shrinkage

The limitation of the SUBI model especially with respect to the lack of accounting for stiffness anisotropy are discussed in Shiu & Billaux (2014).

The following Chapter 7 provides recommended parameter sets for geomechanical, numerical modelling for engineering feasibility purposes.

[9] Cf. Nagra (2002) and Chapter 7.

7 Recommended parameter values for numerical modelling

7.1 Geomechanical parameters

The data base in Chapter 3 demonstrated that mineralogy and geotechnical index properties of Opalinus Clay are comparable for different locations across northern Switzerland. In contrast, a fairly systematic positive correlation is recognized for porosity with greater current burial depth or overconsolidation ratio. Chapter 4 provided ample evidence that stiffness, swelling and strength parameters are inversely proportional to water content, which is a measure of porosity. In particular, samples from the URL MT were shown to exhibit greater porosity and lower stiffness, swelling and strength values than samples from Benken and Schlattingen-1. In Chapter 6.1 this observation was brought into a constitutive framework. For engineering feasibility assessment, a simplified material law is being used (chapter 6.2). Table 7-1 provides a recommendation of parameter values for numerical modelling using a SUBI elasto-plastic material law. To honour the dependency of strength and stiffness parameters on porosity in a pragmatic way, two geomechanical data sets are proposed.

Tab. 7-1: Recommended parameter sets for Opalinus Clay for effective stress analysis using a bi-linear Mohr-Coulomb constitutive law with tension cut-off.

[a]E-Moduli constrained in unload-reload cyclces. [b]Bi-linear regression for data set Opalinus Clay deep ($0 \leq p' \leq 25$ / $p' > 25$ MPa, where p' = effective mean stress defined as 1/3 x $[\sigma_1' + \sigma_2' + \sigma_3']$). Mohr-Coulomb strength values are listed as best fit values from regression analysis.

Parameter	Unit	Opalinus Clay shallow (<400m b.g.)		Opalinus Clay deep (400-900m b.g.)	
		Value ∥ bedding	Value ⊥ bedding	Value ∥ bedding	Value ⊥ bedding
Bulk density (natural)	[g/cm3]	2.43		2.52	
Bulk density (dry)	[g/cm3]	2.33		2.43	
Grain density (dry)	[g/cm3]	2.71			
Water content	[wt.%]	6.4		4.5	
Physical porosity	[vol.%]	16		11	
E-Modulus					
Drained[a]	[GPa]	2		4	
Undrained[a]	[GPa]	8	4	18	9
Poisson ratio	[-]	0.35	0.25	0.27	0.27
Uniaxial Compressive Strength (UCS)	[MPa]	17	18	33	31
Uniaxial Tensile Strength (UTS)	[MPa]	1.1	1.8	1.4	2.7
Mohr-Coulomb shear strength					
Peak strength[b]					
Matrix - effective cohesion	[MPa]	3.1		7.1 / 14.6	
Matrix - effective angle of internal friction	[°]	29.0		33 / 18	
Bedding - effective cohesion		1.7		3.9 / 7.4	
Bedding - effective angle of internal friction		19		24 / 17	
Residual strength					
Matrix - effective cohesion	[MPa]	2.3		5.2	
Matrix - effective angle of internal friction	[°]	22.0		22.0	
Bedding - effective cohesion		1.0		2.3	
Bedding - effective angle of internal friction		17		20	
Dilation angle	[°]	0		0	
Biot coefficient (alpha)	[-]	0.8		0.8	

A first data set is hereafter referred to as *Opalinus Clay shallow*, and it is based on physical and geomechanical properties from the URL MT as shown in Chapter 3 and 4. It is considered the representative geomechanical data set for relatively shallow depths up to approximately 400 m below ground. A second data set is termed *Opalinus Clay deep* as it is considered representative for current burial depths between 400 and 900 m. The geomechanical data set Opalinus Clay deep is based on data from core samples of Benken and Schlattingen-1.

Stiffness (E-Moduli)

The stress dependency of stiffness is honoured by the formulation of different values in the two data sets of Tab. 7-1, which in turn are recommended for different depth intervals. The values were estimated from Fig. 4-9 at the effective stress levels considered typical with respect to the different depth of application of the two data sets, i.e. at $\sigma_3' \approx 5$ MPa for the *Opalinus Clay shallow*, and at $\sigma_3' \approx 10$ MPa for *the Opalinus Clay deep*.

A stiffness-anisotropy (perpendicular to bedding vs. parallel to bedding) of two is recommended in both of the two different geomechanical data sets of Tab. 7-1. For numerical modelling in engineering analysis using a constitutive law with an isotropic E-Moduli the lower values[10] (perpendicular to bedding) are recommended as a base case.

Strength parameters

The strength values formulated in Tab. 7-1 differ from those compiled in Tab. 4-5. This is because the data base for regression was extended or was re-evaluated to be more consistent with the conceptual framework described in Chapter 6:

- For the data set *Opalinus Clay deep* (Figs. 7-1 and 7-2):
    - UCS test results are also considered for regression analysis to complement the data set in the low stress range (notably at $p' < 10$ MPa).
    - A bi-linear fit in the range between $0 \leq p' \leq 70$ MPa is adapted as opposed to just a linear fit between $0 \leq p' \leq 30$ MPa
- *Opalinus Clay shallow* (Figs. 7-3 to 7-5):
    - The regression for the matrix post-peak values, and the bedding peak and post-peak values were forced to intersect the q-axis at a specified value which was derived in the q-e plane (Fig. 7-3, see below). This led essentially to greater effective cohesion values.

The UCS test results were considered in the case of the deep data set since no triaxial test results are available for $p' < 7$ MPa, in contrast to the shallow data set. Since the effective stress state at failure is not known in UCS tests, it is assumed that pore fluid pressure is equal to zero. In reality pore fluid pressure can be elevated in response to the high strain-rate of this test procedure in combination with the low intrinsic hydraulic properties of Opalinus Clay, or even negative due to suction. UCS tests are therefore assigned a very low ranking for regression. In the absence of robust test results at low effective stresses and given that unconstrained and unsaturated conditions will also occur at the tunnel face after excavation the integration of UCS test result in the regression is considered appropriate.

[10] This is a conservative approach as lower E-Moduli will enhance convergence during tunnel excavation.

Tests conducted at p' > 30 MPa on samples from the Benken borehole (from Rummel & Weber 1999) were also included and following Nagra (2002) a bilinear regression was fitted. The break of slope in the bilinear fit was forced at p' = 25 MPa for both matrix and bedding peak strength. Strength data in the stress range of p' > 30 MPa are virtually absent for the URL MT. A physical explanation of the apparent break in slope would be that some tests conducted at elevated p' follow the roscoe surface during yielding (cf. Figs. 6-1 and 6-2). In the absence of new tests at elevated stresses, the bi-linear regression was adapted from Nagra (2002). For engineering application, it is noted that effective stresses in excess of p' = 30 MPa are not expected in Opalinus Clay for the considered depth range up to 900 m. Hence the high-stress branch of the bi-linear fit is irrelevant for tunnel stability analysis.

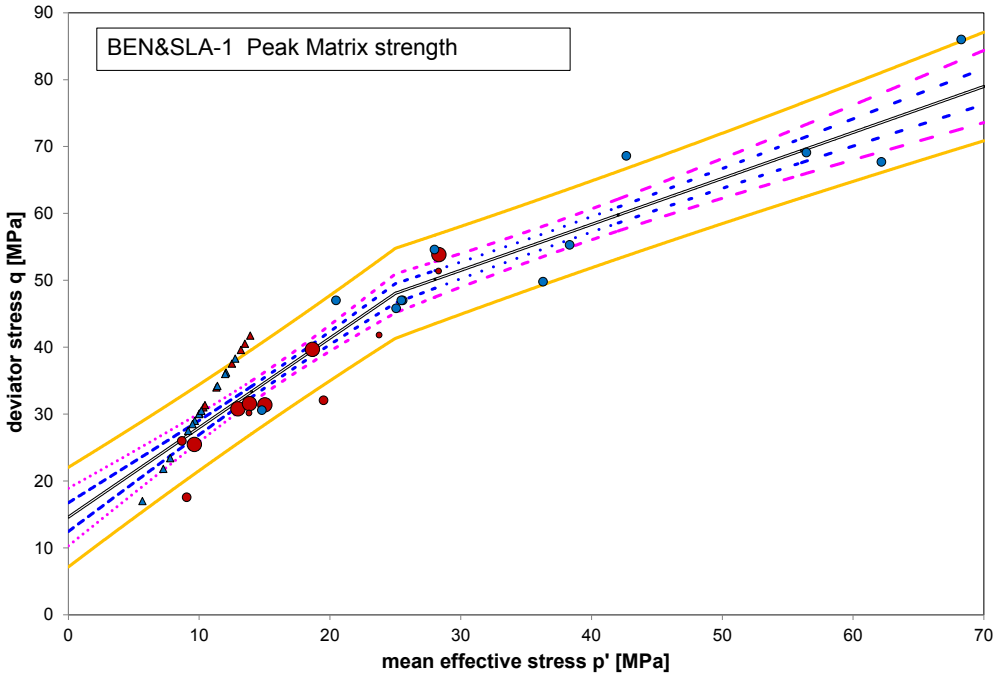

Fig. 7-1: Bilinear regression for matrix strength from Benken and Schlattingen-1.

UCS test data are indicated as triangles, triaxial test results as circles as in Fig. 4-20. Black line = bilinear regression fit accounting for data weighting (sample size), blue dashed line = 68% confidence bands, pink dotted line = 95% confidence bands and orange line = 95% prediction bands.

It is noted that the fit lines depicted in Figures 7-1 and 7-2 were derived from a data set assuming a constant pore fluid pressure of $P_f = 0.2$ MPa for the tests of Rummel & Weber (1999). A later regression analysis with the measured pore fluid pressures showed virtually no effect on the fit lines in the stress range of $0 \leq p' \leq 25$ MPa, and therefore the parameter recommendations (Tab. 7-1) were not adjusted (see also Appendix B).

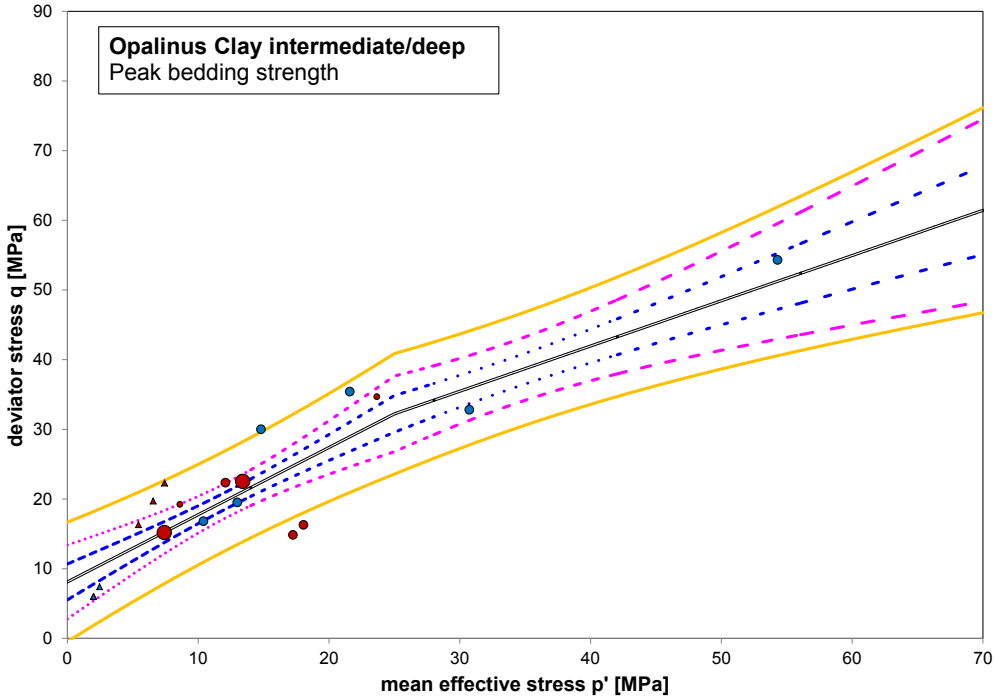

Fig. 7-2: Bilinear regression for bedding strength from Benken and Schlattingen-1.

UCS test data are indicated as triangles, triaxial test results as circles as in Fig. 4-22. Colour code of fit lines as in Fig. 7-1.

As discussed in Chapters 4.7.2 and 5 the triaxial test results from Mont Terri used to constrain the *Opalinus Clay shallow* data set shows considerable scatter, which cannot be reconciled by the variations of water contents only. The data was therefore re-evaluated by considering a conceptual relationship with the data set *Opalinus Clay deep*. To this end, in analogy with Fig. 4-24 the test data were plotted in q-*v* space (log q vs. water content), separated by matrix and bedding values (Fig. 7-3). The regression line of the peak matrix shear strength is considered as reasonably well constrained as it broadly matches the data with the highest quality level (Fig. 4-17, Tab. 4-5). In a next step, the matrix peak strength values at p' = 0 for both the *Opalinus Clay shallow* and *deep* data sets are plotted in q-v space (black squares in Fig. 7-3, above). Equation 6-4 suggests that the slope of the line through these two points may be related to the compression index (λ). The constructed black line yields a value of $\lambda = 0.06$ (or Cc = 0.14), which is roughly consistent with the findings of one-dimensional compression, although it corresponds to the highest reported values by Péron et al. (2009).

It is then assumed that the slope is constant also for matrix post-peak strength values and bedding strength values. Using the post-peak matrix strength of the data set *Opalinus Clay deep* the equivalent point can then be constructed for the *Opalinus Clay shallow* at a water content of w = 6.4%. The derived value (q = 4.9 MPa) is then used for a forced regression of the post-peak matrix strength in p'-q space (Fig. 7-4). The same procedure is applied also for the bedding strength analysis (Fig. 7-3 below and Figs. 7-5 and 7-6). The forced regression analysis is also documented in *8_LinearFits_p'-q.opj* and in *10_MT_matrix.xlsx* and *11_MT_bedding.xlsx*.

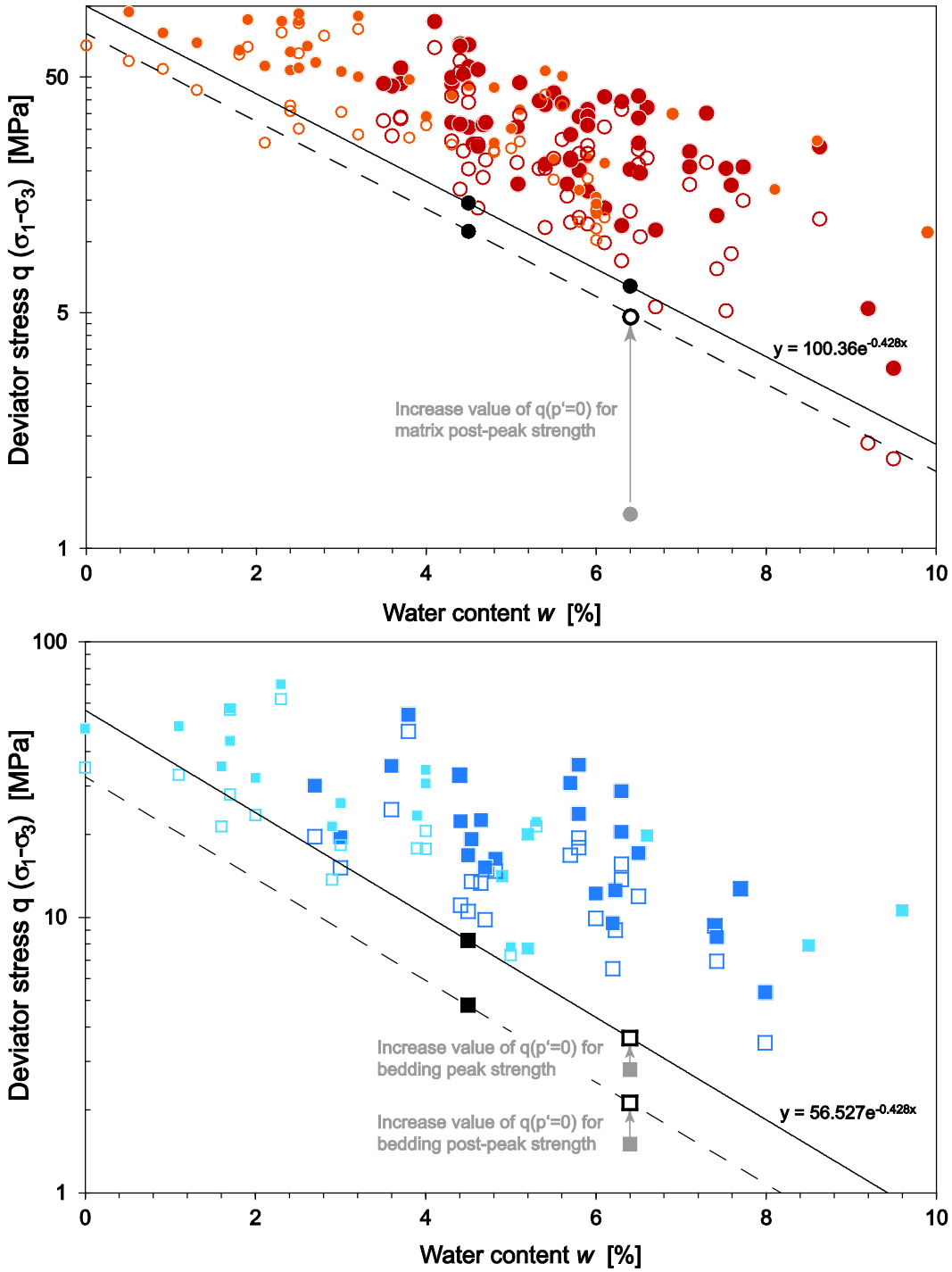

Fig. 7-3: Strength results projected onto q-*v* section.

See Fig. 4-24 for comparison, but here strength is expressed by deviator stress q instead of undrained shear strength Su (= q/2). Specific volume *v* is expressed by water content (cf. Fig. 6-1). *Above:* test results in P and S configuration (matrix). *Below:* test results in X and Z configuration (bedding). Black circles and squares denote intersections of strength fits from the p'-q section with the q-*v* section (p' = 0) for the data set Opalinus Clay deep (w = 4.5%) and shallow (w = 6.4%), respectively. Grey symbols show intersections for MT according to Tab. 4-5. Open circles and squares show adjusted intersections by lifting the grey symbols to a line with constant slope.

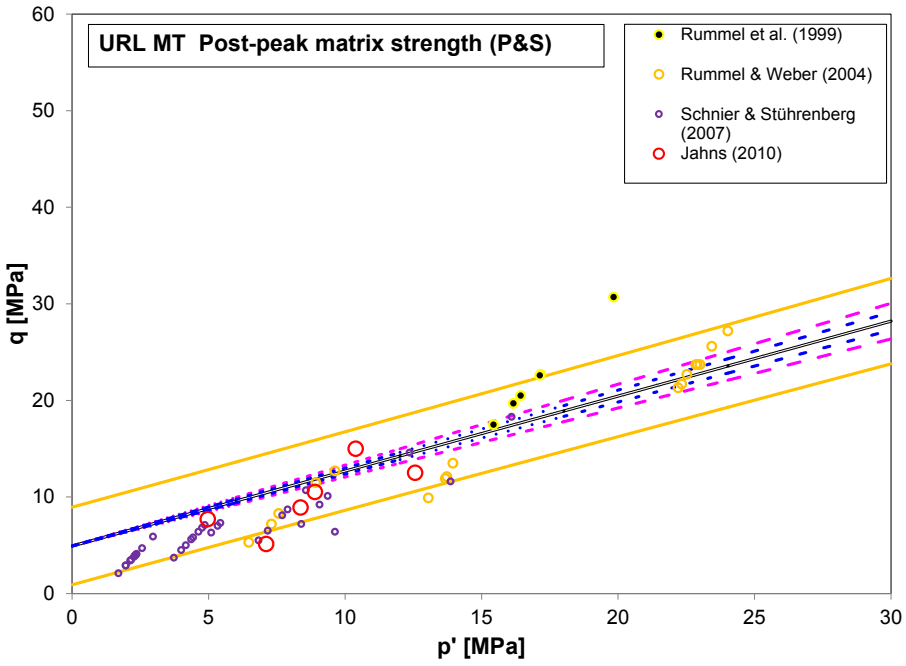

Fig. 7-4: Forced regression for matrix post-peak strength of Mont Terri test results.

Test results as in Fig. 4-17, but with a forced intercept of q = 4.9 MPa at p' = 0. Black line = linear regression fit accounting for data weighting (sample size), blue dashed line = 68% confidence bands, pink dotted line = 95% confidence bands and orange line = 95% prediction bands.

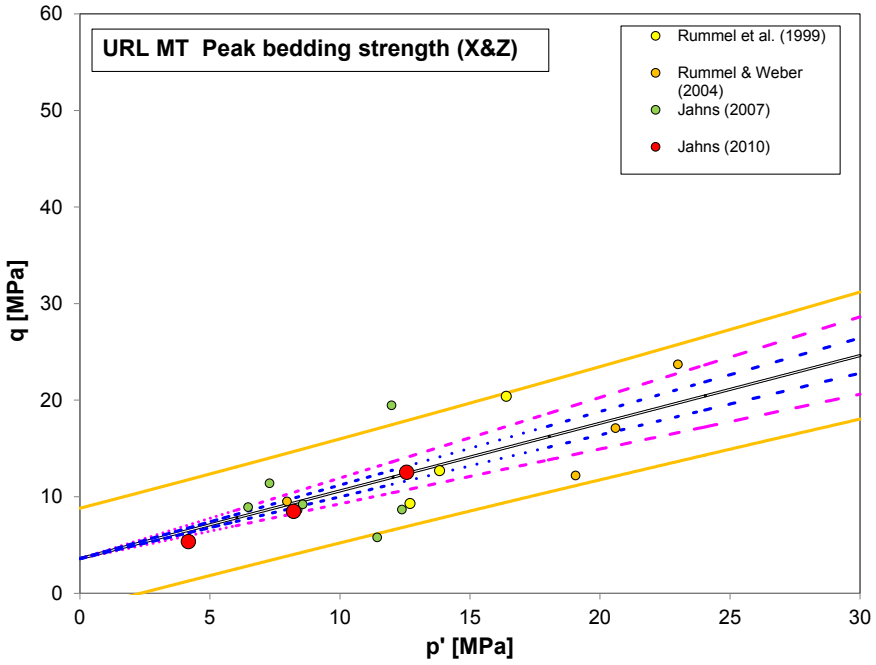

Fig. 7-5: Forced regression for bedding peak strength of Mont Terri test results.

Test results as in Fig. 4-19, but with a forced intercept of q = 3.6 MPa at p' = 0. Open circles were ignored for regression. Colour code of fit lines as in Fig. 7-4.

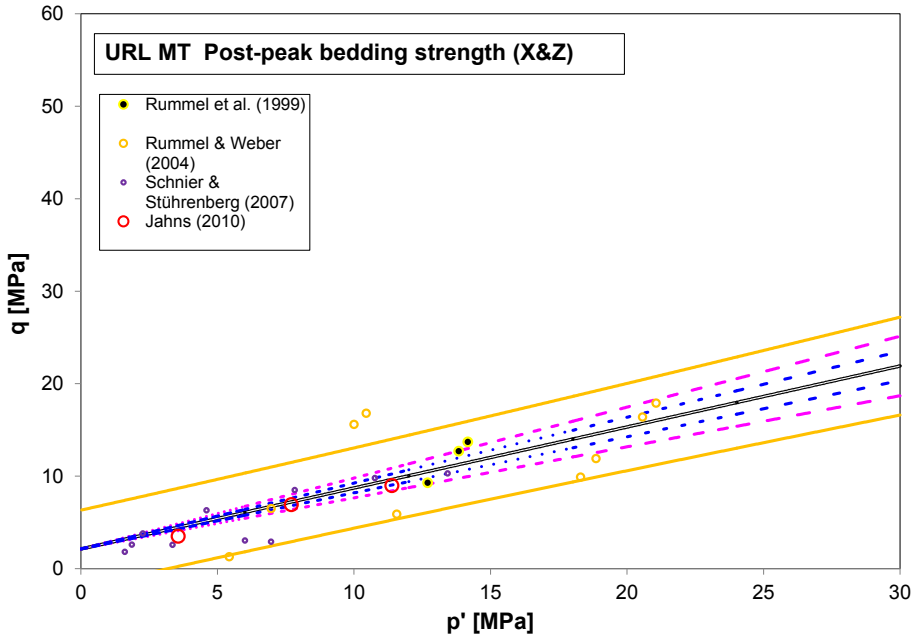

Fig. 7-6: Forced regression for bedding post-peak strength of Mont Terri test results.

Test results as in Fig. 4-19, but with a forced intercept of q = 2.1 MPa at p' = 0. Black line linear regression fit accounting for data weighting (sample size), blue dashed line = 68% confidence bands, pink dotted line = 95% confidence bands and orange line = 95% prediction bands.

Dilatancy angle

As emphasized in Chapter 4.7.1 the detailed assessment of the volumetric behavior during triaxial deformation remains difficult. In their recommendation to "numeric in geotechnics", the German Geotechnical Society advocates to use a dilation angle $\psi = 30° - \varphi$ for materials with a friction angle of $\varphi \geq 30°$, and $\psi = 0°$ for materials with a friction angle of $\varphi < 30°$ (Schanz 2006). For large strains, ψ is recommended as 0° irrespective of the angle of friction. This is consistent with the findings in shear tests of Opalinus Clay (Chapter 4.9).

Biot coefficient alpha

ABiot coefficient $\alpha = 1.0$ was assumed for the analysis of triaxial test results in effective stress space (chapter 4.7). Limited experimental evidence with Opalinus Clay and comparison with findings of a very similar claystone (cf. Chapter 4.6) suggests slightly lower values. In model calibrations using the SUBI constitutive model in FLAC software a value of $\alpha = 0.8$ was used (Shiu & Billaux 2014). The same value is also adapted in the parameter recommendation in Table 7-1.

7.2 Swelling parameters

Values of swelling pressure and swelling heave are derived from constrained and free swelling tests, respectively. Values for the *shallow* and *deep* data sets are comparable parallel to bedding, but swelling pressures are a factor of two greater perpendicular to bedding for the *deep* data set.

Tab. 7-2: Recommended swelling parameters for Opalinus Clay.

Parameter	Unit	Opalinus Clay shallow (<400m b.g.)		Opalinus Clay deep (400-900m b.g.)	
		Value ∥ bedding	Value ⊥ bedding	Value ∥ bedding	Value ⊥ bedding
Swelling pressure	[MPa]	0.2	0.5	0.2	1.0
Swelling heave	[%]	1	6	3	6

7.3 Rock models ('Gebirgsmodelle')

As discussed in Chapter 2.2 planar discontinuities such as fractures or veins are generally rare in cores of Opalinus Clay from boreholes of Northern Switzerland. Typical frequencies are less than 1/m or even 1/10 m (Fig. 2-3). The exceptions are the lowermost 20 – 30 m of Opalinus Clay in the boreholes of Riniken and Schafisheim with strongly destructured, tectonized zones. At the URL MT frequencies are also elevated with respect to findings of cores in boreholes of Northern Switzerland (e.g. Yong 2007; Blümling & Vietor 2009).

It is acknowledged that structural discontinuities are also to be expected in Opalinus Clay at greater depth (i.e. at repository level) in Northern Switzerland, and their effect is to lower the rock mass strength with respect to "intact" samples as tested in the laboratory. Fig. 7-7 illustrates the envisaged destructuring of intact, anisotropic Opalinus Clay to an essentially isotropic gouge material ("ultimate state" in terms of critical state soil mechanics). The destructuring can be seen as the evolution by increasing tectonic overprint, with strength reduction occurring primarily either along the bedding, or the matrix (i.e. any other direction), or affecting both the bedding and matrix. The strength reduction can be linked to laboratory strength measurements as schematically shown by the colour coding in Fig. 7-8 to define specific *rock models ("Gebirgsmodelle", referred to as GM's hereafter)*. The rock models are numbered from 1 to 7 in Fig. 7-7. For example, the intact rock model GM1 is assigned peak strength for both bedding and matrix. In rock model GM3, bedding peak strength is reduced by approximately two standard deviations, but peak matrix is considered intact. Note that the rock models shown in Fig. 7-7 refer to a continuum approach and – combined with Fig. 7-8 – reflect a strength *appraisal* of the rock mass, not a description.

The partial reduction of strength applies to disturbed samples without an interconnected fracture network and also arises conceptually from the self-sealing behavior of Opalinus Clay. Tectonic fractures are expected to recover strength by swelling at depths where the mean normal stress is above the swelling pressure (i.e. typically at depths greater than 100 – 200 m). Accordingly, these structures should be considered as "potential fractures" (potenzielle Trennflächen, SIA 1998) rather than "effective fractures" (effektive Trennflächen) in Opalinus Clay for depths relevant for potential repositories.

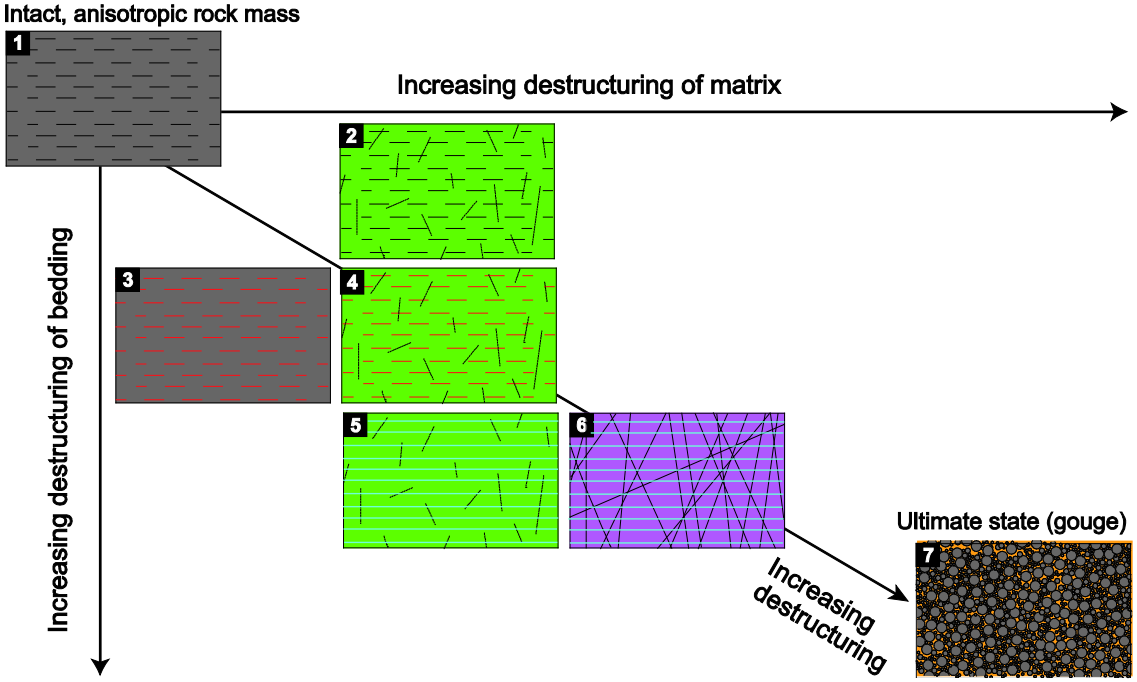

Fig. 7-7: Schematic destructuring of intact, anisotropic Opalinus Clay rock mass.

Numbers indicate rock models ("Gebirgsmodelle").

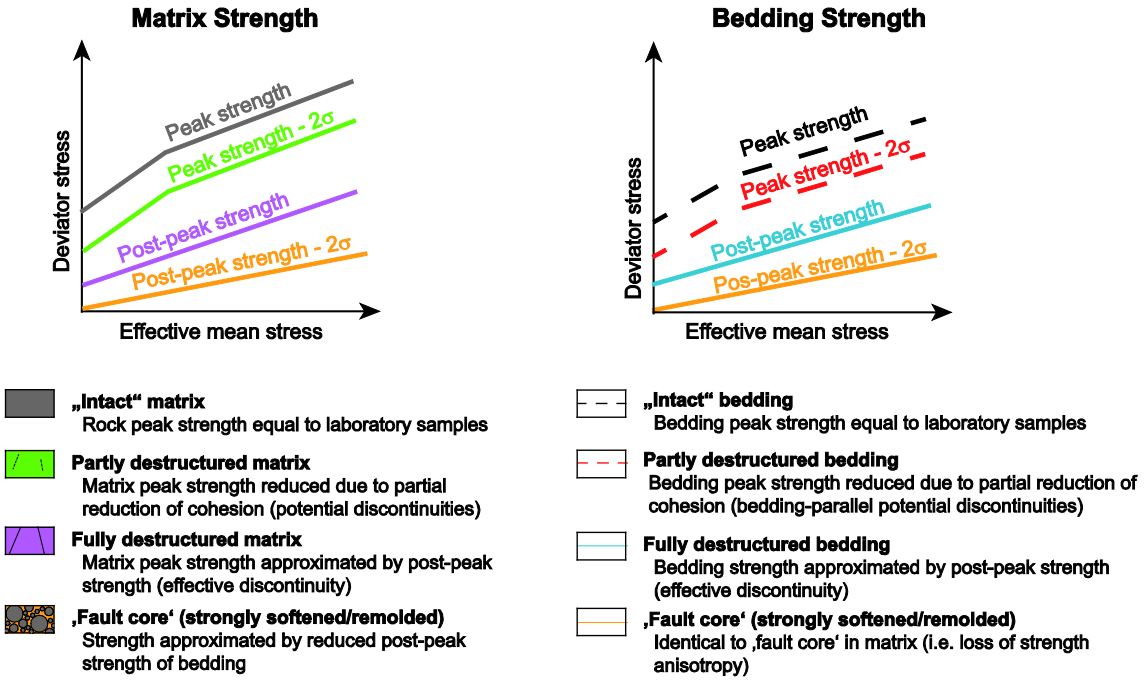

Fig. 7-8: Schematic of assigned laboratory strength parameters to progressively destructured Opalinus Clay.

Symbols and colours refer to Fig. 7-7. Reading example: Rock model 5 consists of a partly destructured matrix and a fully destructured bedding. The matrix strength is reduced from peak strength observed in laboratory samples (green line), and the bedding strength is approximated by the post-peak bedding strength observed in the laboratory (blue line).

Rock models with strength reduced to post-peak strength along bedding (GM5), and both bedding and matrix (GM6) are shown in Fig. 7-7 to cover the spectrum in the framework of progressive tectonic destructuring, but they are not considered as realistic, representative rock models for any of the proposed siting areas (see below). With respect to Chapter 2.2, the different rock models can be compared to the following field examples:

- GM1: The bulk interval of boreholes Weiach and Benken without fractures (Fig. 2-3)
- GM2: Borehole intervals with isolated fractures of moderate to steep inclination
- GM3: Borehole intervals with isolated fractures of bedding-parallel orientation. Distinction from "discing" (i.e. splitting perpendicular to core axis) is generally difficult in core analysis (cf. Ebert 2014).
- GM4: Variably fractured zone in the periphery of major slip surface as in Fig. 2-5
- GM5 & 6: Tectonized zones at the base of Opalinus Clay in boreholes Schafisheim and Riniken.
- GM7: Fault core material as illustrated by grey shading in examples of Fig. 2-5

Specific values for peak (GM1) and post-peak strength (GM5 for bedding, GM6 for matrix) were adapted from Tab. 7-1. Values of reduced strength were constructed based roughly on the 95% confidence bands and plausible values at p' = 0 (e.g. incremental decrease: intact, reduced, post-peak and strongly softened). The resulting values are given in Tab. 7-3 and are illustrated in p'-q space in Figs. 7-9 and 7-10.

Tab. 7-3: Recommended Mohr-Coulomb effective strength parameters for the different rock models.

C' = effective cohesion. φ' = effective friction angle. For the data set Opalinus Clay deep the values for p' ≥ 25 MPa are given in brackets (bi-linear regression).

Rock Model	Opalinus Clay shallow (< 400 m)				Opalinus Clay deep (400 – 900 m)			
	Matrix		Bedding		Matrix		Bedding	
	C′ [MPa]	φ′ [°]	C′ [MPa]	φ′ [°]	C′ [MPa]	φ′ [°]	C′ [MPa]	φ′ [°]
GM 1	3.1	29	1.7	19	7.1 (14.5)	33 (18)	3.9 (7.5)	24 (17)
GM 2	2.6	28	1.7	19	6.0 (13.4)	32 (17)	3.9 (7.5)	24 (17)
GM 3	3.1	29	1.3	18	7.1 (14.5)	33 (18)	2.9 (5.8)	21 (18)
GM 4	2.6	28	1.3	18	6.0 (13.4)	32 (17)	2.9 (5.8)	21 (18)
GM 5	2.6	28	1.0	17	6.0 (13.4)	32 (17)	2.3 (2.3)	20 (20)
GM 6	2.3	22	1.0	17	5.2 (5.2)	22 (22)	2.3 (2.3)	20 (20)
GM 7	0.3	17	0.3	17	0.5 (0.5)	17 (17)	0.5 (0.5)	17 (17)

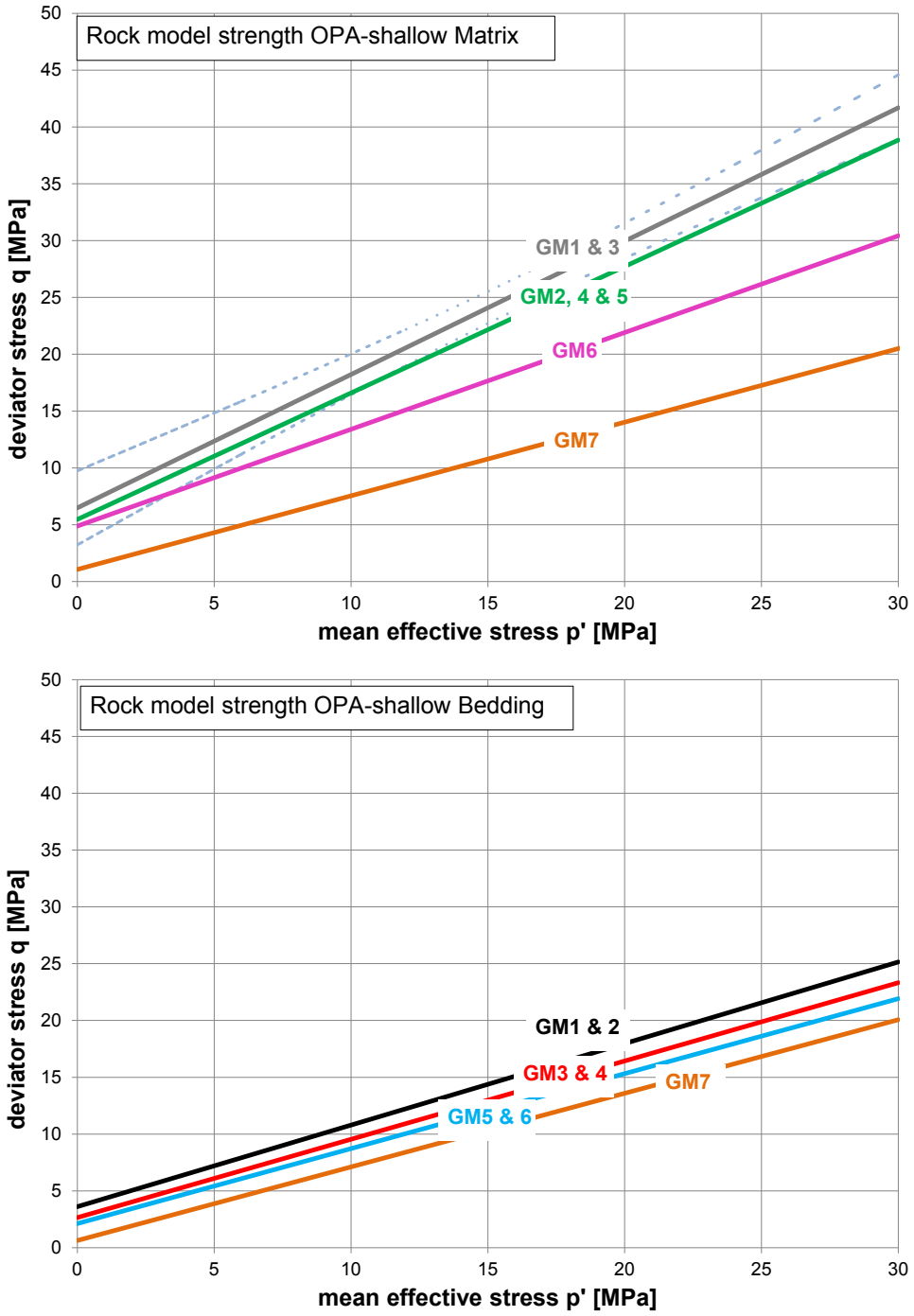

Fig. 7-9: Strength values of different rock models for *Opalinus Clay shallow*.
For colour coding see Figs. 7-7 and 7-8.

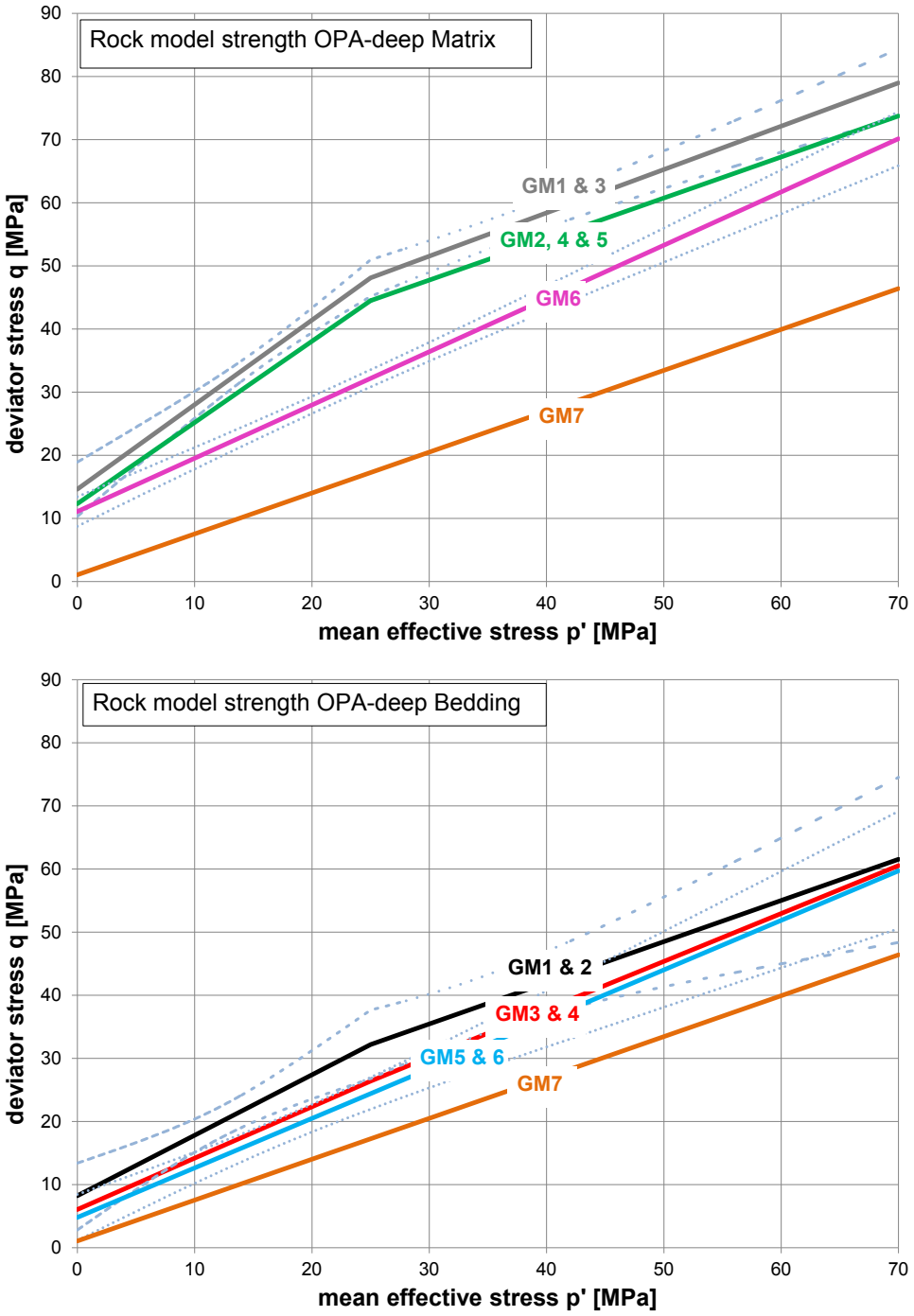

Fig. 7-10: Strength values of different rock models for *Opalinus Clay deep*.
For colour coding see Figs. 7-7 and 7-8.

In Fig. 4-24 the undrained triaxial test results were plottet as undrained shear strength S_u[11] with respect to the water content. For the forced regression analysis a relationship between S_u and water content according to Equation 6-4 was used (Fig. 7-3). Equation 6-4 can be rearranged in the following way.

$$S_u = \mathrm{A} \cdot \exp(-\mathrm{B} \cdot \mathrm{w}) \quad (7\text{-}1)$$

Where A and B are related to intrinsic material parameters. The triaxial test results can therefore also be interpreted as a function of water content and expressed as undrained shear strength rather than in the effective stress space (p'-q).

Similar to the above analysis in p'-q space, different rock models can also be derived in v-q space (Su vs. water content). Such an analysis is provided in Table 7-4 and Figure 7-11. A regression analysis was conducted for the peak strength tests of matrix and bedding to constrain GM1. The slopes for these two fit analyses were then held constant for all other rock models in the respective orientations (matrix and bedding). The lower 95% confidence band[12] was also used to constrain the y-axis intercept values for the reduced peak strength fits (GM2, 4&5 for matrix and GM3&4 for bedding, respectively). Post peak strength intercept values values with the y-axis were constrained by 'fitting' the lower boundary of the experimental data (GM6 for matrix and GM5&6 for bedding, respectively).

Tab. 7-4: Recommended parameter values to derive undrained shear strength values (Su) for different rock models at a given water content.

*Values for S_u can be derived according to Equation (7-1) using values A and B for either matrix (subscript M) or bedding (subscript S) and the water content. It should be noted that for the calculation of S_u water content is expressed in decimal values and not percentage, as shown in Fig. 7-11).

Rock Model	Material parameters to derive* values fort he undrained shear strength S_u					
	Matrix values			Bedding values		
	A_M [MPa]	B_M [-]	λ_M [-]	A_S [MPa]	B_S [-]	λ_S [-]
GM 1	61.5	23.5	0.12	42.4	28.9	0.09
GM 2	35.0	23.5	0.12	42.4	28.9	0.09
GM 3	61.5	23.5	0.12	30.0	28.9	0.09
GM 4	35.0	23.5	0.12	30.0	28.9	0.09
GM 5	35.0	23.5	0.12	18.0	28.9	0.09
GM 6	20.0	23.5	0.12	18.0	28.9	0.09

[11] According to Equation 4-11.

[12] See data file *20_Su-wc.opj* for details

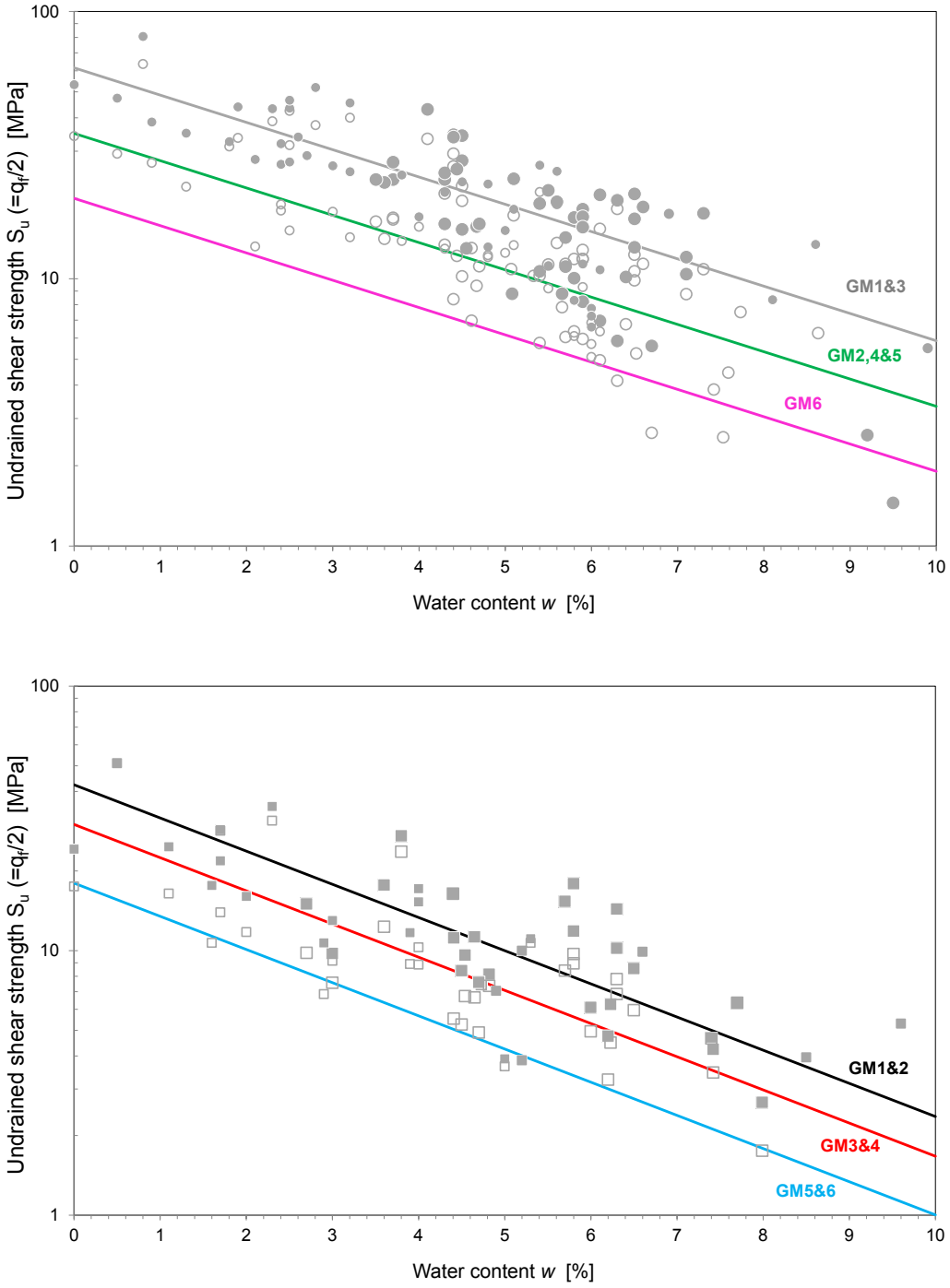

Fig. 7-11: Rock models interpreted in Su-w space.

For colour coding see Figs. 7-7 and 7-8.

7.4 In-situ stress

Reference minimum horizontal stress

$$Sh_{ref} = K_{Sh/Sv\_ref} \times S_v = 0.95 \times S_v \quad (7\text{-}2a)$$

Reference maximum horizontal stress

$$SH_{ref} = K_{SH/Sh\_ref} = 1.35 \times Sh_{ref} \quad (7\text{-}2b)$$

These reference values relate to the constrained magnitudes from hydraulic fracturing in the Benken borehole at a depth of 630 m (Nagra 2001). Relative to S_v they are fixed at a constant ratio within the considered depth range (Fig. 6-3).

A lower bound value for the minimum horizontal stress can be formulated assuming that lateral stresses are controlled *only by the overburden* (i.e. no tectonic stresses) and following the approach by Mayne and Kulhawy (1982) for overconsolidated claystones (Appendix C):

$$Sh_{min} = \frac{(1-\sin\varphi)\times OCR^{\sin\varphi}\times(Sv-Pp)+Pp}{Sv} \times S_v$$

where OCR is the overconsolidation ratio according to Equation 4-1, φ is the angle of internal friction [°] and Pp the pore fluid pressure [MPa]. Assuming further a hydrostatic pore pressure gradient and constant overburden density, and using Equation 4-1 with the minimum estimated overconsolidation ratio (OCR) (cf. Equation B3-1b in Appendix C), the above equation can be simplified to:

Low-end minimum horizontal stress

$$Sh_{min} = S_v \times \left[0.35 \times \left(1 + \frac{300}{z}\right)^{0.42} + 0.4\right] \quad (7\text{-}3a)$$

Low-end maximum horizontal stress

$$SH_{min} = K_{SH/Sv\_min} = 1.35 \times Sh_{min} \quad (7\text{-}3b)$$

Note that the approach of Mayne & Kulhawy (1982) relates only the vertical stress to a horizontal stress and assumes that $S_h \approx S_H$. By holding $K_{SH/Sh}$ constant at 1.35 it is here assumed that in addition to the lateral stresses exerted by the vertical load, lateral tectonic loading leads to a differential stress between S_H and S_h, i.e. tectonic loading only increases the S_H magnitude, but not S_h. Evidence for an ambient lateral differential stress in Opalinus Clay comes from the observation that directed breakouts are recorded in Opalinus Clay in the boreholes of Benken, Weiach and Schafisheim (Heidbach & Reinecker 2013).

Tab. 7-5: Reference principal total normal stress values as a function of depth.
See also Fig. 7-11 for graphical visualization.[a]z = depth in meters below ground.

Stress magnitudes	**Unit**	**Values for any depth**	**Values for specific depth [m b.g.]**		
			500	**700**	**900**
Overburden stress S_v (ρ = 2500 kg/m^3)	[MPa]	0.0245z[a]	12.3	17.2	22.1
Horizontal stresses					
Reference horizontal stresses (RSR_{ref})					
Minimum horizontal stress magnitude ($S_{h\ ref}$).	[MPa]	Eq. 7-2a	11.6	16.3	21.0
Maximum horizontal stress magnitude ($S_{H\ ref}$)	[MPa]	Eq. 7-2a	15.7	22.0	28.3
$K_{Sh/Sv}$	[-]		0.95	0.95	0.95
$K_{SH/Sv}$	[-]		1.28	1.28	1.28
Alternative values at low tectonic stresses (RSR_{min})					
Minimum horizontal stress magnitude ($S_{h\ min}$)	[MPa]	Eq. 7-3a	10.1	13.8	17.5
Maximum horizontal stress magnitude ($S_{H\ min}$)	[MPa]	Eq. 7-3b	13.7	18.7	23.7
$K_{Sh/Sv}$	[-]		0.83	0.81	0.79
$K_{SH/Sv}$	[-]		1.12	1.09	1.07
Alternative values at high tectonic stresses (RSR_{max})					
Minimum horizontal stress magnitude ($S_{h\ max}$)	[MPa]	Eq. 7-4b	17.2	23.8	30.5
Maximum horizontal stress magnitude ($S_{H\ max}$)	[MPa]	Eq. 7-4a	23.2	32.2	41.1
$K_{Sh/Sv}$	[-]		1.40	1.39	1.38
$K_{SH/Sv}$	[-]		1.89	1.87	1.86

High-end maximum horizontal stress

$$SH_{max} = S_v \times \frac{1+\sin(\varphi)}{1-\sin(\varphi)} + 2\,C \times \frac{\cos(\varphi)}{1-\sin(\varphi)} \quad (7\text{-}4a)$$

where φ and C are the Mohr-Coulomb angle of internal friction [°] and cohesion [MPa]. Since the strength of Opalinus Clay would be the limiting factor, residual strength parameters are recommended for this scenario with φ = 17° and C = 0.3 MPa.

In a compressive regime Sh should be greater than Sv. For consistency with the reference and the low-end stress field, the ratio between SH and Sh is held constant at a factor 1.35:

High-end minimum horizontal stress

$$Sh_{max} = SH_{max}/1.35 \quad (7\text{-}4b)$$

SH but sensitivity analyses (Heidbach et al. 2014) suggest that S_h is not very sensitive to lateral tectonic loading. Therefore, Sh_{max} is recommended as:

Table 7-4 summarises the three scenarios of ambient stress fields for the Opalinus Clay and Fig. 7-11 graphically visualizes the evolution with depth. Simpson (1997) defined the *Regime Stress Ratio (RSR)* as:

$$RSR = (n + 0.5) + (-1)^n(R - 0.5) \tag{7-5}$$

Where $R = \frac{\sigma_2 - \sigma_3}{\sigma_1 - \sigma_3}$ and $n = \begin{cases} 0 & S_h < S_H < S_v \quad \text{normal faulting} \\ 1 & S_h < S_v < S_H \quad \text{strike-slip faulting} \\ 2 & S_v < S_h < S_H \quad \text{thrust faulting} \end{cases}$

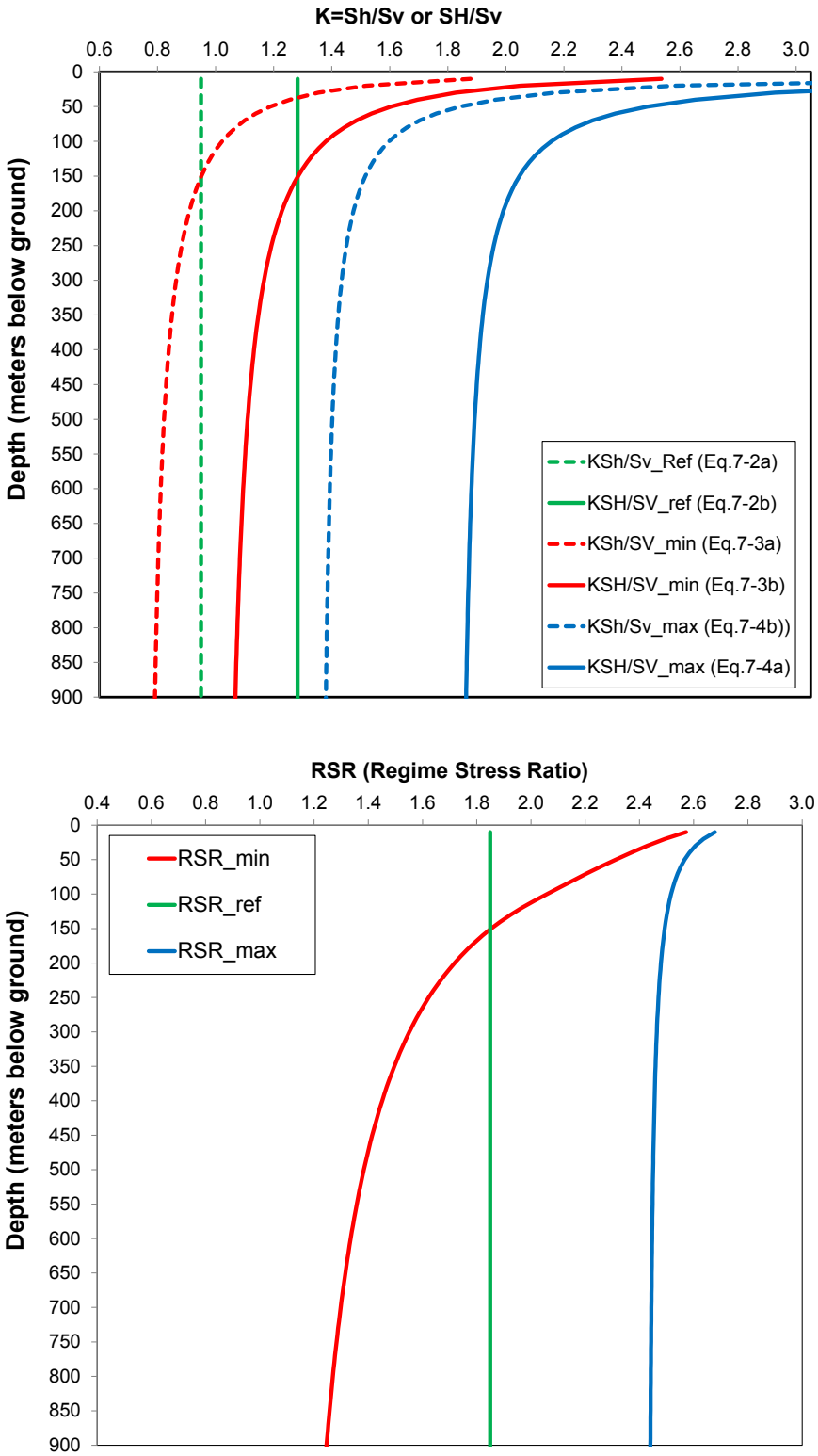

Fig. 7-12: Recommended depth trend of reference and alternative stress scenarios.

Above: Lateral stresses S_h and S_H expressed with respect to overburden stress S_v. Green = reference scenario, red = minimum stress scenario and blue = maximum stress scenario. *Below:* The same stress ratios expressed as RSR values.

Hence the advantage of the RSR is that it expresses the relative magnitudes of the three principal stresses as a continuous value between 0 (pure normal faulting) and 3 (pure thrust faulting). The three stress field scenarios are therefore referred to as RSR_{ref}, RSR_{min} and RSR_{max} in Tab. 7-4 and they are graphically visualized in Fig. 7-11.

7.5 Site-specific reference data sets

A recommendation of the reference data sets to be considered for site specific analyses of engineering appraisal is provided in Tab. 7-6. The recommendation of the reference geomechanical dataset (Tab. 7-1) is based on the mean depth of Opalinus Clay in the siting regions (Tab. 2-1). Since Opalinus Clay in the siting regions Jura Ost and Südranden is at a mean depth of approximately 400 m, the geomechanical parameter set of *Opalinus Clay shallow* may be considered as an alternative data set to *Opalinus Clay deep*.

All three stress scenarios (RSR_{ref}, RSR_{min}, RSR_{max}) are considered plausible at the level of Opalinus Clay in the different siting regions. This also applies to Zürich Nordost, where hydraulic fracturing data is available from the borehole Benken. The scenario RSR_{max} covers roughly the upper bound of the estimated SH in Benken based on the "measured" Sh magnitude.

The rock models GM1 to GM4 should be considered for comparative, site specific analyses. The other rock models (GM5-7) are formulated to cover the range of observation, but they are not considered as representative of the Opalinus Clay in the siting areas. As outlined in Chapter 2.1, Opalinus Clay in the Subjurassic zone (JS) and the deformed Tabular Jura (JO, NL) was transported to the north during Neogene shortening. It is therefore considered appropriate to assume a slightly less favorable rock model for the sites of JS, JO and NL (GM2 to GM4 instead of GM1 to GM3 in ZNO and SR). This assumption is corroborated by generally higher structural frequencies in boreholes from Benken to Schafisheim (i.e. from east to west in Fig. 2-3) and by ongoing analyses of seismic data (Madritsch et al. 2013).

Tab. 7-6: Recommended geomechanical reference datasets for site specific analyses.

	Jura-Südfuss	**Jura Ost**	**Nördlich Lägern**	**Zürich Nordost**	**Südranden**
Geomechanical data					
Reference	$OPA_{interm/deep}$	$OPA_{interm/deep}$	$OPA_{interm/deep}$	$OPA_{interm/deep}$	$OPA_{interm/deep}$
Alternative	-	$OPA_{shallow}$	-	-	$OPA_{shallow}$
Stress regime					
Scenario 1	RSR_{ref}	RSR_{ref}	RSR_{ref}	RSR_{ref}	RSR_{ref}
Scenario 2	RSR_{min}	RSR_{min}	RSR_{min}	RSR_{min}	RSR_{min}
Scenario 3	RSR_{max}	RSR_{max}	RSR_{max}	RSR_{max}	RSR_{max}
Rock model					
Scenario 1	GM3	GM3	GM3	GM1	GM1
Scenario 2	GM2	GM2	GM2	GM2	GM2
Scenario 3	GM4	GM4	GM4	GM3	GM3

References

Al-Bazali, T., Zhang, J., Chenevert, M.E. & Sharma, M.M. (2008): Experimental and numerical study on the impact of strain rate on failure characteristics of shales. Journal of Petroleum Science and Engineering 60, 194-204.

Albert, W. (2000): Sondierbohrung Benken: Auswertung von Bohrlochrandausbrüchen und induzierten Rissen. Unpubl. Nagra Int. Bericht. Nagra, Wettingen.

Albert, W. & Schwab (2013): Analyse des Tonmineralgehalts anhand von Bohrlochmessungen in Bohrungen der Nordschweiz. Nagra Arbeitsbericht NAB 12-56. Nagra, Wettingen.

Amann, F.; Kaiser, P. & Button, E.A. (2012): Experimental Study of Brittle Behavior of Clay Shale in Rapid Triaxial Compression. Rock Mechanics and Rock Engineering 45, 21-33.

Aristorenas, G.V. (1992): Time-dependent behavior of tunnels excavated in shale. Doctor of Philosophy at the Massachusetts Institute of Technology.

Azizi, F. (1999): Applied analyses in geotechnics. E & FN Spon, London.

Backers, T. (2010): Brasilianische Zugversuche an Proben aus Opalinus Ton bei verschiedenen Wassergehalten. Nagra Arbeitsbericht NAB 10-08. Nagra, Wettingen.

Beauheim, R. (2013): Hydraulic conductivity and head distributions in the host rock formations of the proposed siting regions. Nagra Arbeitsbericht NAB 13-13. Nagra, Wettingen.

Bellwald, P. (1990): A contribution to the design of tunnels in argillaceous rock. Doctor of Science in Civil Engineering at the Massachusetts Institute of Technology.

Bemer, E., Longuemare, P. & Vincké, O. (2004): Poroelastic parameters of Meuse/ Haute Marne argillites: effect of loading and saturation states. Applied Clay Science 26, 359-366.

Blümling, P. & Vietor, T. (2009): Felsmechanisch relevante Eigenschaften von Trennflächen-systemen in Opalinuston. Unpubl. Nagra Int. Bericht. Nagra, Wettingen.

Bock, H. (2009): RA Experiment: updated review of rock mechanics properties of the Opalinus Clay of Mont Terri URL based on laboratory and field testing. Mont Terri Technical Report TR 2008-04.

Bock, H., Dehandschutter, B., Martin, C.D., Mazurek, M., de Haller, A., Skoczylas, F. & Davy, C. (2010): Self-sealing of fractures in argillaceous formations in the context of geological disposal of radioactive waste. Review and synthesis, OECD/NEA, Paris.

Boisson, J.-Y. (2005): Clay club catalogue of characteristics of argillaceous rocks. OECD Nuclear Energy Agency OECD/NEA, Paris.

Brooker, E.W. & Ireland, H.O. (1965): Earth pressures at rest related to stress history. Canadian Geotechnical Journal 11/1, 1-15.

Büchi & Müller AG (1983): Beurteilung der Abbaumöglichkeiten für Opalinuston im Bereich Birchbüel-Chrügeli, Gemeinde Gächlingen und Siblingen/SH. Bericht Nr. 1794.

Büchi & Müller AG (1988): Geordnete regionale Deponie Pflumm, Gemeinde Gächlingen. Bericht Nr. 2701.

Charlez, P.A. (1997): Rock mechanics volume 2, petroleum applications. Éditions Technip, Paris.

Chiffoleau, S. & Robinet, J.C. (1999): HE Experiment: determination of the hydromechanical characteristics of the Opalinus Clay. Mont Terri Technical Note TN 98-36.

Czaikowski, O. (2011): Laborative und rechnerische Untersuchungen zu geomechanisch-geohydraulischen Wechselwirkungen im Tongestein im Hinblick auf die Endlagerung radioaktiver Abfälle. Dissertation, ISBN 978-3-86948-181-4, TU Clausthal.

Favero, V., Ferrari, A. & Laloui, L. (2013): Diagnostic analyses of the geomechanical database from cores of the Borehole Schlattingen SLA-1. Nagra Arbeitsbericht NAB 13-45. Nagra, Wettingen.

Ebert, A. (2014) Strukturgeologische Kernaufnahmen der Wirtgesteine aus Tiefbohrungen der Nordschweiz. Nagra Arbeitsbericht NAB 13-89. Nagra, Wettingen.

Ferrari, A., Gruaz, G., Salager, S. & Laloui, L. (2009): HA-project: analysis of Opalinus Clay self sealing: experimental investigation (swelling tests): Mont Terri Technical Note TN 2008-45 rev.

Ferrari, A., Favero, V., Manca, D. & Laloui, L. (2012a): Geotechnical characterizazion of core samples from the geothermal borehole Schlattingen LSA-1. Nagra Arbeitsbericht NAB 12-50. Nagra, Wettingen.

Ferrari, A., Witteveen, P. & Laloui, L. (2012b): Material properties and geomechanical tests on BHG-D1 cores. Mont Terri Technical Note TN 2010-52.

Fjær, E., Holt, R.M., Horsrud, P., Raanen, A.M. & Risnes, R. (2008): Petroleum related rock mechanics, 2nd edition. Elsevier.

Fredlund, D.G. & Rahardjo, H. (1993): Soil mechanics for unsaturated soils. John Wiley & Sons.

Jahns Gesteinslabor (2013): Geomechanical laboratory tests on Opalinus Clay cores from the borehole Schlattingen SLA-1. Nagra Arbeitsbericht NAB 13-18. Nagra, Wettingen.

Jahns Gesteinslabor (2007): Rock mechanics analysis (RA) experiment: rock strength of Opalinus Clay subject to time of storage. Mont Terri Technical Note 2007-30.

Jahns Gesteinslabor (2010): RA Experiment: Opalinus Clay rock characterization. Mont Terri Technical Note 2008-55 rev.

Graham, J. & Houlsby, G.T. (1983): Elastic anisotropy of a natural clay. Géotechnique 33/2, 165-180.

Gutierrez, M., Nygård, R., Høeg, K. & Berre, T. (2008): Normalized undrained shear strength of clay shales. Engineering Geology 99, 31-39.

Haug, C. (2009): Mechanische Charakterisierung präexistenter tektonischer Trennflächen im Opalinuston. Master-Arbeit, Dep. Erdwissenschaften, ETH Zürich.

Heidbach, O. & Reinecker, J. (2013): Analyse des rezenten Spannungsfeldes der Nordschweiz. Nagra Arbeitsbericht NAB 12-05. Nagra, Wettingen.

Heidbach, O., Hergert, T., Reiter, K. & Giger, S.B. (2014). Stress sensitivity analysis – case study Nördlich Lägern. Nagra Arbeitsbericht NAB 13-88. Nagra, Wettingen.

Holtz, R.D., Kovacs, W.D. & Sheahan, T.C. (2009): An Introduction to Geotechnical Engineering. 2nd edition.

Horseman, S.T. & Harrington, J.F. (2002): Laboratory experiments on gas migration in Opalinus Clay samples from the Benken borehole, Switzerland. Unpubl. Nagra Int. Report. Nagra, Wettingen.

Horseman, S.T., Harrington, J.F., Birchall, D.J., Noy, D.J. & Cuss, R.J. (2006): Hydrogeologic analyses and synthesis (HA experiment): consolidation and rebound properties of Opalinus Clay: a long-term, fully drained test. Mont Terri Technical Note TN 2003-03 rev.

Jáky, J. (1944): The coefficient of earth pressure at rest. Journal for Society of Hungarian architects and engineers, 355-358, Budapest, Hungary.

Kulhawym, F.H., Beech, J.F. & Trautman, C.H. (1989): Influence of geologic development on horizontal stresses in soil. Proc. Foundation Engineering Congr. ASCE, Evanston, Illinois, 43-47.

Klee, G. & Rummel, F. (2000): Sondierbohrung Benken: Hydrofrac Spannungsmessungen Teil II – Ergebnisse der Laboruntersuchungen und Abschlussbewertung. Unpubl. Nagra Int. Ber. Nagra, Wettingen.

Klee, G. (2012): Geothermal borehole Schlattingen-1: Hydraulic fracturing stress measurements. Unpubl. Nagra Project Report. Nagra, Wettingen.

Ladd, C.C. (1991): Stability evaluation during staged construction. J. Geotech. Engrg. 117/4, 540-615.

Lambé, R. & Whitman, V. (1979): Soil mechanics. Wiley.

Lux, K.H., Düsterloh, U. & Czaikowski, O. (2007): Laboratory tests on indurated clay. Clausthal University of Technology Final Report for EDZ long term evolution (WP 4.4). European Commission NF-PRO (D4.4.13).

Madritsch, H. & Hammer, P. (2012): Characterisation of Cenozoic brittle deformation of potential geological siting regions for radioactive waste repositories in Northern Switzerland based on structural geological analysis of field outcrops. Nagra Arbeitsbericht NAB 12-41. Nagra, Wettingen.

Madritsch, H., Meier, B., Kuhn, P., Roth, Ph., Zingg, O., Heuberger, S., Naef, H. & Birkhäuser, Ph. (2013): Regionale strukturgeologische Zeitinterpretation der Nagra 2D-Seimik 2011/12. Nagra Arbeitsbericht NAB 13-10. Nagra, Wettingen.

Mathier, J.-F., Egger, P. & Descoeudres, F. (1999): Sondierbohrung Benken: Felsmechanische Untersuchungen an Bohrkernen (Teil 2). Unpubl. Nagra Int. Bericht. Nagra, Wettingen.

Mazurek, M., Hurford, A.J. & Leu, W. (2006): Unravelling the multi-stage burial history of the Swiss Molasse Basin: integration of apatite fission track, vitrinite reflectance and biomarker isomerisation analysis. Basin Research 18, 27-50.

Mazurek, M. (2011): Aufbau und Auswertung der Gesteinsparameter-Datenbank für Opalinuston, den 'Braunen Dogger', Effinger Schichten und Mergel-Formationen des Helvetikums. Nagra Arbeitsbericht NAB 11-20. Nagra, Wettingen.

Minon, S., Salager, S. & Laloui, L. (2010): WS-H experiment: Identification tests and rheological analysis of Opalinus Clay: Shaly facies, sandy facies and wet spot material. Mont Terri Technical Note 2010-61.

Monfared, M., Sulem, J., Delage, P. & Mohajerani, M. (2011): A laboratory investigation on thermal properties of the Opalinus Claytone. Rock Mech. Rock Eng. 44, 735-747. DOI 10.1007/s00603-011-0171-4.

Mayne, P.W. & Kulhawy, F.H. (1982): K_0-OCR relationships in soil. ASCE Journal of Geotechnical Engineering Division 108 (GT6), 851-872.

Matter, A., Peters, Tj., Isenschmid, Ch., Bläsi, H.R. & Ziegler, H.J. (1987): Sondierbohrung Riniken – Geologie. Textband und Beilagenband. Nagra Tech. Bericht NTB 86-02. Nagra, Wettingen.

Matter, A., Peters, Tj., Bläsi, H.R., Schenker, F. & Weiss, H.-P. (1988): Sondierbohrung Schafisheim – Geologie. Textband und Beilagenband. Nagra Tech. Bericht NTB 86-03. Nagra, Wettingen.

Nagra (2001): Sondierbohrung Benken – Untersuchungsbericht. Textband und Beilagenband. Nagra Tech. Bericht NTB 00-01. Nagra, Wettingen.

Nagra (2002): Projekt Opalinuston: Synthese der geowissenschaftlichen Untersuchungsergebnisse – Entsorgungsnachweis für abgebrannte Brennelemente, verglaste hochaktive sowie langlebige mittelaktive Abfälle. Nagra Tech. Bericht NTB 02-03. Nagra, Wettingen.

Nagra (2008): Vorschlag geologischer Standortgebiete für ein SMA- und ein HAA-Lager: Geologische Grundlagen (Bericht zur Geologie). Nagra Tech. Bericht NTB 08-04. Nagra, Wettingen.

Nagra (2010): Beurteilung der geologischen Unterlagen für die provisorischen Sicherheitsanalysen in SGT Etappe 2 – Klärung der Notwendigkeit ergänzender geologischer Untersuchungen. Nagra Tech. Bericht NTB 10-01. Nagra, Wettingen.

Noiret, A., Giot, R., Bemer, E., Giraud, A. & Homand, F. (2011): Hydromechanical behavior of Tournemire argillites: Measurement of the poroelastic parameters and estimation of the intrinsic permeability by oedometric tests. International Journal for Numerical and Analytical Methods in Geomechanics 35, 496-518.

Nüesch, R. (1991): Das mechanische Verhalten von Opalinuston. Diss. ETH Zürich Nr. 9349.

Olalla, C., Martin, M.E. & Sáez, J. (1999): ED-B Experiment: Geotechnical laboratory tests on Opalinus Clay rock samples. Mont Terri Technical Note TN 98-57.

Pellet, F.L., Keshavarz, M. & Boulon, M. (2013): Influence of humidity conditions on shear strength of clay rock discontinuities. Engineering Geology 157, 33-38.

Péron, H., Salager, S., Eichenberger, J., Rizzi, M. & Laloui, L. (2009) : Experimental and numerical analysis of excavation damaged zone (EDZ) along tunnels. Mont Terri Technical Note TN 2008-54.

Popp, T. & Salzer, K. (2006): HE-D experiment: Influence of bedding planes. Mont Terri Technical Note TN 2005-34.

Rummel, F., Hettkamp, T. & Weber, U. (1998): Laboratory experiments for the determination of deformation mechanisms and a constitutive law for time dependent deformation behaviour of the Opalinus Clay (Phase 3). Mont Terri Technical Note TN 98-35

Rummel, F. & Weber, U. (1999): Sondierbohrung Benken: Felsmechanische Laboruntersuchungen am Bohrkernen. Unpubl. Nagra Int. Bericht. Nagra, Wettingen.

Rummel, F., Hettkamp, T. & Weber, U. (1999): DM Experiment: Laboratory experiments for the determination of deformation mechanisms and a constitutive law for time dependent deformation behaviour of the Opalinus Clay. Mont Terri Technical Note TN 99-35.

Rummel, F. & Weber, U. (2004): RA experiment: Rock mechanical testing and characterization on drillcores of boreholes BRA-1 and BRA-2. Mont Terri Technical Note TN 2004-38.

Schanz, T. (2006): Aktuelle Entwicklungen bei Standsicherheits- und Verformungsberechnungen in der Geotechnik (Current developments of stability and deformation calculations in geotechnics). Geotechnik, 29 (1), 13-27.

Schanz, T. & Al-Badran, Y. (2011): Final report for hydro-mechanical characterization of Opalinus Clay. Internal report, Ruhr University, Bochum, Germany.

Schnier, H. & Stührenberg, D. (2007): LT experiment: strength tests on cylindrical specimens, documentation and evaluation (phases 8 & 9). Mont Terri Technical Report TR 2003-04.

Schofield, A. & Wroth, P. (1968): Critical state soil mechanics. Cambridge University.

Shiu, W. & Billaux, D. (2014): Numerical reproduction and sensitivity analysis of undrained triaxial test results. Nagra Arbeitsbericht NAB 13-86. Nagra, Wettingen.

SIA (1998): Erfassung des Gebirges im Untertagebau: Beschreibung des Gebirges; Beurteilung des Gebirges; Geologische, hydrogeologische und geotechnische Berichte. SIA Empfehlung 199. Schweizerischer Ingenieur- und Architekten-Verein, Zürich.

Simpson, R.W. (1997): Quantifying Anderson's fault types, J. Geophys. Res., 102, 17909-17919.

Stark, T.D. & Eid, H.T. (1994): Drained residual strength of cohesive soils. Journal of Geotechnical Engineering 120/5, 856–871.

Suarez-Rivera, R. & Fjær, E. (2013): Evaluating the poroelastic effect of anisotropic, organic-rich mudstone systems. Rock Mech. Rock Eng. 46, 569-580.

SFOE (2008): Sectoral Plan for Deep Geological Repositories, Conceptual Part. Swiss Federal Office of Energy, Bern, Switzerland.

Steiner W. (2000): Choice of construction methods for tunnels in hard soil soft rock: Influence and reliability of site investigations. The geotechnics of hard soils – soft rocks, Evangelista & Picarelli (eds), 2nd Internat. Symp. Hard Soil Soft Rock, Napoli, October 1998, Balkema, Rotterdam, 1547-1554.

Te Kamp, L. (2008): Comparative rock-mechanical modeling of ILW caverns in different host rocks. Nagra Arbeitsbericht NAB 08-45. Nagra, Wettingen.

Terzaghi, K., Peck, R.B. & Mesri, G. (1996): Soil mechanics in engineering practice. Third edition. John Wiley & Sons, New York.

Torabi, A. & Støren Berg, S. (2011): Scaling of fault attributes: A review [PDF Article in Press]. Marine and Petroleum Geology 28/8, 1444-1460.

Traber, D. & Blaser, P. (2013): Gesteinsparameter der Wirtgesteine Opalinuston, 'Brauner Dogger', Effinger Schichten und Helvetische Mergel als Grundlage für die Sorptions-datenbank. Nagra Arbeitsbericht NAB 12-39. Nagra, Wettingen.

Underwood, L.B. (1967): Classification and identification of shales. Proc. ASCE J. soil mechanics and foundation engineering. 93, No. SM 6, 97-116.

Vögtli, B. & Bossart, P. (1998): DT Experiment, swelling experiment on Opalinus Clay drillcores. Mont Terri Technical Note 97-06 (revised).

Wild, K.M., Wymann, L.P., Zimmer, S., Thoeny, R. & Amann, F. (2014): Water retention characteristics and state-dependent mechanical and petro-physical properties of a clay shale. Rock Mech. Rock Eng. doi:10.1007/s00603-014-0565-1.

Wileveau, Y., Cornet, F.H., Desroches, J. & Blümling, P. (2007): Complete in situ stress determination in an argillite sedimentary formation. J. Phys. Chem. Earth 32, 866-878. doi:10.1016/j.pce.2006.03.018.

Yong S. (2007): A three-dimensional analysis of excavation-induced perturbations in the Opalinus Clay at the Mont Terri Rock Laboratory. DISS. ETH Nr. 17575. Eidgenössische Technische Hochschule, Zürich.

Appendix A: Independent evidence

Effective friction angle of intact clays

Opalinus Clay index properties from Chapter 3 are compared to empirical correlations of the same properties with effective friction angles in clays and shales.

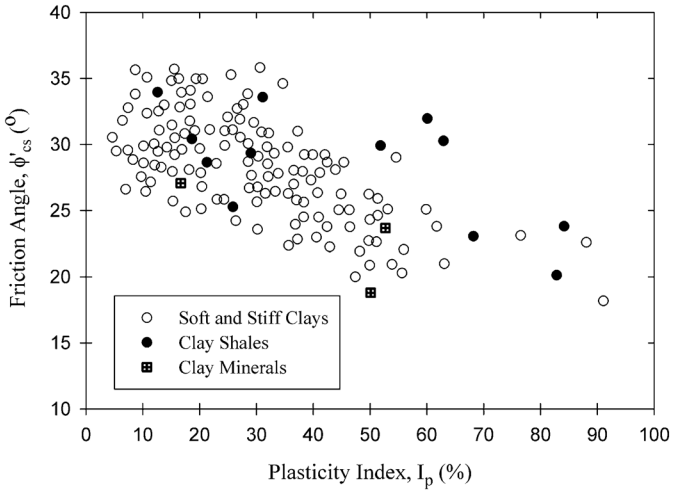

Fig. A1-1: Empirical correlation of effective friction angle with Plasticity Index (I_p or PI) after Terzaghi et al. (1996).

For Opalinus Clay ($10 < PI < 20$), the empirical correlation suggests effective friction angle values of equal to or greater than 25°.

Residual effective friction angle

Opalinus Clay index properties from Chapter 3 are compared to empirical correlations of the same properties with residual friction angles in clays and shales.

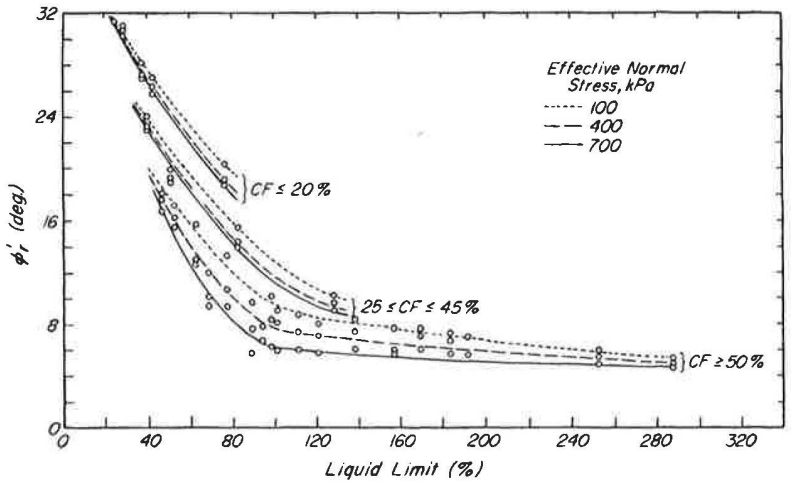

Fig. A1-2: Empirical correlation of effective residual friction angle with liquid limit (w_L) and clay size fraction (CF) after Stark & Eid (1994).

For Opalinus Clay ($30 < w_L < 50$; $20 < CF$ 40%) the empirical correlation suggests residual friction values of greater than 20°.

Undrained shear strength (S_u)

Gutierrez et al. (2008) normalized S_u values of 25 different shales from the North Sea to current in-situ vertical effective stress (σ_{vo}') and plot the results versus the apparent overconsolidation ratio (OCR). For the experimental data, σ_{vo}' corresponds to the effective consolidation stress. The OCR is defined in Equation 4-1. In Fig. A-3, triaxial test results of Opalinus Clay from the boreholes of Schlattingen-1 (Gesteinslabor Jahns 2013) and near Diepflingen (Bellwald 1990 and Aristorenas 1992) are compared to the fit line of Gutierrez et al. (2008). To calculate the OCR values with respect to the effective consolidation stress the maximum past effective stress σ_p' for Schlattingen-1 was assumed 20 MPa and 15 MPa for the area of Diepflingen (cf. Tab. 4-1).

The general positive correlation of normalized shear strength with OCR is also observed in Opalinus Clay. The slope and actual values are especially comparable to the North Sea shales data for the Opalinus Clay with loading inclined to the fabric (it is noted that the tests by Bellwald (1990) and Aristorenas (1992) were also conducted with the fabric inclined to the loading direction).

Using the relationship of Gutierrez et al. (2008; Fig. 7) and assuming a maximum burial depth for Opalinus Clay of 1700 m, OCR values calculated on the basis of Equation 4-1, hydrostatic pore pressure gradient and a total vertical stress gradient of 0.025 MPa/m yields values of $S_u \approx$ 8-9 MPa in the relevant depth range for repositories (400 – 900 m).

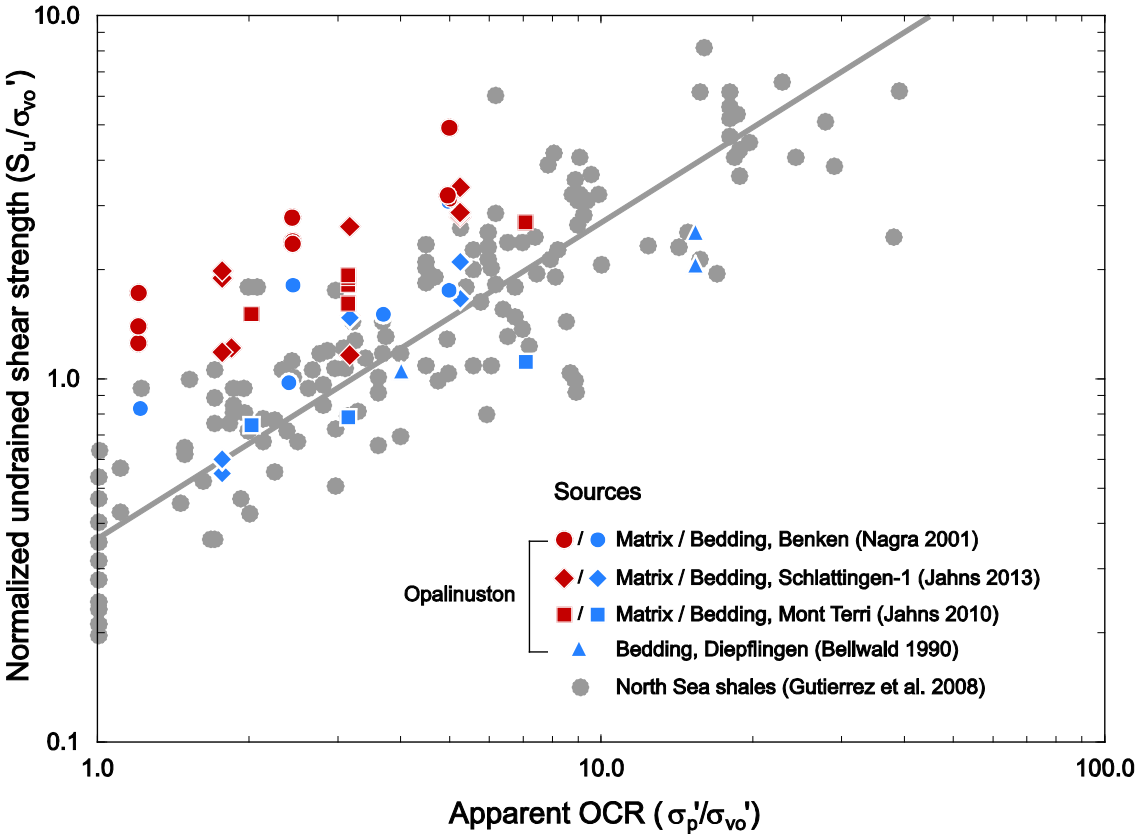

Fig. A1-3: Comparison of normalized undrained shear strength between Opalinus Clay and North Sea shales.

Appendix B: Effect of pore pressure in regression lines of Benken data

Rummel & Weber (1999) mention, that a pore fluid pressure of $P_f \approx 0.3 – 0.4$ MPa was applied for consolidation prior to shear testing, but they did not document details of the pore pressure evolution during testing in their report. The only indication was a pore pressure vs. time curve of a representative test, in which pore pressure dropped slowly during consolidation and reached a value of approximately $P_f \approx 0.2$ MPa. In an early fit analysis, the pore fluid pressure for all data of Rummel & Weber (1999) was therefore assumed as $P_f = 0.2$ MPa. This is documented in the electronic file *16_BilinearFits_p'-q.opj* and *17_BENSLA1_matrix_BiLinear.xlsx* and *18_BENSLA1_bedding_BiLinear.xlsx*. (see Appendix D).

The original data files of the tests were then recoverd, including details of the pore pressure evolution during shearing. The data was re-interpreted with the measured pore fluid pressures. It was found that the regression at values of p' < 25 MPa was hardly affected (Tab. B1-1). Values at p' > 25 MPa were slightly affected by the new regression, but these values are not relevant for the depth range considered (< 900 m b.g., cf. Table 7-1 and 7-4). Given these small differences in the regression analysis the recommended parameters were not adjusted.

Tab. B1-1: Comparison of fit analysis with variable pore fluid pressure values for the geomechanical tests by Rummel & Weber (1999).

	Matrix strength			Bedding strength		
	Pf = 0.2	Pf measured	**Ref-value (Tab 7-1)**	Pf = 0.2	Pf measured	**Ref-value (Tab 7-1)**
Peak values						
C'_1 [MPa]	7.1	7.3	**7.1**	3.9	4.1	**3.9**
φ'_1 [MPa]	33	33	**33**	24	24	**24**
C'_2 [MPa]	14.6	14.1	**14.6**	7.4	6.4	**7.4**
φ'_2 [MPa]	18	19	**18**	17	19	**17**
Post-peak values						
C' [MPa]	5.3	5.1	**5.2**	2.4	2.2	**2.2**
φ' [MPa]	22	22	**22**	20	22	**20**

Appendix C: Estimation of minimum horizontal stress magnitudes

In soil mechanics, the ratio of horizontal to vertical stress (K = Sh/Sv) for *normally consolidated (NC)* clays can be approximated by the relationship K_{NC} = 1-sin(φ)' (Jaky 1944), where φ is the effective friction angle. Empirical correlations have shown that K-values of stiff, overconsolidated shales during unloading (e.g. exhumation) are elevated with respect to values at identical depth during initial loading (e.g. Brooker & Ireland 1965). This is because swelling occurs mainly in vertical direction (assuming horizontal stratification), and therefore the horizontal effective stresses reduce by only a portion of the load removed (Kulhawy et al. 1989). Mayne & Kulhawy (1982) suggested that K-values of overconsolidated clays be approximated by the following relationship:

$$K_{OCR} = K_{NC} \times OCR^{\sin(\varphi)} = (1 - \sin(\varphi)) \times OCR^{\sin(\varphi)} \quad \text{(C1-1)}$$

In the absence of lateral tectonic stresses, it can be assumed that $K_{Sh/Sv}' \approx K_{OCR}$. The apostrophe indicates that the empirical relationships were constrained in drained Oedometer tests, i.e. they relate to *effective* stresses (absolute stress values minus pore fluid pressure). Hydraulic fracturing results and modelling input generally relate to absolute stress values. Therefore, absolute stress ratios are calculated from effective stress ratios:

$$K_{\frac{Sh}{Sv}} = \frac{\frac{K'_{Sh}(S_v - P_p)}{Sv} + P_p}{S_v} \quad \text{(C2-1a)}$$

Which can be rearranged assuming constant overburden density of ρ = 2500 kg/m^3 and hydro-static pore fluid pressure gradient to:

$$K_{Sh} = 0.6K'_{Sh} + 0.4 \quad \text{(C2-1b)}$$

As a reminder, overconsolidation ratio was defined in Equation 4-1 as:

$$OCR = 1 + z_1/z$$

where z_1 = removed (eroded) sediment thickness and z = present burial depth. Iterative fitting of Equation 4-1 to estimated OCR values at the URL MT and the boreholes of Benken and Schlattingen-1 resulted in values of $z_{1,min}$ = 300 (minimum OCR), $z_{1,\,avg}$ = 650 (average OCR) and $z_{1,max}$ = 1000 (maximum OCR). Using a constant angle of internal friction of φ = 25°, and assuming hydrostatic pore fluid pressure and a constant overburden density of ρ = 2500 kg/m^3 then leads to the following relationships:

$$K_{Sh\_min}' = 0.58 \times (1 + \frac{300}{z})^{0.42} \quad \text{(C3-1a)}$$

$$K_{Sh\_min} = 0.35 \times (1 + \frac{300}{z})^{0.42} + 0.4 \quad \text{(C3-1b)}$$

$$K_{Sh\_avg}{}' = 0.58 \times (1 + \frac{650}{z})^{0.42} \quad \text{(C3-1c)}$$

$$K_{Sh\_avg} = 0.35 \times (1 + \frac{650}{z})^{0.42} + 0.4 \quad \text{(C3-1d)}$$

$$K_{Sh\_max}{}' = 0.58 \times (1 + \frac{1000}{z})^{0.42} \quad \text{(C3-1e)}$$

$$K_{Sh\_max} = 0.35 \times (1 + \frac{1000}{z})^{0.42} + 0.4 \quad \text{(C3-1f)}$$

Appendix D: Electronic datafiles

The electronic data files comprising the data base and regression analyses used for this report is included in this report as a CD. The following table provides an overview of the different data files and specifies the different tables and figures for which the data was used. It is noted that the compiled data in this report is not exhaustive (especially for the extensive data base of the Mont Terri underground lab) but considered representative. The numbering corresponds to the order of appearance in the report.

Tab. D1-1: Overview of electronic datafiles.

Data file	**Content**	**Used in Table#**	**Used in Figure#**
1_Grainsize.xlsx	Grain size distribution		3-4
2_Plasticity.xlsx	Plasticity chart		3-5
3_Swelling.xlsx	Swelling parameters	7-2	4-4
4_Poisson ratio.xlsx	Compilation of Poisson's ratio		
5_E-Moduli.xlsx	Youngs moduli	7-1	4-7, 4-8, 4-9
6_TensileStrength.xlsx	Tensile strength (Brazilian) tests	4-3, 7-1	
7_UCS.xlsx	Uniaxial compressive strengths	4-4	4-11, 4-12, 4-23
8_LinearFits_p'-q.opj	Statistical analysis of linear regression lines in Origin software	Basis for data files# 9, 10, 11, 12, 14	
9_EffectiveStress	Calculation of mean effective stress values (p') from test data	Basis for data files# 10, 11-13, 15-19	
10_MT_matrix.xlsx	Compilation of data used for linear fits of P&S tests with samples from Mont Terri (*including forced-fit data from Chapter 7).	4-5, 7-1*	4-17, 7-4*
11_MT_bedding.xlsx	Compilation of data used for linear fits of X&Z tests with samples from Mont Terri (*including forced-fit data from Chapter 7)	4-5, 7-1*	4-19, 7-5*, 7-6*
12_BENSLA1_matrix.xlsx	Compilation of data used for linear fits of P&S tests with samples from Benken and Schlattingen-1	4-5, 7-1	4-20
13_BENSLA1_ bedding.xlsx	Compilation of data used for linear fits of X&Z tests with samples from Benken and Schlattingen-1	4-5, 7-1	4-22
14_Su-wc.xlsx	Compilation of undrained shear strength Su vs. water content (*including basis for forced-fit and rock models in Su-w plane in Chapter 7)	7-4*	4-24, 7-3*, 7-11*
15_BENSLA1_matrix_ alpha0.6.xlsx	Comparison of regression fit using alpha = 0.6 instead of 1.0		
16_BilinearFits_p'-q.opj	Statistical analysis of bi-linear regression lines in Origin software	Basis for data files# 17–19	

Data file	Content	Used in Table#	Used in Figure#
17_BENSLA1_matrix_ BiLinear.xlsx	Compilation of data used for bi-linear fits of P&S tests with samples from Benken and Schlattingen-1	7-1	7-1
18_BENSLA1_bedding_ BiLinear.xlsx	Compilation of data used for bi-linear fits of X&Z tests with samples from Benken and Schlattingen-1	7-1	7-2
19_StrengthRockModels. xlsx	Compilation of rock models in p'-q space (note: rock models in v-q space is included in 13_Su-wc.xlsx)	7-3	7-9, 7-11
20_Su-wc.opj	Statistical analysis (Origin software) of exponential regression lines for rock models in v-q plane	Basis for data files# 14 (rock models in Su-w space)	
21_Normalized_Su.xlsx	Normalized shear strength vs. overconsolida-tion ratio – comparison of Opalinus Clay with North Sea shales		A1-3